

**EXPLORING GERM GRANULE FUNCTION IN
SMALL RNA BIOLOGY**

By

John Paul Tsu Ouyang

A dissertation submitted to Johns Hopkins University in conformity with the requirements for
the degree of Doctor of Philosophy

Baltimore, Maryland

August, 2021

Abstract

P granules protect RNA interference genes from silencing by piRNAs

P granules are perinuclear condensates in *C. elegans* germ cells proposed to serve as hubs for self/non-self RNA discrimination by Argonautes. We report that a mutant (*meg-3 meg-4*) that does not assemble P granules in primordial germ cells loses competence for RNA-interference over several generations and accumulates silencing small RNAs against hundreds of endogenous genes, including the RNA-interference genes *rde-11* and *sid-1*. In wild-type, *rde-11* and *sid-1* transcripts are heavily targeted by piRNAs, accumulate in P granules, but maintain expression. In the primordial germ cells of *meg-3 meg-4* mutants, *rde-11* and *sid-1* transcripts disperse in the cytoplasm with the small RNA biogenesis machinery, become hyper-targeted by secondary sRNAs, and are eventually silenced. Silencing requires the PIWI-class Argonaute PRG-1 and the nuclear Argonaute HRDE-1 that maintains trans-generational silencing of piRNA targets. These observations support a “safe harbor” model for P granules in protecting germline transcripts from piRNA-initiated silencing.

Two parallel sRNA amplification cycles contribute to transgenerational RNAi in C. elegans

RNA-mediated interference (RNAi) is a conserved mechanism that uses small RNAs (sRNAs) to tune gene expression. In *C. elegans*, exposure to dsRNA induces the production of gene-specific sRNAs that are propagated to progeny not exposed to the dsRNA trigger. We present evidence that RNAi inheritance is mediated by two parallel sRNA amplification loops. The first loop, dependent on the nuclear Argonaute HRDE-1, targets nascent transcripts, and reduces but does not eliminate productive transcription at the locus. The second loop, dependent on the conserved helicase ZNFX-1, targets mature transcripts and concentrates them in perinuclear condensates (nuage). Each amplification loop generates a distinct class of sRNAs that perpetuate silencing into the next generation, with the ZNFX-1 loop responsible for the bulk of sRNA production. We speculate that nuage is a germline adaptation that allows for cytoplasmic transcripts to be used as templates for robust sRNA amplification in the absence of the original trigger.

Readers: Geraldine Seydoux, PhD. and John Kim, PhD.

Acknowledgements

I would like to dedicate this thesis to my past and present scientific mentors: to Dr. Caren Chang (UMD), who fostered the budding scientific interests of a naïve college freshman; to Dr. John Clay (UMD), who mentored me with incredible patience in the midst of his busy graduate work; to Dr. Michael Lichten (NIH), who helped support me in my pursuit of graduate school; to Dr. Chih-Yung Sean Lee (JHU), who taught me all the techniques I needed to succeed (and who kept me calm in the midst of strife); and of course, to Dr. Geraldine Seydoux, whose incredible mentorship shaped the very basis of my critical thought and got me excited about a life in science! I would also like to dedicate this thesis to all the members of the Seydoux lab, who have helped make my research a fun experience; particularly, to Dr. Dominique Rasolison, who always made sure I was well fed! I would like to dedicate this work to my thesis committee, Dr. John Kim, Dr. Jeff Corden, and Dr. Tatjana Trcek, for their many insightful comments and recommendations throughout the years. To soon-to-be Dr. Thao Phan, who helped me through many a tough time. To my undergraduate students, Lauren Bernard and Lucy Zhang, who did many a PCR. To Taylor Swift, whose music was the fuel for my scientific research. And last, but certainly not least, my family: Mom, Dad, Suzanne, Kathleen, William, Anna Rita, Josie, and Christina. The support and love that you have all given me has been so important in what I do. Thank you for keeping me grounded in this crazy world! XOXO

Table of Contents

Abstract ii

Acknowledgements iii

Table of Contents iv

List of Tables v

List of Figures vi

Chapter 1: Introduction..... 1

Chapter 2: P granules protect RNA interference genes from silencing by piRNAs..... 5

 Abstract.....5

 Introduction.....6

 Results.....8

 Discussion.....17

 Figures.....23

 List of tables.....48

 Methods.....49

 References.....59

Chapter 3: Two parallel sRNA amplification cycles contribute to transgenerational RNAi in C. elegans 66

 Abstract.....66

 Introduction.....67

 Results.....69

 Discussion.....76

 Figures.....84

 Methods.....116

 References.....125

Chapter 4: Conclusions and Final Remarks 137

Curriculum Vitae..... 139

List of Tables

<i>Table S1. Genes with sRNAs up in all four meg-3 meg-4 strains.</i>	<i>48</i>
<i>Table S2. Genes with sRNAs down in all four meg-3 meg-4 strains.....</i>	<i>48</i>
<i>Table S3. Genes involved in RNAi.</i>	<i>48</i>
<i>Table S4. Misregulated meg-3 meg-4 sRNAs rescued in hrde-1; meg-3 meg-4.....</i>	<i>48</i>
<i>Table S5. List of guides, repair templates, and oligos used in this study.....</i>	<i>48</i>
<i>Table S6. List of high-throughput sequencing libraries used in this study</i>	<i>48</i>

List of Figures

Chapter 2: P granules protect RNA interference genes from silencing by piRNAs

<i>Fig. 1: Segregation of P granules in wild-type and meg-3 meg-4 embryos.....</i>	<i>23</i>
<i>Fig. 2: meg-3 meg-4 mutants lose competency for RNA-interference and are defective in the production of secondary siRNAs.....</i>	<i>25</i>
<i>Fig. 3: meg-3 meg-4 mutants misregulate sRNAs that target hundreds of loci</i>	<i>28</i>
<i>Fig. 4: meg-3 meg-4 phenotypes are suppressed by loss-of-function mutations in hrde-1 and prg-1</i>	<i>30</i>
<i>Fig. 5: Localization of epigenetic factors during embryonic development in wild-type and meg-3 meg-4 mutants</i>	<i>32</i>
<i>Fig. 6: Localization of rde-11 and sid-1 transcripts in wild-type and meg-3 meg-4 primordial germ cells.....</i>	<i>34</i>
<i>Fig. 7: Model illustrating the fate of rde-11 transcripts in wild-type and meg-3 meg-4 primordial germ cells.....</i>	<i>36</i>
<i>Fig. S1: related to Fig. 2</i>	<i>38</i>
<i>Fig. S2: related to Fig. 3</i>	<i>40</i>
<i>Fig. S3: related to Fig. 4</i>	<i>42</i>
<i>Fig. S4: related to Fig. 5</i>	<i>44</i>
<i>Fig. S5: related to Fig. 6</i>	<i>46</i>

Chapter 3: Two parallel sRNA amplification cycles contribute to transgenerational RNAi in *C. elegans*

<i>Figure 1. mex-6 RNA expression in the C. elegans germline</i>	<i>84</i>
<i>Figure S1. Related to Figure 1</i>	<i>86</i>
<i>Figure 2. Evolution of mex-6 RNA during 24-hour RNAi treatment (P0 generation)</i>	<i>88</i>
<i>Figure S2. Related to Figure 2</i>	<i>90</i>
<i>Figure 3. mex-6 RNA in adult progeny (F1 generation) of animals exposed to mex-6 dsRNA..</i>	<i>92</i>
<i>Figure S3. Related to Figure 3</i>	<i>94</i>
<i>Figure 4. HRDE-1 is required for RNAi-induced changes in nascent transcripts</i>	<i>96</i>
<i>Figure S4. Related to Figure 4</i>	<i>98</i>
<i>Figure 5. ZNFX-1 is required for enrichment of RNAi-targeted transcripts in germ granules.</i>	<i>100</i>

Figure S5. Related to Figure 5 102
Figure 6. ZNFX-1 and HRDE-1 function in separate pathways contributing to transgenerational RNAi..... 104
Figure S6. Related to Figure 6 106
Figure 7. ZNFX-1 is required for pUG RNA localization to germ granules 108
Figure S7. Related to Figure 7 110
Figure S8. Related to Discussion..... 112
Figure S9. Related to Methods..... 114

Chapter 1: Introduction

First identified in *C. elegans* (Lee et al., 1993), small RNAs (sRNAs) of 20-30 nucleotides in length are now known to be universally employed across the different kingdoms of life in order to control gene expression. Working in complex with a class of proteins known as “Argonautes,” sRNAs can specifically target transcripts via RNA base-pairing and regulate mRNA levels by modulating RNA transcription, stability and/or translation (Billi et al., 2014; Carthew and Sontheimer, 2009; Hoogstrate et al., 2014). sRNAs can be derived from either exogenous or endogenous sources: introduction of exogenous double-stranded RNA (dsRNA) in cells leads to the production of sRNAs that can then target complementary transcripts for degradation (RNAi; Fire et al., 1998). Additionally, many organisms produce a multitude of genomically-encoded sRNAs, such as microRNAs (miRNAs) and Piwi-interacting RNAs (piRNAs), that participate in a variety of gene regulatory networks contributing to fertility and development through base-pairing with their targeted substrates (Bartel, 2018; Billi et al., 2014; Hoogstrate et al., 2014).

A common theme observed in sRNA biology is the amplification of sRNA responses. In the “ping-pong” sRNA amplification cycle of *Drosophila* and mammalian piRNA systems, the piRNA Argonautes have been shown to co-opt the targeted RNA substrates for the generation of new sRNAs, leading to their entry into another cycle of sRNA targeting/subsequent sRNA synthesis (Czech and Hannon, 2016a). In plants, fungi, and nematodes, sRNAs have been shown to be amplified by RNA-dependent RNA polymerases (RdRPs) that use sRNA-targeted transcripts as templates for further sRNA production (Billi et al., 2014; Martienssen and Moazed, 2015; Willmann et al., 2011). Following sRNA amplification, the newly generated sRNAs are loaded onto secondary Argonautes to allow for greater regulation of the targeted RNA (Yigit et al., 2006). In *C. elegans*, sRNAs generated directly from an exogenous dsRNA trigger (or from genomically-encoded piRNAs) have been termed “primary sRNAs;” the sRNAs produced following the primary sRNA targeting event are referred to as “secondary sRNAs.” More recently, the mechanisms of sRNA amplification have begun to be elucidated. It has been found that targeting of mRNAs by primary sRNAs, such as those derived from exogenous RNAi triggers, can lead to transcript cleavage by the endonuclease RDE-8 (Tsai et al., 2015). Following cleavage, the poly(UG)

polymerase MUT-2 has been shown to add poly-UG repeats to the 5' cleavage fragment in a process termed "pUGylation" (Shukla et al., 2020). The "pUG-tail" is sufficient to recruit RdRPs to the RNA fragment for subsequent amplification of secondary sRNAs (Shukla et al., 2020). In some cases, the production of "tertiary sRNAs" proceeds downstream of secondary sRNA targeting events (Sapetschnig et al., 2015), but this is thought to be a regulated event so as to prevent runaway sRNA amplification from inappropriately silencing transcripts with homology to others (Pak et al., 2012).

One intriguing feature of the RdRP-dependent sRNA amplification phenomenon in *C. elegans* is that sRNA-based silencing events present in the parental generation can be inherited transgenerationally (Alcazar et al., 2008; Fire et al., 1998; Grishok et al., 2000; Rechavi and Lev, 2017). The duration of silencing varies depending on the gene being targeted, but has been observed in some instances to occur upwards of ten generations (Rechavi and Lev, 2017). Key to sRNA inheritance is the secondary Argonaute HRDE-1/WAGO-9, which localizes specifically to germline nuclei (Ashe et al., 2012; Buckley et al., 2012; Shirayama et al., 2012). The current model for this nuclear RNAi pathway is as follows: following binding to a secondary sRNA, HRDE-1 can enter into the nucleus and bind to nascent transcripts (Billi et al., 2014; Weiser and Kim, 2019). The HRDE-1 complex can then induce stalling of RNA pol II and recruit downstream nuclear RNAi factors (NRDE-1/2/4) that recruit chromatin modifying enzymes that can help silencing the genomic locus (Billi et al., 2014; Weiser and Kim, 2019). This nuclear RNAi pathway has also been shown to function in the production of tertiary sRNAs (Sapetschnig et al., 2015), which is believed to help perpetuate RNAi in subsequent generations when the dsRNA trigger is absent (Rechavi and Lev, 2017; Weiser and Kim, 2019).

In addition to RNAi factors residing within the nucleus, cell biological analysis has revealed that many protein factors involved in sRNA biology also reside in liquid-like condensates within the germline, known generally as either "germ granules" or "nuage" (Dodson and Kennedy, 2020; Sundby et al., 2021). Germ granules exhibit perinuclear patterning in the adult germline but interestingly become cytoplasmically dispersed in the oocyte-to-zygote transition (Seydoux, 2018; Updike and Strome, 2010; Voronina et al., 2011; Wang and Seydoux, 2013). They later become perinuclear in the germline founder cell following cytoplasmic partitioning of germ

granule proteins into the embryonic germ cell lineage (Seydoux, 2018; Updike and Strome, 2010; Voronina et al., 2011; Wang and Seydoux, 2013). Intriguingly, the germ granules of *C. elegans* have been shown to exhibit an exquisite spatial organization in the adult germline: Argonautes, RdRPs, and other proteins required for sRNA amplification/biogenesis are assembled into distinct, adjacent germ granule sub-compartments (Sundby et al., 2021). Thus far, five distinct phases have been characterized: the P granule (Strome and Wood, 1982), Mutator foci (Phillips et al., 2012), R2 bodies (Yang et al., 2014), Z granules (Wan et al., 2018), and SIMR foci (Manage et al., 2020). Different functions have been prescribed to these perinuclear granules based on the loss-of-function phenotypes associated with genetic loss of their respective constituents. However, how and whether these functions are actually enabled by the granule properties/environment of these proteins is not known.

One speculated function of germ granules is that they serve as sites for transcript surveillance and sRNA amplification (Sundby et al., 2021; Updike and Strome, 2010; Dodson and Kennedy, 2020). It has been proposed that the collective assembly of Argonautes and sRNA biogenesis factors around the nucleus serves to catch and silence inappropriately expressed transcripts that could be deleterious for germline immortality. Such a hypothesis is rooted in the observation that many small RNA factor/germ granule component mutants exhibit sterility phenotypes (Sundby et al., 2021). However, the function of germ granules may differ depending on the developmental stage, as germ granule composition is known to change throughout the lifetime of the worm (Seydoux, 2018; Updike and Strome, 2010). In the past few years, increasing evidence has emerged that germ granules function in preserving sRNA-based transgenerational epigenetic memory, as the ability to maintain transgenerational RNAi has been shown to depend on germ granule components (Ishidate et al., 2018a; Wan et al., 2018; Xu et al., 2018). However, the precise mechanism for how this is achieved and how these granules function with respect to the nuclear RNAi pathway in order to maintain transgenerational RNAi remains unknown.

As a composite, this thesis focuses on furthering our understanding on the role of germ granules in sRNA biology. This thesis is outlined as follows:

- Chapter 2 describes how transient loss of germ granules in *C. elegans* primordial germ cells leads to disrupted sRNA homeostasis, inappropriate silencing of transcripts

- required for RNAi (*rde-11* and *sid-1*), and thus RNAi-insensitivity. We find that this aberrant transcript silencing is mediated by piRNA-dependent sRNAs and can be alleviated by loss of the piRNA Argonaute PRG-1 as well as the downstream nuclear Argonaute HRDE-1. In wild-type animals, we find that the *rde-11* and *sid-1* transcripts normally are concentrated in the germ granules of primordial germ cells. However, when these germ granules are lost (such as in the *meg-3 meg-4* mutant), these transcripts become cytoplasmically dispersed, where they become prone to silencing.
- Chapter 3 describes how exogenous RNAi leads to the initiation of two parallel amplification pathways that underly the perpetuation of transgenerational RNAi. The first cycle is the previously characterized nuclear RNAi pathway that depends upon the nuclear Argonaute HRDE-1 and targets nascent transcripts for sRNA amplification. The second cycle is a cytoplasmic pathway dependent upon the germ granule helicase ZNFX-1 that functions to maintain the continuous production of pUGylated transcripts for small RNA amplification.
 - Chapter 4 details concluding remarks.

Chapter Two: P granules protect RNA interference genes from silencing by piRNAs

Published August 08, 2019 in Developmental Cell

DOI: <https://doi.org/10.1016/j.devcel.2019.07.026>

Supplemental tables can be found online.

Authors: John Paul T. Ouyang¹, Andrew Folkmann¹, Lauren Bernard¹, Chih-Yung Lee¹, Uri Seroussi², Amanda G. Charlesworth², Julie M. Claycomb² and Geraldine Seydoux^{1,3}.

1. HHMI and Dept. of Molecular Biology and Genetics, Johns Hopkins University School of Medicine, Baltimore MD USA

2. Department of Molecular Genetics, University of Toronto, Toronto, Canada.

3. Corresponding author: gseydoux@jhmi.edu

Key Words: RNA-mediated interference, epigenetic silencing, Argonautes, P granules, piRNAs.

Abstract

P granules are perinuclear condensates in *C. elegans* germ cells proposed to serve as hubs for self/non-self RNA discrimination by Argonautes. We report that a mutant (*meg-3 meg-4*) that does not assemble P granules in primordial germ cells loses competence for RNA-interference over several generations and accumulates silencing small RNAs against hundreds of endogenous genes, including the RNA-interference genes *rde-11* and *sid-1*. In wild-type, *rde-11* and *sid-1* transcripts are heavily targeted by piRNAs, accumulate in P granules, but maintain expression. In the primordial germ cells of *meg-3 meg-4* mutants, *rde-11* and *sid-1* transcripts disperse in the cytoplasm with the small RNA biogenesis machinery, become hyper-targeted by secondary sRNAs, and are eventually silenced. Silencing requires the PIWI-class Argonaute PRG-1 and the nuclear Argonaute HRDE-1 that maintains trans-generational silencing of piRNA targets. These observations support a “safe harbor” model for P granules in protecting germline transcripts from piRNA-initiated silencing.

Introduction

In the germ cells of animals, dense RNA-protein condensates accumulate on the cytoplasmic face of the nuclear envelope. These condensates, collectively referred to as nuage, contain components of the small RNA (sRNA) machinery that scan germline transcripts for foreign sequences. For example, in *Drosophila*, components of the piRNA machinery in nuage amplify small RNAs that target transcripts from transposable elements for destruction (Huang et al., 2017). In *C. elegans*, the PIWI-class Argonaute PRG-1 associates with ~15,000 piRNAs encoded in the genome that scan most, if not all, germline mRNAs (Zhang et al., 2018; Shen et al., 2018). PRG-1 accumulates in nuage condensates called P granules that overlay nuclear pores (Batista et al., 2008; Wang and Reinke, 2008). Targeting by PRG-1/piRNA complexes recruits RNA-dependent RNA polymerases that synthesize 22 nucleotide RNAs (22G-RNAs) complementary to the targeted transcript (Lee et al., 2012; Shen et al., 2018). Synthesis of 22G-RNAs requires proteins in two other nuage condensates: Z granules (ZNF-1) and mutator foci (MUT-16) that form adjacent to P granules (Ishidate et al., 2018; Wan et al., 2018; Phillips et al., 2012; Zhang et al., 2012). 22G-RNAs in turn are bound by other Argonautes that silence gene expression, including HRDE-1, a nuclear Argonaute that generates a heritable chromatin mark that silences targeted loci for several generations (Buckley et al., 2012). Silencing by exogenous triggers, such as dsRNAs introduced by injection or feeding (exogenous RNAi), also requires 22G-RNA synthesis (Pak and Fire, 2007; Sijen et al., 2007) and HRDE-1 activity, which propagates the RNAi-induced silenced state over generations (Buckley et al., 2012).

The observation that PRG-1/piRNA complexes engage most germline transcripts suggests the existence of mechanisms that restrain PRG-1/HRDE-1 silencing activity (Zhang et al., 2018; Shen et al., 2018). One mechanism involves protection by CSR-1, an opposing Argonaute also present in P granules. CSR-1 binds to abundant 22G-RNAs that target many germline-expressed mRNAs (Seth et al., 2013; Wedeles et al., 2013). CSR-1 opposes the engagement of PRG-1/piRNA complexes (Shen et al., 2018) and is thought to license genes for germline expression (Wedeles et al., 2013; Seth et al., 2013; Cecere et al., 2014; Shen et al., 2018), although some genes are also modestly silenced by CSR-1 (Gerson-Gurwitz et al., 2016). The mechanisms that determine the balance of licensing and silencing 22G-RNAs for each germline-expressed locus are not

understood. Inheritance of piRNAs and 22G-RNAs from previous generations is likely to play a role: progeny that inherit neither piRNAs nor 22G-RNAs from their parents and that are competent to synthesize their own 22G-RNAs silence germline genes and become sterile (Phillips et al., 2015; de Albuquerque 2015). P granules could mediate the inheritance of maternal piRNAs and/or 22G-RNAs since P granules contain Argonaute proteins and are maternally inherited (Fig. 1). Segregation of Argonautes and proteins required for 22G-RNA production into distinct nuage compartments (P granules versus Z granules and mutator foci) could also play a role in sorting 22G-RNAs or limiting their production (Wan et al., 2018). A direct test of these hypotheses, however, has been difficult to obtain as complete loss of P granules causes sterility.

We previously identified a mutant that affects P granule coalescence only during embryogenesis (Wang et al., 2014). MEG-3 and MEG-4 are intrinsically-disordered proteins present in the germ plasm, a specialized cytoplasm that is partitioned with the germ lineage during early embryonic cleavages (Wang and Seydoux, 2013). MEG-3 and MEG-4 form gel-like scaffolds that recruit and stimulate the coalescence of P granule proteins in germ plasm to ensure their partitioning to the embryonic germline and the primordial germ cells Z2 and Z3 (Fig. 1; Putnam et al., 2019). In *meg-3 meg-4* embryos, P granules do not coalesce in germ plasm, causing granule components to be partitioned equally to all cells and turned over (Fig. 1; Wang et al., 2014). Despite lacking P granules during embryogenesis, *meg-3 meg-4* assemble P granules *de novo* when the primordial germ cells resume divisions in the first larval stage to generate the ~2000 germ cells that constitute the adult germline. Unlike other P granule mutants, *meg-3 meg-4* mutants are mostly fertile and can be maintained indefinitely (Wang et al., 2014).

In this study, we have examined *meg-3 meg-4* mutants for defects in small RNA (sRNA) homeostasis. We find that *meg-3 meg-4* mutants become progressively deficient in exogenous RNA-mediated interference over several generations and accumulate abnormally high levels of sRNAs that silence endogenous genes. The silenced genes belong to a class of genes that in wild-type are targeted primarily by the silencing Argonautes PRG-1 and HRDE-1, and include *rde-11* and *sid-1*, two genes required for exogenous RNAi. *rde-11* and *sid-1* transcripts are retained in P granules in wild-type, but in *meg-3 meg-4* mutants, the transcripts become dispersed in the cytoplasm with Z granules and mutator foci components. Our findings suggest a role for P

granules in protecting certain germline transcripts from run-away, trans-generational silencing initiated by piRNAs and amplified by HRDE-1-associated 22Gs.

Results

***meg-3 meg-4* mutants are defective in exogenous RNA-mediated interference**

JH3475 is a strain in which both the *meg-3* and *meg-4* open reading frames have been deleted by genome editing (Smith et al., 2016; Paix et al., 2017). This strain (*meg-3 meg-4*^{#1}) has been passed over 100 times. In the course of conducting experiments with *meg-3 meg-4*^{#1} worms, we noticed that *meg-3 meg-4*^{#1} adults appeared resistant to exogenous RNA-mediated interference. To examine this phenotype systematically, we fed *meg-3 meg-4*^{#1} hermaphrodites bacteria expressing double-stranded RNA (dsRNA) against the *pos-1* gene. *pos-1* is a maternally-expressed gene required for embryonic viability (Tabara et al., 1999). As expected, wild-type control hermaphrodites laid on average only 6.5% viable embryos after *pos-1(RNAi)* (Fig. 2A). In contrast, *meg-3 meg-4*^{#1} laid on average 76% viable embryos after *pos-1(RNAi)* (Fig. 2A). We obtained similar results by administering the double-stranded RNA by injection, and by targeting two other maternally-expressed genes required for embryogenesis (*mex-5* and *mex-6*) (Fig. 2A and S1A). Abnormal RNAi behavior of strains with loss of function mutations in *meg-3* and *meg-4* has also been reported by others (Wan et al., 2018; Lev et al., 2019).

meg-3 and *meg-4* are required maternally for the formation of P granules in embryos (Wang et al., 2014). To determine whether *meg-3* and *meg-4* were also required maternally for RNAi competence, we tested *meg-3 meg-4* homozygous hermaphrodites derived from heterozygous *meg-3 meg-4*^{#1/++} mothers (M1Z0) and *meg-3 meg-4*^{#1/++} heterozygous hermaphrodites derived from homozygous mutant mothers (M0Z1) (see Fig. S1B for crosses). We found that M1Z0 hermaphrodites had normal sensitivity to RNAi, whereas M0Z1 hermaphrodites were defective, consistent with a maternal requirement for *meg-3 meg-4* (Fig. 2A). To test this further, using genome editing (Paix et al., 2017), we regenerated the *meg-4* deletion in a line carrying the *meg-3* deletion to generate three new *meg-3 meg-4* lines (*meg-3 meg-4*^{#2}, *meg-3 meg-4*^{#3}, and *meg-3 meg-4*^{#4}). Strikingly, we found that the newly generated *meg-3 meg-4* lines remained competent for RNAi for at least five generations before beginning to exhibit resistance.

After generation six, the degree of RNAi resistance varied from generation to generation and between strains (Fig. 2B). In contrast, three sibling strains that only contained the *meg-3* deletion remained sensitive to RNAi throughout the course of the experiment (Fig. S1C). We conclude that *meg-3 meg-4* mutants exhibit a defect in RNAi that is acquired progressively over several generations.

***meg-3 meg-4* mutants exhibit reduced accumulation of secondary siRNAs triggered by *pos-1*(RNAi)**

Silencing of gene activity after ingestion of a long double-stranded RNA trigger requires production of primary sRNAs derived from the trigger, and synthesis of secondary sRNAs templated from the targeted RNA (Yigit et al., 2006; Pak and Fire, 2007; Sijen et al., 2007). To determine which step is affected in *meg-3 meg-4* mutants, we sequenced sRNAs from wild-type and *meg-3 meg-4*^{#1} adult hermaphrodites fed bacteria expressing *pos-1* dsRNA. As an additional control, we also sequenced sRNAs from *rde-11* hermaphrodites fed *pos-1* RNAi bacteria. *rde-11* mutants generate primary sRNAs but fail to generate secondary sRNAs and are defective in exogenous RNAi (Yang et al., 2012; Zhang et al., 2012). Primary and secondary sRNAs can be differentiated by the presence of a 5' monophosphate on primary sRNAs and a 5' triphosphate on secondary sRNAs (Pak and Fire, 2007; Sijen et al., 2007). Therefore, for each genotype, we prepared two types of libraries: one where the RNA was left untreated to preferentially clone primary siRNAs and one where the RNA was treated with a 5' polyphosphatase to allow the cloning of both primary and secondary sRNAs. As expected, we found that wild-type hermaphrodites accumulate many sRNAs at the *pos-1* locus that target sequences both within and outside the trigger (Fig. 2C). *rde-11* mutants in contrast accumulate fewer sRNAs at the *pos-1* locus and all of these target sequences within the trigger region, consistent with normal production of primary sRNAs and defective production of secondary sRNAs as reported previously (Fig. 2C and Zhang et al., 2012). Similar to *rde-11*, *meg-3 meg-4* mutants accumulated fewer sRNAs at the *pos-1* locus, and these sRNAs mapped primarily to the trigger (Fig. 2C). Quantification of primary sRNAs at the *pos-1* locus revealed similar levels of primary sRNAs in all genotypes (no treatment samples), and reduced overall levels of sRNAs in *rde-11* and *meg-3 meg-*

4 compared to wild-type (5' polyphosphatase-treated samples) (Fig. 2D). We conclude that, like *rde-11* mutants, *meg-3 meg-4* mutants are defective in the production of secondary sRNAs generated in response to an exogenous RNA trigger.

***meg-3 meg-4* mutants have elevated numbers of sRNAs against *rde-11* and five other genes implicated in small RNA pathways.**

MEG-3 and MEG-4 proteins are expressed primarily in embryos (Fig. S2A), and so are unlikely to have a direct role in the production of secondary sRNAs in larval and adult hermaphrodites. The generational delay in the appearance of the RNAi defective phenotype also suggests an indirect effect. To understand the origin of the RNAi defect in *meg-3 meg-4* mutants, we sequenced sRNAs in mixed populations of *meg-3 meg-4*^{#1}, *meg-3 meg-4*^{#2}, *meg-3 meg-4*^{#3}, and *meg-3 meg-4*^{#4} under normal feeding conditions (no exogenous RNAi). We considered three classes of sRNAs: piRNAs and microRNAs, which are genomically encoded, and sRNAs that are antisense to coding genes. The latter can be sub-divided further based on published lists of sRNAs immunoprecipitated with specific Argonautes (Methods). We detected all major classes of sRNAs in *meg-3 meg-4* mutants, including piRNAs, microRNAs and sRNAs mapping to loci targeted by the Argonautes WAGO-1, WAGO-4, HRDE-1, and CSR-1 (Fig. S2B; Gu et al., 2009; Xu et al., 2018, Buckley et al., 2012; Claycomb et al., 2009). All classes accumulated at levels similar to wild-type, with the exception of microRNAs which appeared slightly elevated in *meg-3 meg-4* mutants (Fig. S2B). We also compared the sRNA length distribution and 5' nucleotide preference in wild-type and *meg-3 meg-4*^{#1} sRNA libraries and found no overt differences (Fig. S2C-D).

We compared the frequency of sRNA reads at every annotated locus in the genome in *meg-3 meg-4* mutants versus wild-type. Surprisingly, we identified hundreds of loci with misregulated sRNAs (Fig. 3A and Fig. S2E-G). Combining data for all four strains, we identified 303 and 316 loci that were targeted by more or fewer sRNAs, respectively, in all four strains compared to wild-type (Tables S1-S2). Interestingly, nearly 50% of those loci have been reported to be targeted by sRNAs associated with HRDE-1 in wild-type hermaphrodites (Fig. 3B). HRDE-1-associated sRNAs target 1,208 loci in wild-type, and 25% (306) of those loci exhibit mis-regulated sRNAs in *meg-3 meg-4* mutants (Fig. 3C). In contrast, CSR-1-associated sRNAs target over 4,000

transcripts, but only 1.2% (50) of these exhibited misregulated sRNAs in *meg-3 meg-4* mutants (Fig. 3C). We conclude that *meg-3 meg-4* mutants misregulate sRNA at many loci that are primarily targeted by the silencing Argonaute HRDE-1.

We reasoned that upregulation of silencing sRNAs against loci required for RNAi could explain the RNAi defective phenotype of *meg-3 meg-4* mutants. To investigate this possibility, we cross-referenced the 303 genes with upregulated sRNAs with a list of 332 genes implicated in small RNA pathways compiled from the “gene silencing by RNA” Gene Ontology classification of WormBase WS270, Kim et al., 2005, and Tabach et al., 2013 (Table S3). This analysis identified 6 genes: *rde-11*, *sid-1*, *hda-3*, *zfp-1*, *set-23* and *wago-2*. *rde-11* codes for a RING finger domain protein required for exogenous RNAi as described above (Yang et al., 2012; Zhang et al., 2012). *sid-1* codes for a dsRNA transporter required for exogenous RNAi by feeding (Winston et al., 2002; Feinberg and Hunter 2003; Minkina and Hunter, 2017). *hda-3* and *zfp-1* are chromatin factors identified in a screen for genes required for exogenous RNAi (Kim et al., 2005). *set-23* is a predicted histone methyltransferase identified in a screen for genes that co-evolved with known RNAi factors (Tabach et al., 2013). *wago-2* is a member of the 27 Argonautes present in the *C. elegans* genome (Yigit et al., 2006) and a predicted pseudogene (WormBase WS270). sRNAs against the six genes were elevated in all four strains, but the extent of upregulation varied from strain to strain and gene to gene, with *rde-11* and *sid-1* showing the highest increase in three and one of the four strains, respectively (Fig. 3D). We reasoned that elevated sRNAs might result in downregulation of the corresponding mRNA transcript. For those analyses, we used *meg-3 meg-4*^{#1}, the oldest *meg-3 meg-4* strain with a strong RNAi-resistant phenotype. We found that expression of the six genes appeared reduced in *meg-3 meg-4*^{#1} compared to wild-type as determined by RNAseq (Fig. 3D – the difference for *zfp-1* did not score as statistically significant). The RNAseq data, however, must be interpreted cautiously since RNAseq was performed on populations of adult worms, which in the case of *meg-3 meg-4*^{#1} include ~ 30% worms lacking a germline (Wang et al., 2014), but see below for a more direct measurement of *rde-11* transcript levels. Together, these observations suggest that the RNAi defect of *meg-3 meg-4* mutants is caused by increased targeting by sRNAs (and likely lower mRNA expression) of 4 genes with a

demonstrated requirement in exogenous RNAi (*rde-11*, *sid-1*, *hda-3*, and *zfp-1*) and two genes (*set-23* and *wago-2*) with potential roles in sRNA pathways.

We also cross-referenced the sRNAs downregulated in *meg-3 meg-4* with sRNA pathway genes and identified only one gene (*haf-4*). Expression of this gene did not change significantly in *meg-3 meg-4*^{#1}. We noticed, however, that 34% of loci with downregulated sRNAs in *meg-3 meg-4* mutants also exhibited downregulated sRNAs in *rde-11* mutants (Fig. 3E). This observation suggests that downregulation of some sRNAs in *meg-3 meg-4* mutants may be an indirect consequence of reduced *rde-11* activity.

The nuclear Argonaute *hrde-1* is required for upregulation of sRNAs at the *rde-11* and *sid-1* loci in *meg-3 meg-4* mutants

Nearly 50% of the genes with misregulated sRNAs in *meg-3 meg-4* mutants (306 of 619 genes) are targeted by HRDE-1-associated sRNAs in wild-type (Fig. 3B). HRDE-1 is a nuclear Argonaute that recruits the nuclear RNAi machinery to nascent transcripts. Interestingly, we noticed that the distribution of sRNAs mapping to the *rde-11* locus in *meg-3 meg-4* mutants is consistent with silencing by the nuclear RNAi machinery. *rde-11* is transcribed as part of an operon that includes *B0564.2*, a gene immediately 3' of *rde-11*. Operons are transcribed as single, long transcripts that are broken up into shorter transcripts by trans-splicing in the nucleus before transport to the cytoplasm (Blumenthal and Gleason, 2003). In wild-type, only exons three and four of *rde-11* were targeted by sRNAs, with fewer sRNA mapping to the other exons of *rde-11* or to *B0564.2*. In contrast, in *meg-3 meg-4* mutants, all exons of both genes were heavily targeted by sRNAs (Fig. 4A and Fig. S3A). As observed for *rde-11*, *B0564.2* mRNA levels were also significantly downregulated in *meg-3 meg-4*^{#1} as determined by RNAseq (Fig. S3A). The observation that *rde-11* and *B0564.2* are co-targeted by small RNAs in *meg-3 meg-4* mutants is consistent with targeting by a nuclear Argonaute (Guang et al., 2008).

We reasoned that if HRDE-1 were required for silencing the *rde-11* operon, a loss of function mutation in *hrde-1* should block sRNA amplification against the *rde-11* and *B0564.2* loci and restore transcripts levels back to wild-type. To test this, we crossed *meg-3 meg-4* hermaphrodites with males carrying a mutation in *hrde-1* to generate the triple mutant *hrde-1*;

meg-3 meg-4 (see Fig. S3B for crosses). Consistent with our hypothesis, we observed lower levels of sRNAs against the *rde-11* and *B0564. 2* transcripts in *hrde-1; meg-3 meg-4* compared to *meg-3 meg-4* (Fig. 4A). sRNAs against *sid-1*, were also significantly reduced (Fig. S3C), whereas sRNAs against the other sRNA pathway genes (*wago-2*, *hda-3*, *set-23*, and *zfp-1*) did not show changes that reached statistical significance (Fig. S3C). Of the 303 transcripts with upregulated sRNAs in *meg-3 meg-4* mutants, only 39 were partially rescued (lowered) in *hrde-1; meg-3 meg-4* (Table S4). Although this analysis is likely to be complicated by sRNA defects inherent to loss of *hrde-1* activity, we conclude that *hrde-1* is responsible for some, but not all, of the upregulation of sRNAs in *meg-3 meg-4* mutants. Other Argonautes that overlap in function with HRDE-1 may be responsible for the remainder (Shirayama et al., 2012; Gu et al., 2009).

***rde-11* and *sid-1* are engaged by PRG-1-piRNA complexes and not by CSR-1-sRNA complexes**

HRDE-1 has been shown to act downstream of the piRNA Argonaute PRG-1 to perpetuate a sRNA epigenetic memory (Ashe et al., 2012; Shirayama et al., 2012). Using previously published Cross Linking and Selection of Hybrids (CLASH) data (Shen et al., 2018), we assigned a rank to each protein coding gene based on degree of targeting by PRG-1/piRNA complexes. We found that *rde-11* and *sid-1* rank among the top 50 genes in the genome most targeted by PRG-1/piRNAs complexes (average rank among coding genes across two CLASH replicates: #15 for *rde-11*, #33 for *sid-1*). 123 unique piRNA sites were identified in the *rde-11* transcript and 75 in the *sid-1* transcript (Shen et al., 2018). Consistent with targeting by piRNAs, sRNAs targeting *rde-11* and *sid-1* were reduced in *prg-1* mutants as compared to wild-type whereas *rde-11* and *sid-1* mRNA levels were increased in *prg-1* mutants (Lee et al., 2012; Shen et al., 2018; McMurchy et al., 2017, Fig. S3D-E). Silencing of endogenous genes by PRG-1 is countered by the Argonaute CSR-1, which licenses germline genes for expression (Wedeles et al., 2013; Seth et al., 2013; Cecere et al., 2014; Shen et al., 2018). Interestingly, a published list of sRNAs that co-immunoprecipitate with CSR-1 did not contain sRNAs against *rde-11* or *sid-1* (Claycomb et al., 2009). In fact, as noted above, more than 90% of loci with misregulated sRNAs in *meg-3 meg-4* mutants do not appear to be targeted by CSR-1-associated sRNAs (Fig. 3B). These observations suggest that misregulated genes in *meg-3 meg-4* mutants may be in a “sensitized” state in wild-

type: hyper-targeted by silencing PRG-1/piRNA complexes and hypo-targeted by protective CSR-1/sRNA complexes.

PRG-1 and HRDE-1 are required for *rde-11* silencing and for the RNAi-defective phenotype of *meg-3 meg-4* mutants

We reasoned that if PRG-1 and HRDE-1 are responsible for the hyper-targeting of loci required for exogenous RNAi in *meg-3 meg-4* mutants, loss of function mutations in *prg-1* and *hrde-1* should restore competence for exogenous RNAi to *meg-3 meg-4* mutants. As predicted, we found that, unlike *meg-3 meg-4* mutants, *hrde-1; meg-3 meg-4* and *prg-1; meg-3 meg-4* mutants were competent for RNAi (Fig. 4B; see Fig. S3F for cross). In contrast, mutations in a different Argonaute WAGO-4 did not suppress the *meg-3 meg-4* phenotype (Fig. 4B; see Fig. S3F for cross). CSR-1 mutants are sterile and so could not be tested in this assay (Yigit et al., 2006; Claycomb et al., 2009). ZNFX-1 is a conserved helicase required for sRNA amplification (Ishidate et al., 2018; Wan et al., 2018). We found that *znfx-1; meg-3 meg-4* worms were competent for RNAi, suggesting that ZNFX-1, like PRG-1 and HRDE-1, is required for hypertargeting of RNAi loci in *meg-3 meg-4* mutants (Fig 4B; see Fig. S3F for cross).

To examine whether *rde-11* expression is restored in *meg-3 meg-4* mutants that also lack *prg-1* or *hrde-1*, we used single-molecule fluorescent *in situ* hybridization to directly measure *rde-11* transcript levels in adult germlines. We focused on *rde-11* since that locus showed the greatest reduction in mRNA level in a population of *meg-3 meg-4*^{#1} adults (Fig. 3B). We found that, as expected, *rde-11* is expressed robustly in wild-type germlines and at much lower levels in *meg-3 meg-4*^{#1} germlines (Fig. 4C and Fig. S3G). Remarkably, wild-type levels of *rde-11* transcripts were restored in *hrde-1; meg-3 meg-4* and *prg-1; meg-3 meg-4* germlines (Fig. 4C and Fig. S3G). We conclude that PRG-1 and HRDE-1 are required for silencing of the *rde-11* locus in *meg-3 meg-4* adult germlines.

P granule proteins, including PRG-1, fail to coalesce into granules in *meg-3 meg-4* embryos

Previous studies using the P granule marker PGL-1 showed that P granules assemble normally post-embryogenesis in *meg-3 meg-4* germlines (Wang et al., 2014). We verified this

observation and confirmed that formation of Z granules and mutator foci was also unaffected in adult *meg-3 meg-4* germlines (Fig. S4A-B, Wan et al., 2018). Additionally, PRG-1 and CSR-1 protein levels appeared unchanged in *meg-3 meg-4* adults compared to wild-type as determined by western analyses (Fig. S4C). Silencing of the *rde-11* locus in adult germlines, therefore, is unlikely to be due to gross defects in nuage organization at this stage.

During the oocyte-to-embryo transition, the canonical P granule component PGL-1 relocates from the nuclear periphery to cytoplasmic granules that are asymmetrically partitioned to the embryonic germ lineage during the first embryonic cleavages (Strome and Wood, 1982). Whether other nuage components behave similarly has not yet been reported systematically. Using fluorescently-tagged alleles generated by genome editing, we compared the distribution of PRG-1, CSR-1, ZNFX-1, and MUT-16 to that of PGL-1 (Fig. 5A; Methods, Shen et al., 2018, Wan et al., 2018). We found that like PGL-1, PRG-1 and ZNFX-1 localize to granules that segregate preferentially with the germ lineage during early cleavages (also see Wan et al., 2018). CSR-1 exhibited a similar pattern, except that CSR-1 granules did not appear as strongly asymmetrically segregated (Fig 5A). Around the 28-cell stage, PGL-1 becomes concentrated in autophagic bodies in somatic cells and is turned over (Zhang et al., 2009). We observed a similar pattern of turnover for PRG-1, CSR-1 and ZNFX-1 in somatic lineages. By comma-stage, PGL-1, PRG-1, CSR-1 and ZNFX-1 could only be detected in the primordial germ cells Z2 and Z3 (Fig. 5A).

In *meg-3 meg-4* embryos, PGL-1, PRG-1, CSR-1 and ZNFX-1 granules were segregated evenly to all cells and turned over in somatic cells after the 28-cell stage (Fig. 5B). Consistent with failed preferential segregation to the germ lineage, by mid-embryogenesis (comma-stage), PGL-1, PRG-1, and ZNFX-1 levels were severely reduced in *meg-3 meg-4* compared to wild-type (Fig. 5B). In contrast, CSR-1 levels appear comparable to wild-type. At this stage, in wild-type, PGL-1, PRG-1, ZNFX-1 and CSR-1 are concentrated in granules around the nuclei of Z2 and Z3 (Fig. 5A). In contrast, in *meg-3 meg-4* mutants, these proteins were mostly cytoplasmic in Z2 and Z3 forming only rare puncta, with the exception of PGL-1 which formed many small cytoplasmic puncta (Fig. 5B).

Unlike P granule-associated proteins, the mutator foci protein MUT-16 was segregated uniformly to all cells of early wild-type embryos, and remained as an abundant cytoplasmic

protein in most cells throughout embryogenesis. Bright perinuclear MUT-16 puncta could be observed in many cells, including Z2 and Z3. This pattern was not disrupted significantly in *meg-3 meg-4* mutants (Fig. 5B).

Finally, we also examined the embryonic distribution of HRDE-1, using a GFP-tagged allele (Methods). HRDE-1 was present in all cells in early embryos and became restricted to the germline founder cell P₄ by the 28-cell stage by an unknown mechanism. This pattern was not disrupted in *meg-3 meg-4* embryos. In comma-stage embryos, HRDE-1 was present exclusively in Z2 and Z3 in both wild-type and *meg-3 meg-4* mutants (Fig. 5A-B). The only observed difference was that the nuclear-to-cytoplasm ratio of HRDE-1 was higher in *meg-3 meg-4* primordial germ cells compared to wild-type (Fig. 5A-B and S4G-H). No such difference was seen when comparing HRDE-1 in oocytes of *meg-3 meg-4* and wild-type hermaphrodites (Fig. S4G-H). Intriguingly, increased nuclear-to-cytoplasm ratio has been correlated with 22G-RNA loading for the somatic nuclear Argonaute, NRDE-3 (Guang et al., 2008).

In summary, we find that primordial germ cells in *meg-3 meg-4* mutants maintain mutator foci and nuclear HRDE-1, but fail to assemble perinuclear P and Z granules. P (PRG-1, CSR-1, PGL-1) and Z (ZNF-1) granule proteins are still present in these cells, but are dispersed throughout the cytoplasm.

***rde-11* and *sid-1* transcripts are transcribed and accumulate in P granules in wild-type, but not *meg-3 meg-4* primordial germ cells**

The dramatic nuage assembly defect in *meg-3 meg-4* embryos led us to investigate whether *rde-11* and *sid-1* might be expressed in Z2 and Z3 during embryogenesis. We performed fluorescent *in situ* hybridization for *rde-11* and *sid-1* on wild-type embryos expressing GFP::PRG-1. Consistent with expression in the adult maternal germline, we detected cytoplasmic *rde-11* and *sid-1* transcripts in early embryos (Fig. S5). In comma-stage embryos, we observed scattered single *sid-1* and *rde-11* transcripts in somatic cells and clusters of *rde-11* and *sid-1* transcripts in Z2 and Z3 (Fig. S5). The clusters overlapped with perinuclear granules positive for GFP::PRG-1 (Fig. 6A). We also detected a few transcripts in the cytoplasm away from GFP::PRG-1 granules, but these were a minority (Fig. 6B). Consistent with zygotic transcription at this stage, we

detected nuclear signal in 9 of 14 comma-stage embryos examined for *rde-11* expression and 4 of 5 comma-stage embryos examined for *sid-1* expression. These observations suggest that *rde-11* and *sid-1* are transcribed in Z2 and Z3 during embryogenesis and accumulate in P granules with PRG-1.

Next, we examined *rde-11* and *sid-1* transcripts in *gfp::prg-1; meg-3 meg-4* embryos. *meg-3 meg-4* primordial germ cells accumulated fewer *rde-11* and *sid-1* transcripts compared to wild-type (Fig. 6A, C). We detected nuclear transcripts in 3 of 8 embryos examined for *rde-11* expression and 3 of 8 embryos examined for *sid-1* expression. Consistent with the fact that PRG-1 forms fewer and smaller granules in *meg-3 meg-4* mutants, a smaller proportion of cytoplasmic *rde-11* and *sid-1* transcripts were enriched in granules compared to wild-type and most transcripts were dispersed in the cytoplasm (Fig. 6A and B). We conclude that *rde-11* and *sid-1* loci are also transcribed in *meg-3 meg-4* primordial germ cells, albeit at a potentially lower efficiency compared to wild-type. *rde-11* and *sid-1* transcripts accumulate with PRG-1 in P granules in wild-type primordial germ cells, but not in *meg-3 meg-4* where they disperse with PRG-1 in the cytoplasm.

DISCUSSION

In this study, we take advantage of a mutant deficient in nuage coalescence during embryogenesis to examine the function of nuage compartments in regulating endogenous gene expression. We find that *meg-3 meg-4* mutants become RNAi-deficient over several generations and that this phenotype requires PRG-1 and HRDE-1 activities. *meg-3 meg-4* mutants upregulate sRNAs against ~300 loci, including four genes required for exogenous RNAi (*rde-11*, *sid-1*, *hda-3*, *zfp-1*) and two genes implicated in sRNA pathways (*wago-2* and *set-23*). The genes with upregulated sRNAs in *meg-3 meg-4* mutants belong to a unique class of loci that are targeted by PRG-1-piRNA and HRDE-1-sRNA complexes, and not targeted by CSR-1-sRNA complexes. *rde-11* and *sid-1* transcripts are expressed in primordial germ cells where they accumulate in perinuclear P granules in wild-type, but not in *meg-3 meg-4* mutants where the transcripts scatter in the cytoplasm mixing with other dispersed nuage components. Together, these observations suggest

that coalescence of nuage into distinct condensates restrains 22G-RNA amplification initiated by piRNAs, especially at loci required for exogenous RNAi.

Maternal inheritance of P granules is not essential for inheritance of epigenetic traits

In *Drosophila*, maternally-deposited piRNAs defend progeny against active transposable elements (Brennecke et al., 2008). Similarly, in *C. elegans*, maternal piRNAs are required to restore transposon silencing and the proper balance of 22G-RNAs in animals that do not inherit 22G-RNAs from their parents (Phillips et al., 2015; de Albuquerque 2015). How piRNAs and other sRNAs are transmitted from germline to germline across generations is not known. In principle, P granules (and their equivalent in *Drosophila*, the polar granules) are ideal conduits, since P granules concentrate Argonaute proteins and are actively partitioned to the embryonic germline during early embryonic cleavages. Our observations with *meg-3 meg-4* mutants, which break the cycle of maternal P granule inheritance, however, challenge this hypothesis. First, the fact that most germline genes are expressed normally in *meg-3 meg-4* mutants demonstrates that maternal inheritance of P granules is not essential to license most germline gene expression. Second, *meg-3 meg-4* become RNAi defective only after several generations, consistent with transmission of an epigenetic signal that is amplified over generational time. Finally, the RNAi-defective phenotype of *meg-3 meg-4* mutants is inherited maternally, providing direct evidence for epigenetic inheritance in the absence of embryonic P granules. We conclude that P granules are not essential to deliver epigenetic signals to the next generation. This conclusion does not exclude the possibility that some epigenetic signals may rely on embryonic P granules for maximal transmission (such as PRG-1/piRNAs complexes, see below).

The nuclear Argonaute HRDE-1 is likely to be the conduit for at least part of the epigenetic inheritance we observe in *meg-3 meg-4* mutants. HRDE-1 is required for the RNA-interference defect of *meg-3 meg-4* mutants. Nuclear HRDE-1 segregates with the embryonic germ line and this distribution was not affected in *meg-3 meg-4* mutants. CSR-1 and PRG-1 could also be detected in the cytoplasm of *meg-3 meg-4* primordial germ cells, despite not being in perinuclear condensates. These observations suggest that at least some of the maternal pool of Argonautes present in zygotes segregates with the embryonic germ lineage independent of P

granules. In zygotes, the polarity regulators PAR-1 and MEX-5 collaborate to drive asymmetric segregation of germ plasm (a collection of maternally-inherited RNA-binding proteins) to the germline founder cell P₄ (Schubert et al., 2000; Folkmann and Seydoux, 2019). It will be important to investigate the mechanisms that segregate HRDE-1 and other Argonautes to the embryonic germline and ensure transmission of epigenetic signals from one generation to the next.

P granules protect *rde-11* and *sid-1* from PRG-1/HRDE-1-driven silencing

Several lines of evidence suggest that the RNAi deficient phenotype of *meg-3 meg-4* is due to silencing of genes required for exogenous RNAi, in particular *rde-11* and *sid-1*. First, like *rde-11* mutants (Zhang et al., 2012), *meg-3 meg-4* mutants exhibit both reduced production of secondary sRNAs in response to an exogenous trigger and reduced levels of endogenous sRNAs at 108 loci also affected in *rde-11* mutants. Second, like *sid-1* mutants (Wang and Hunter, 2017), *meg-3 meg-4* mutants are partially resistant not only to dsRNA introduced by feeding but also to dsRNA introduced by injection. Third, sRNAs mapping to the *rde-11* and *sid-1* loci were elevated in four independent *meg-3 meg-4* lines, and both transcripts were reduced in the original *meg-3 meg-4* line. Fourth, loss of *hrde-1* in *meg-3 meg-4* restored both competence for RNAi and *rde-11* transcript levels in adult gonads. Although silencing of *rde-11* and *sid-1* are likely to be the main drivers of the *meg-3 meg-4* RNAi-defective phenotype, they may not be the only contributors. sRNAs against two other genes required for RNAi (*hda-3* and *zfp-1*) and two genes implicated in sRNA pathways (*wago-2* and *set-23*) were also elevated in *meg-3 meg-4* strains. To what extent silencing of these and other genes additionally contributes to the *meg-3 meg-4* RNAi-defective phenotype remains to be determined.

Of the thousands of genes expressed in germ cells, what makes *rde-11* and *sid-1* so prone to silencing in *meg-3 meg-4* mutants? Examination of recent transcriptome-wide data for PRG-1/piRNA engagement on endogenous transcripts revealed that *rde-11* and *sid-1* are among the top 50 most targeted messages in the entire *C. elegans* transcriptome (Shen et al., 2018). In contrast, *rde-11* and *sid-1* do not appear to be targeted by sRNAs associated with the protective Argonaute CSR-1. This combination of excessive targeting by PRG-1 and hypo-targeting by CSR-1

may be a contributing factor for why *rde-11* and *sid-1* are selectively silenced in *meg-3 meg-4* mutants.

Another characteristic of *rde-11* and *sid-1* is that they are expressed in primordial germ cells during embryogenesis. Only three other genes so far have been documented to be transcribed in primordial germ cells before hatching (Subramaniam and Seydoux, 1999; Kawasaki et al., 1998; Mainpal et al., 2015), which has been described as a period of low transcriptional activity for the germline (Schaner et al., 2003). This is also precisely the developmental period during which *meg-3 meg-4* mutants lack P granules, suggesting that expression in the absence of P granules is what triggers silencing of *rde-11* and *sid-1* in *meg-3 meg-4* mutants.

We propose the following model (Fig. 7). In wild-type, upon emergence from the nucleus, *rde-11* and *sid-1* transcripts accumulate in P granules where they associate with PRG-1/piRNA complexes. Transcript retention in P granules limits their use as templates for 22G-RNA synthesis in Z granules and mutator foci. Consequently, only a moderate number of HRDE-1-associated 22Gs accumulate against *rde-11* and *sid-1* in wild-type, allowing the loci to remain expressed. In contrast, in *meg-3 meg-4* mutants, *rde-11* and *sid-1* transcripts are released directly in the cytoplasm where they are free to mix with dispersed nuage components. 22G-RNA synthesis is accelerated, causing HRDE-1 to become hyper-loaded with sRNAs against *rde-11* and *sid-1*, enter the nucleus and silence the *rde-11* and *sid-1* loci. The observed increase in HRDE-1 nuclear-to-cytoplasmic ratio in *meg-3 meg-4* primordial germ cells is suggestive of elevated HRDE-1 nuclear activity.

It may appear counterintuitive that *rde-11* and *sid-1* transcripts experience an increase in PRG-1-driven silencing, given that PRG-1 levels are much lower overall in *meg-3 meg-4* primordial germ cells compared to wild-type (Fig. 5). In certain genetic contexts, maternal inheritance of PRG-1 has been shown to *protect* germline mRNAs from silencing by preventing misrouting of 22G-RNAs into silencing Argonaute complexes (Phillips et al., 2015). One possibility is that targeting by PRG-1/piRNA complexes in the context of the P granule environment marks transcripts for potential silencing but also protects them from mutator activity in the cytoplasm by retaining most transcripts in granules. In the absence of P granules, however, the protective influence of PRG-1/piRNA complexes is lost and transcripts are free to engage with the sRNA

amplification machinery in the cytoplasm. The low levels of PRG-1 in *meg-3 meg-4* primordial germ cells may explain why several rounds of cytoplasmic exposure (generations) are needed before sufficiently high numbers of HRDE-1/sRNA complexes are generated to silence the RNAi genes.

In this edition of *Developmental Cell*, another study describing the non-Mendelian inheritance of the *meg-3 meg-4* mutant's RNAi-insensitive phenotype was also published (Dodson and Kennedy, 2019). There, they similarly showed that newly generated *meg-3 meg-4* mutants exhibit a transgenerationally lagged acquisition of RNAi-insensitivity (Dodson and Kennedy, 2019). Additionally, they demonstrated that the wild-type decedents of RNAi-insensitive *meg-3 meg-4* hermaphrodites that have been mated to wild-type males strikingly remain insensitive for 9-11 generations (Dodson and Kennedy, 2019). Similar to what was described in this study, they found that the *meg-3 meg-4* RNAi insensitive phenotype was dependent upon the nuclear Argonaute HRDE-1 and that the RNAi-insensitivity of *meg-3 meg-4* worms correlates with sRNA upregulation against the RNAi genes *sid-1* and *rde-11* (Dodson and Kennedy, 2019). We find that this study further strengthens the findings of our paper.

A mechanism for fine tuning the RNA-interference machinery?

piRNAs are genomically-encoded so presumably the heavy targeting of *rde-11* and *sid-1* is beneficial to *C. elegans*. The ability to mount an RNAi response in *C. elegans* has been reported to be tunable across generations (Houry-Ze'evi et al., 2016). Transgenerational duration of an RNAi response to a primary dsRNA trigger is extended when progeny are exposed to an unrelated second dsRNA trigger. Furthermore, exposure to dsRNA changes the level of sRNAs that target genes in the RNA-interference machinery, including *rde-11* and *sid-1* and many others (Houry-Ze'evi et al., 2016). Small changes in temperature have also been shown to affect piRNA biogenesis leading to changes in gene expression in subsequent generations (Belicard et al., 2018). These observations suggest that environmental influences can modulate the potency and specificity of the sRNA machinery. We suggest that this modulation is achieved in part by piRNA-targeting and sequestration in P granules of transcripts coding for epigenetic factors, such as *rde-11* and *sid-1*. An exciting possibility is that P granules modulate the rate of delivery of piRNA-

targeted transcripts to mutator foci as a function of maternal experience and this process begins as soon as transcription initiates in the primordial germ cells. In this way, embryos could integrate ancestral inputs to fine-tune their own epigenetic machinery before hatching and taking their first meal.

Acknowledgments

We thank the Johns Hopkins Neuroscience Research Multiphoton Imaging Core (NS050274) and the Johns Hopkins Integrated Imaging Center (S10OD023548) for excellent microscopy support. We thank the Phillips and Mello labs for strains, the Mello lab for help with analyzing CLASH data, the Miska lab for guidance with sRNAseq, Anne Dodson and Scott Kennedy for sharing data before publication, and Charlotte Choi, Anne Dodson, Scott Kennedy, John Kim, Craig Mello, Eric Miska, the Baltimore Worm Club and the Seydoux lab for many helpful discussions. JPTO thanks Taylor Swift for inspiration. JPTO was supported by the JHU SOM Biochemistry, Cellular, and Molecular Biology NIH training grant (T32 GM007445). GS is an investigator of the Howard Hughes Institute.

Author Contributions

JPTO, AWF, LB conducted the experiments; JPTO, AWF, LB, CYL and GS analyzed the data; US, AGC, and JMC constructed the GFP::CSR-1 and GFP::HRDE-1 strains, JPTO and GS designed the experiments and wrote the paper.

Declaration of Interests

G.S. serves on the Scientific Advisory Board of Dewpoint Therapeutics, Inc.

Figure 1

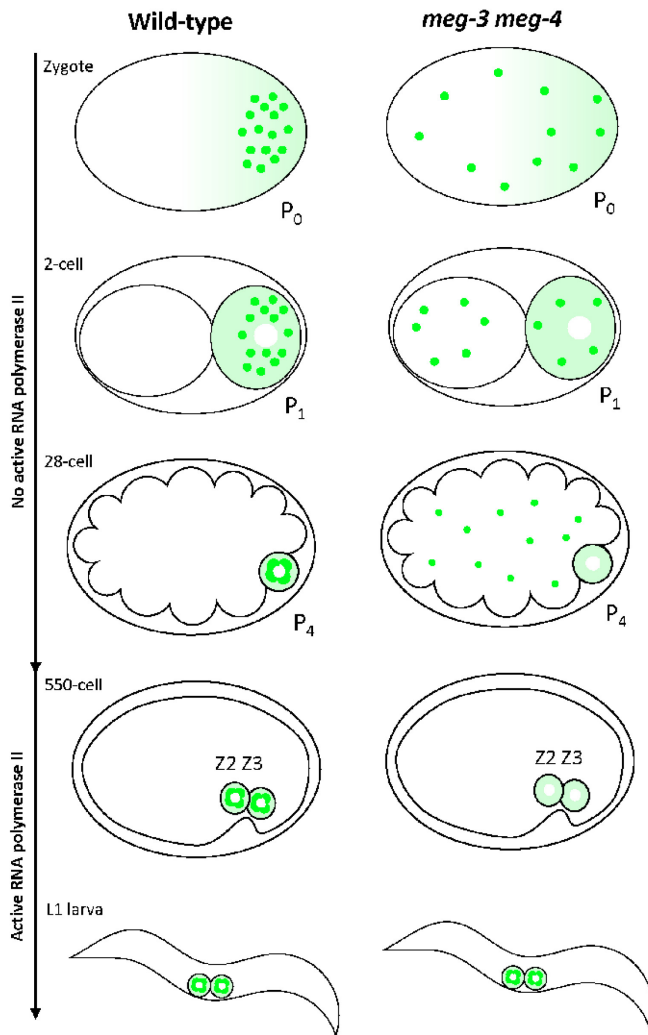
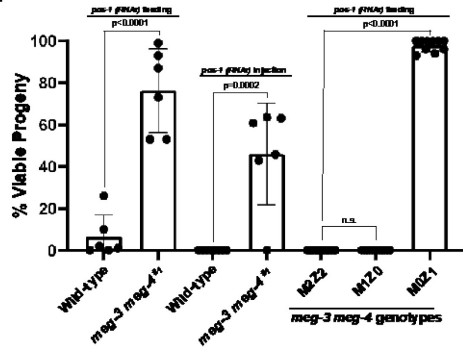


Fig. 1: Segregation of P granules in wild-type and *meg-3 meg-4* embryos

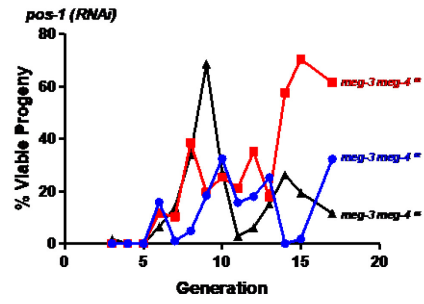
Schematics of *C. elegans* embryos at successive stages of development from the 1-cell zygote to the first larval stage post hatching. RNA polymerase II activity is repressed in the P lineage until gastrulation when P₄ divides to generate Z2 and Z3. In wild-type, P granules (green dots) are segregated preferentially with the germ plasm (lighter green color) to the P lineage that gives rise the primordial germ cells Z2 and Z3. In *meg-3 meg-4* mutants, P granules are partitioned to all cells and are eventually dissolved/turned over. Germ plasm, however, segregates normally in *meg-3 meg-4* mutants. Despite lacking maternal P granules, *meg-3 meg-4* mutants assemble perinuclear P granules *de novo* during late embryogenesis and into the first larval stage (Wang et al., 2014).

Figure 2

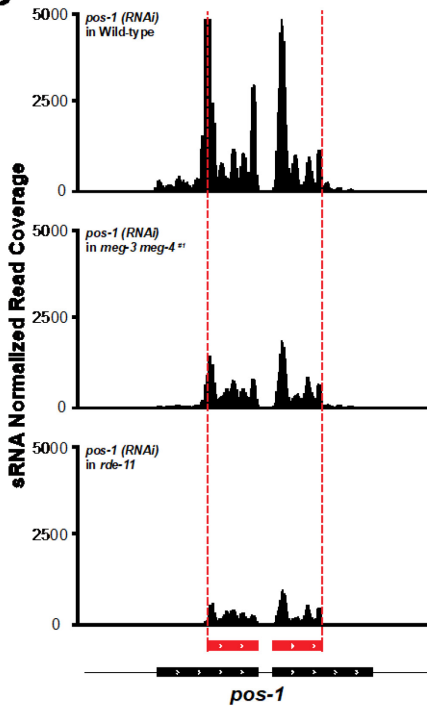
A



B



C



D

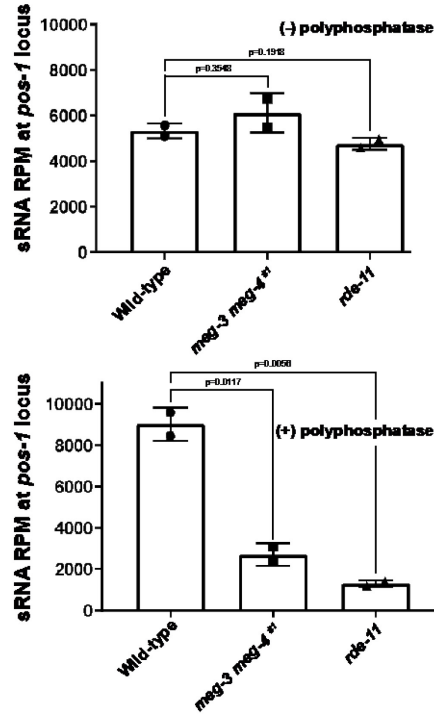


Fig. 2: *meg-3 meg-4* mutants lose competency for RNA-interference and are defective in the production of secondary siRNAs.

A. Graph showing the percentage of viable embryos laid by hermaphrodites of the indicated genotypes upon treatment with *pos-1* dsRNA. First two bars depict the embryonic viability from populations of ~20 hermaphrodites fed starting at the L1 stage (each dot represents an experiment performed on a distinct population). On average, roughly 200 embryos were scored per RNAi experiment. The following two bars represent the percent viable progeny of mothers ~16 hours following injection with 200 ng/uL of *pos-1* dsRNA (each dot represents the progeny of a single injected young adult hermaphrodite that laid more than 15 embryos). The last three bars represent viable progeny from M2Z2, M1Z0, and M0Z1 hermaphrodites fed starting at the L4 stage (each dot represents the progeny of a single hermaphrodite that laid more than 15 embryos). The “M” and “Z” designations refer to the number of wild-type *meg-3 meg-4* alleles present in the mother (M) or hermaphrodite (Z) tested for RNAi. Bar height represents the mean; error bars represent the standard deviation. P-values were calculated using an unpaired t-test.

B. Graph showing the percentage of viable embryos among broods (~12 mothers) laid by newly generated *meg-3 meg-4* hermaphrodites fed with bacteria expressing *pos-1* dsRNA (from L4 stage). Three independently derived strains are shown. “Generation” refers to the number of generations since the *meg-4* gene was deleted by genome editing in the starting strain carrying only a *meg-3* deletion. See Fig. S1C for RNAi sensitivity of three sibling strains carrying only the original *meg-3* deletion. See Fig. S1D for CRISPR breeding scheme.

C. Genome browser view of sRNA reads mapping to the *pos-1* locus in adult hermaphrodites of indicated genotypes fed with bacteria expressing a dsRNA trigger (red in figure) against a central region of the *pos-1* locus.

D. Graphs showing the abundance of sRNA reads mapping to the *pos-1* locus in adult hermaphrodites of the indicated genotypes fed *pos-1* RNAi. The upper panel shows primary sRNAs (directly derived from the ingested trigger), the bottom graph shows all sRNAs (both primary and secondary) from phosphatase treated library samples. Bar height represents the

mean; error bars represent the standard deviation; p-values were calculated using an unpaired t-test.

Figure 3

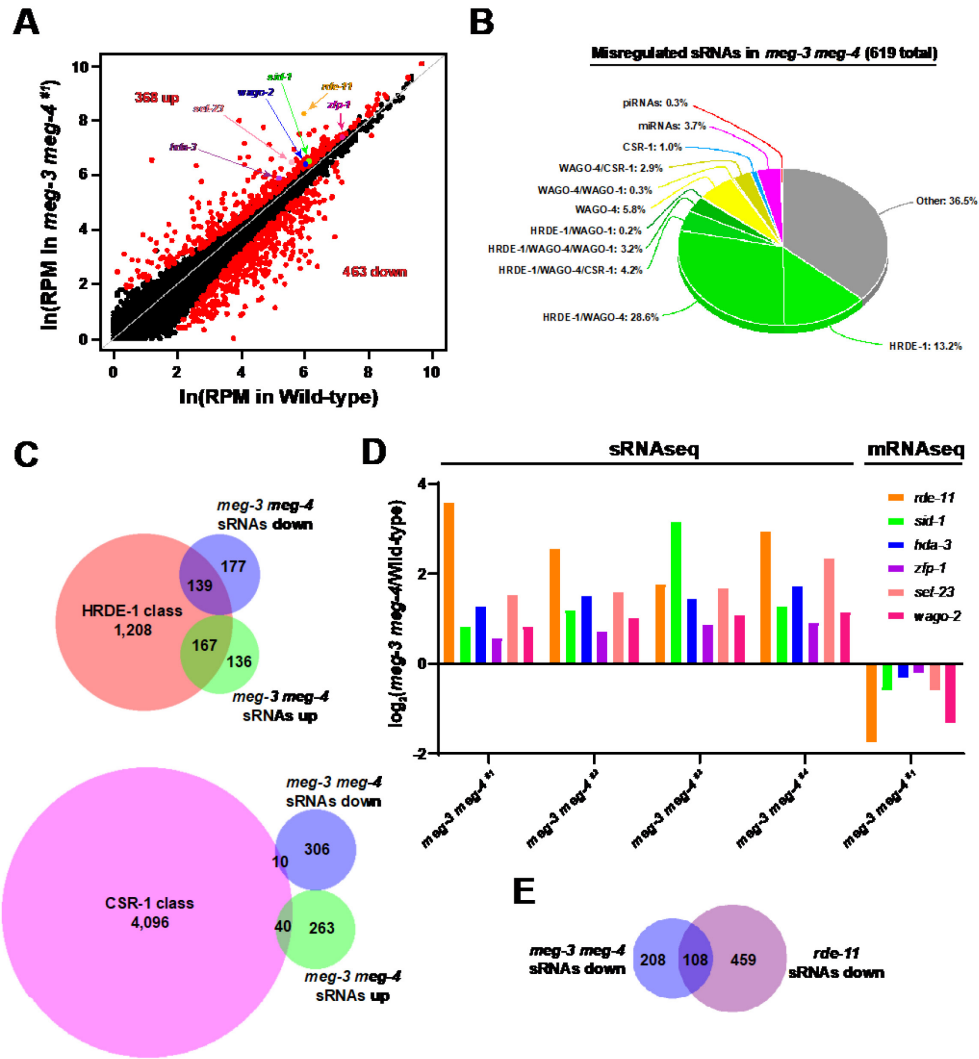


Fig. 3: *meg-3 meg-4* mutants misregulate sRNAs that target hundreds of loci.

A. Scatter plot comparing sRNA abundance in wild-type (X-axis) and *meg-3 meg-4*^{#1} (Y-axis) hermaphrodites. Each dot represents an annotated locus in the *C. elegans* genome. Red dots represent loci with significantly upregulated or downregulated sRNAs comparing two biological replicates each for wild-type and *meg-3 meg-4*^{#1}.

B. Pie chart showing the 619 genes with misregulated sRNAs in *meg-3 meg-4* strains categorized according to the type of sRNAs that target these genes in wild-type. Note that 49.4% of these sRNAs are classified as HRDE-1-associated (Buckley et al., 2012).

C. Venn diagrams showing the overlap between loci with upregulated or downregulated sRNAs in *meg-3 meg-4* mutants and loci targeted by sRNAs that co-immunoprecipitate with HRDE-1 and CSR-1 (Buckley et al., 2012; Claycomb et al., 2009).

D. Bar graph showing the average log₂ fold difference in sRNA abundance for the indicated loci in the four *meg-3 meg-4* strains compared to wild-type. The log₂ fold change represents the average of two biological replicates for each genotype. Last grouping shows the mRNA abundance for each gene in the *meg-3 meg-4*^{#1} adults as determined by RNAseq from two biological replicates.

E. Venn diagrams showing the overlap between loci with downregulated sRNAs in *meg-3 meg-4* mutants and loci with downregulated sRNAs in *rde-11* mutants.

Figure 4

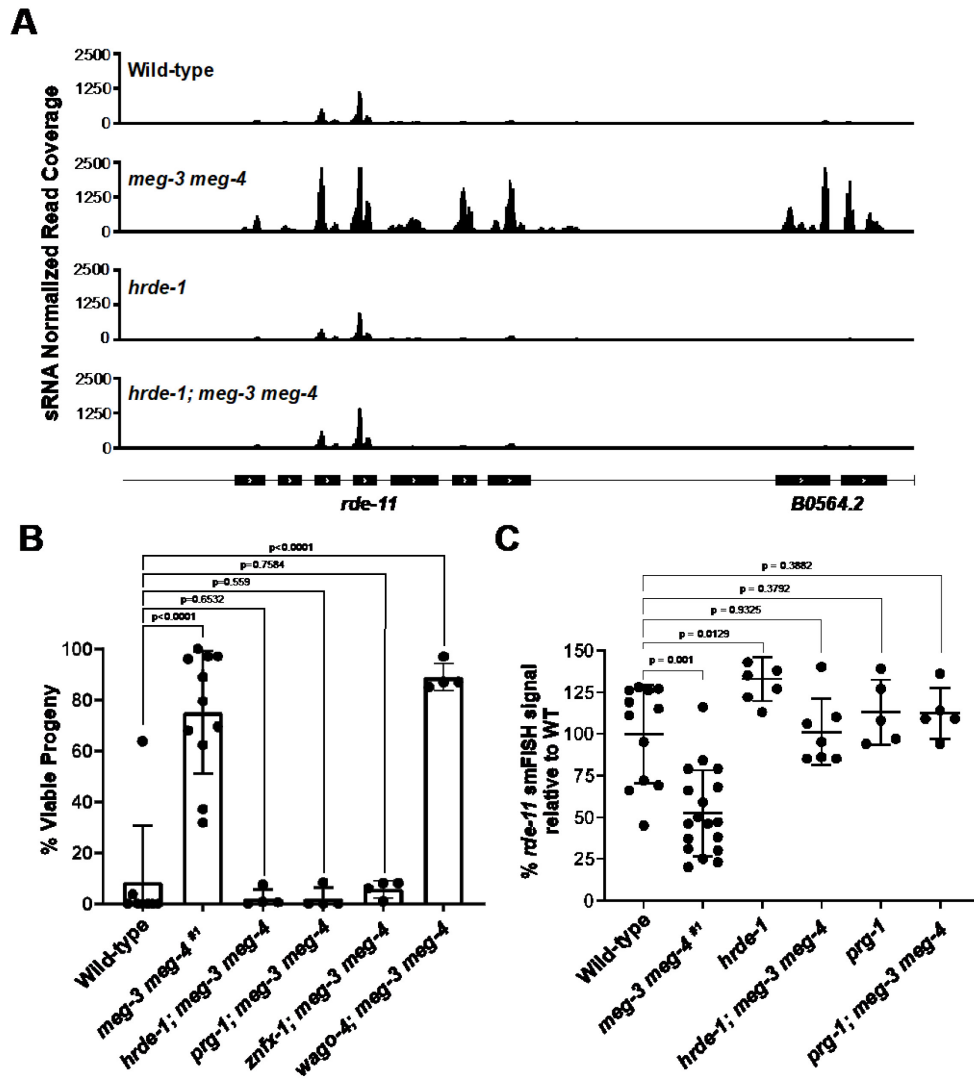


Fig. 4: *meg-3 meg-4* phenotypes are suppressed by loss-of-function mutations in *hrde-1* and *prg-1*

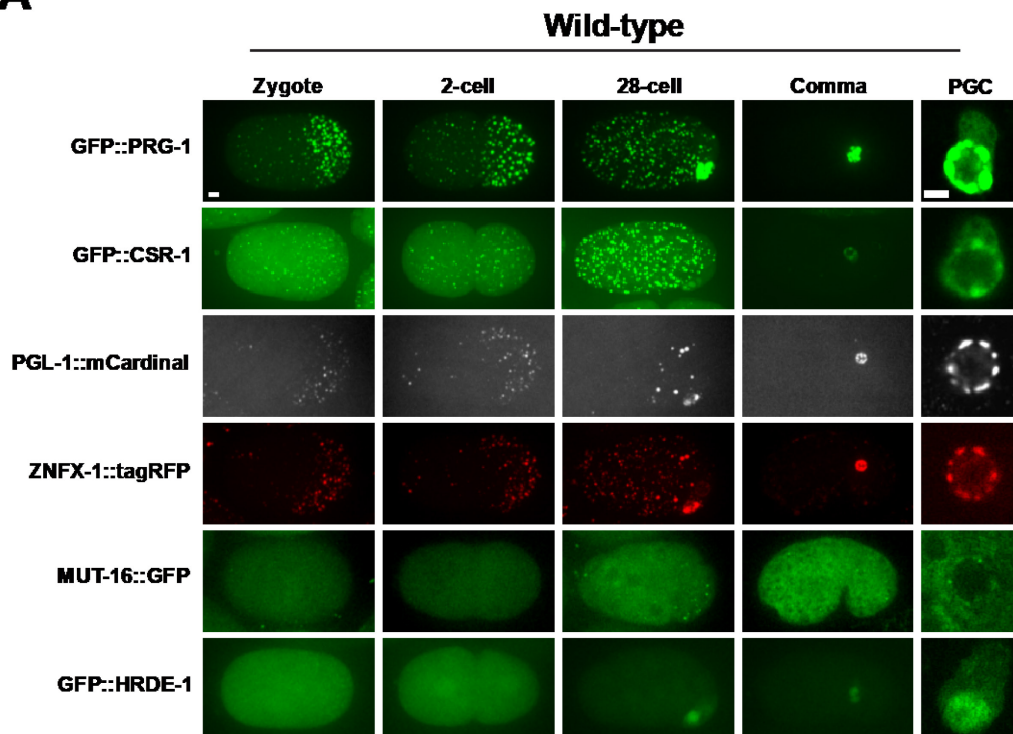
A. Browser view of the *rde-11/B0564.2* locus showing normalized sRNA reads in hermaphrodites of the indicated genotypes.

B. Graph showing the percentage of viable embryos among broods laid by hermaphrodites of the indicated genotypes and fed bacteria expressing *pos-1* dsRNA from the L1 stage. Each dot represents an independent RNAi experiment performed with a cohort of 15-20 hermaphrodites allowed to lay eggs for 1-2 hours. On average, over 200 embryos were scored per RNAi experiment. Note for *prg-1; meg-3 meg-4*, values were normalized to the levels of embryonic lethality the strain exhibits under non-RNAi conditions. Bar height and error bars represent the mean and standard deviation respectively; p-values were obtained using an unpaired t-test.

C. Quantification of smFISH signal normalized to the average wild-type value. Each dot represents a single gonad. Center bar represents the mean and error bars indicate the standard deviation. P values were obtained through an unpaired t-test. See Fig S3G for regions quantified.

Figure 5

A



B

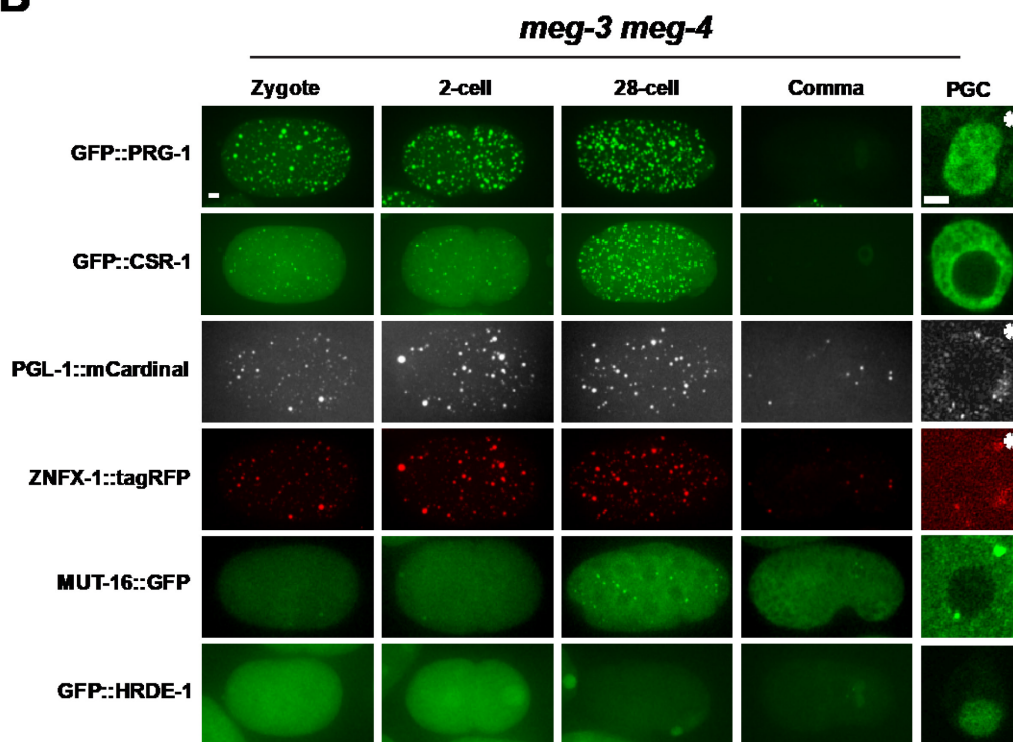


Fig. 5: Localization of epigenetic factors during embryonic development in wild-type and *meg-3 meg-4* mutants.

Photomicrographs of (A) wild-type and (B) *meg-3 meg-4* embryos at the indicated developmental stages expressing fluorescently-tagged nuage proteins and HRDE-1. All tags were introduced at the endogenous locus by genome editing. Last column shows close-ups of a single primordial germ cell (PGC) at comma-stage. Image acquisition and display values were adjusted for each protein and therefore levels cannot be compared between proteins. Wild-type and *meg-3 meg-4* panels for each fusion are comparable, except for panels with asterisks which were adjusted to visualize the much lower levels of fluorescence in *meg-3 meg-4* mutants. See Fig. S4F for non-adjusted panels. Scale bars are 4 μm (embryo panels) and 2 μm (PGC panels).

Figure 6

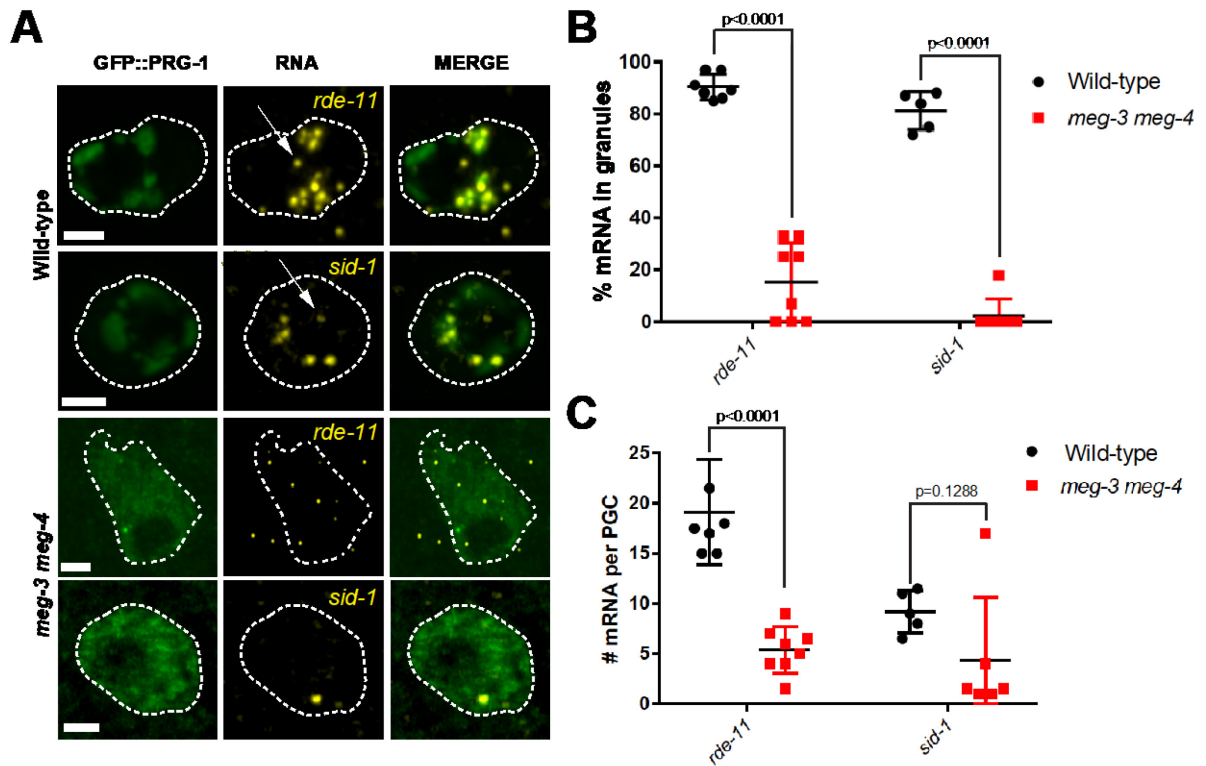


Fig. 6: Localization of *rde-11* and *sid-1* transcripts in wild-type and *meg-3 meg-4* primordial germ cells.

A. Photomicrographs of primordial germ cells in comma-stage embryos hybridized to fluorescent probes to visualize *rde-11* and *sid-1* transcripts (yellow). Embryos also express GFP::PRG-1 fusion (green). Arrows point to nuclear transcripts. Stippled lines indicate cell outline. Scale bar is 2 μm .

B. Graph showing the % of *rde-11* and *sid-1* transcripts in GFP::PRG-1 granules in wild-type vs *meg-3 meg-4* primordial germ cells. Each dot represents one embryo. Error bars represent the standard deviation. P-values were obtained through an unpaired t-test.

C. Graph showing the number of *rde-11* and *sid-1* transcripts in wild-type and *meg-3 meg-4* primordial germ cells. Each dot represents one embryo. Mid bar represents the mean while error bars indicate the standard deviation. P-values were obtained through an unpaired t-test. A significant p-value was obtained between mRNA number in wild-type and *meg-3 meg-4* for *rde-11* mRNA but was not for *sid-1* mRNA due to a single outlier.

Figure 7

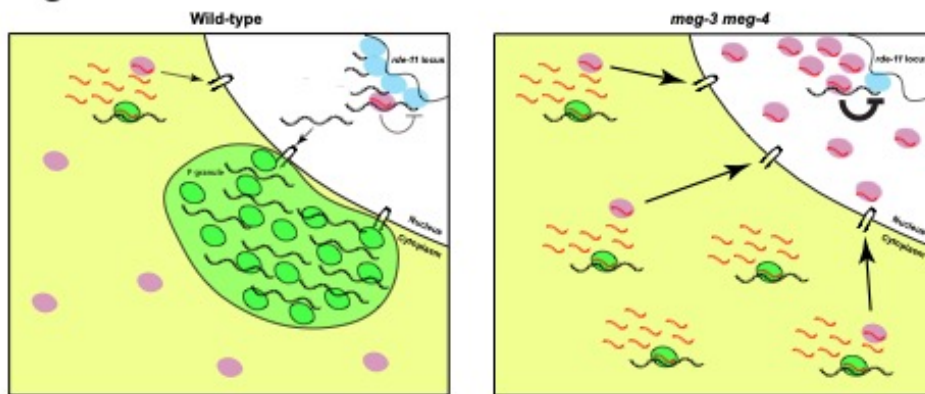


Fig. 7: Model illustrating the fate of *rde-11* transcripts in wild-type and *meg-3 meg-4* primordial germ cells.

In wild-type primordial germ cells, *rde-11* transcripts (black) are transcribed by RNA polymerase II (blue), and accumulate in P granules (green) upon exit from the nucleus. In P granules, *rde-11* transcripts are targeted by PRG-1/piRNA complexes (green) which slows their release into the cytoplasm. Few transcripts reach the cytoplasm (yellow) where mutator activity triggers production of secondary sRNAs (red) that load on HRDE-1 (pink).

In *meg-3 meg-4* primordial germ cells, *rde-11* transcripts immediately disperse in the cytoplasm upon exit from the nucleus. In the cytoplasm, *rde-11* transcripts are targeted by PRG-1/piRNA complexes and by mutator activity which triggers the production of secondary sRNAs. The secondary sRNAs are loaded on HRDE-1 stimulating its nuclear accumulation leading to silencing of the *rde-11* locus.

Figure S1

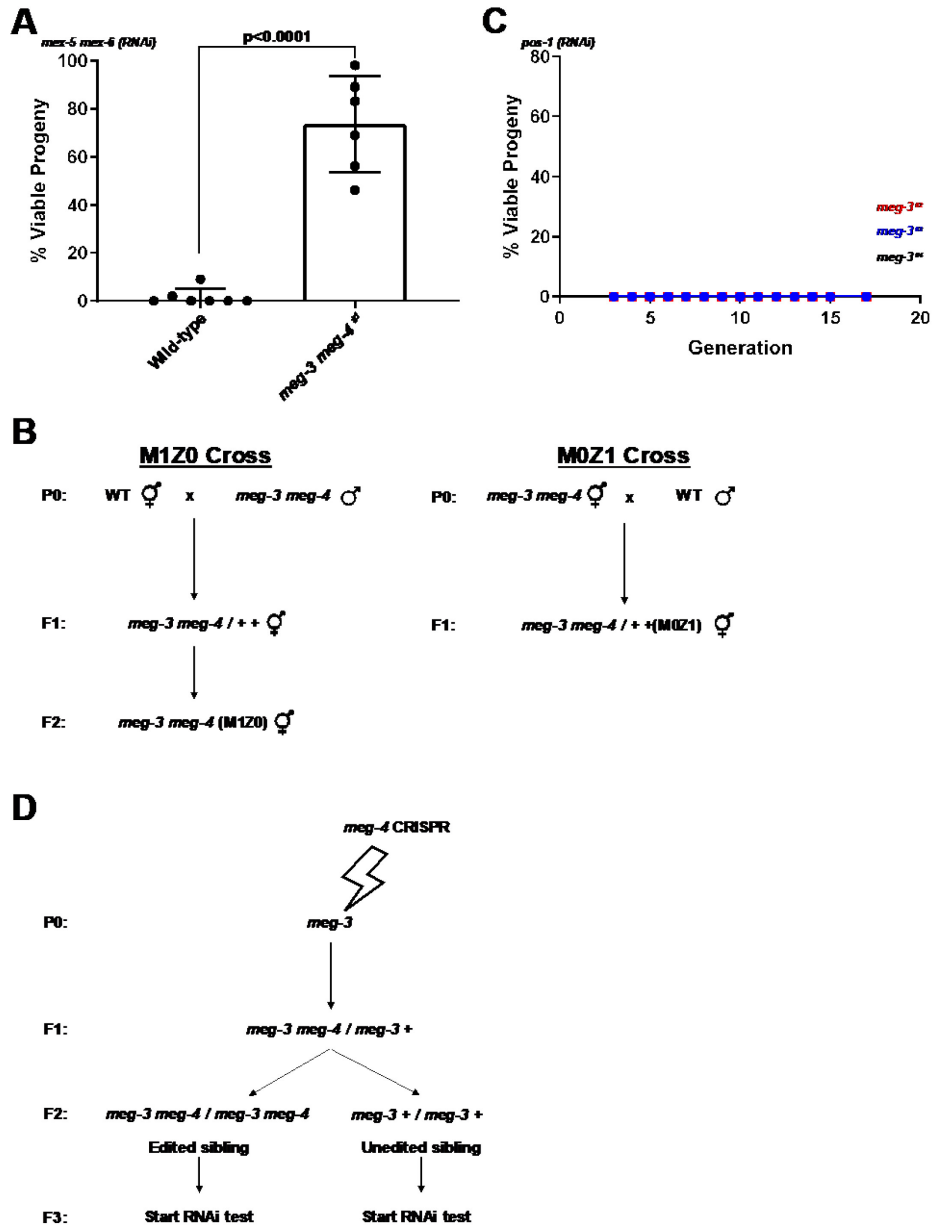


Fig. S1: related to Fig. 2

A. Graph showing the percentage of viable embryos among broods laid by ~20 hermaphrodites of indicated genotypes fed with bacteria expressing *mex-5* and *mex-6* dsRNA from the L1 stage. Bar height represents the mean; error bars represent the standard deviation; the p-value was calculated using an unpaired t-test.

B. Crosses used to generate hermaphrodites with varying numbers of maternal and zygotic *meg-3 meg-4* alleles. *meg-3 meg-4*^{#1} hermaphrodites and males were used in all crosses.

C. Graph showing the percentage of viable embryos among broods laid by ~12 hermaphrodites carrying a deletion at the *meg-3* locus. The three strains shown were generated by cloning non-edited siblings of the *meg-3 meg-4* hermaphrodites analyzed in Fig. 2B. See S1D for CRISPR scheme. Unlike the *meg-3 meg-4* strains, all three *meg-3* strains exhibited complete RNAi penetrance (no viable progeny) throughout the experiment.

D. Genome editing scheme to generate new *meg-3 meg-4* double deletion strains (and control sibling strains) from a strain carrying a deletion in *meg-3*. A single F1 animal was used to establish each *meg-3 meg-4* strain and its control sibling strain. F1 is Generation 1 in Figure 2B.

Figure S2

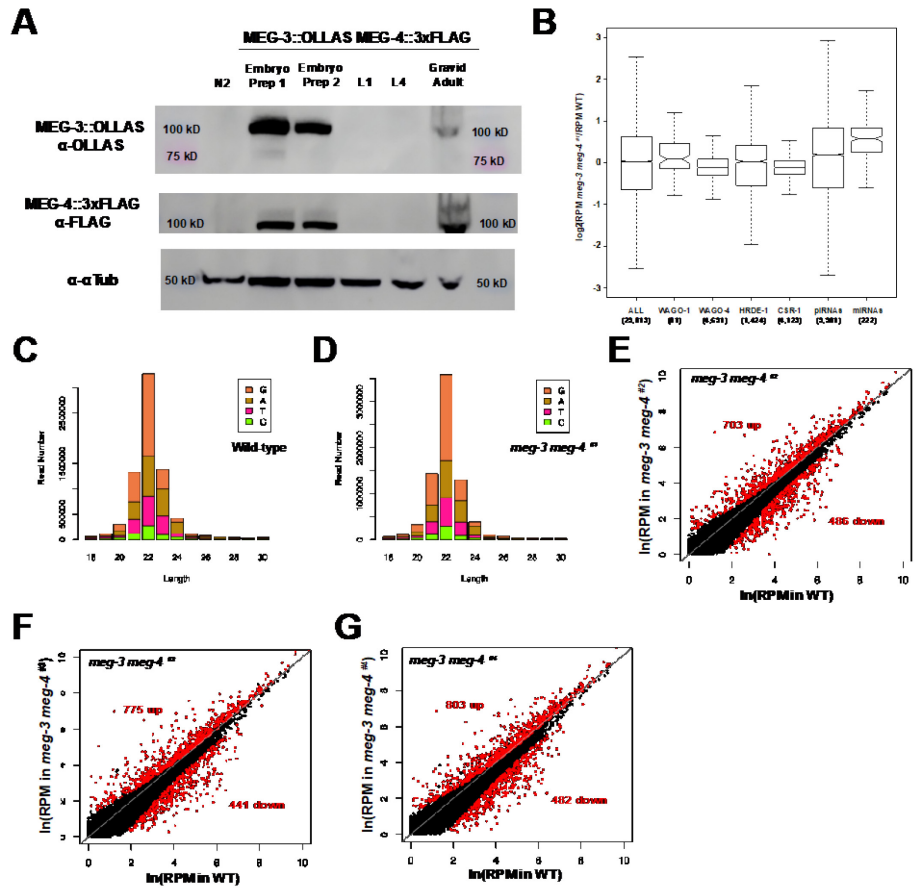


Fig. S2: related to Fig. 3

A. Western blot showing MEG-3 and MEG-4 protein levels in lysates collected at different developmental stages. Proteins were visualized using antibodies against epitope tags inserted at the *meg-3* and *meg-4* loci by genome editing. N2 refers to wild-type worms which do not contain epitope tags at the *meg-3* and *meg-4* loci. All other lanes were loaded with lysates prepared from worms in which *meg-3* and *meg-4* loci were tagged with OLLAS and 3xFLAG, respectively. Embryo Prep 1 lysate was prepared from embryos collected from 1-day old synchronized hermaphrodites. Embryo Prep 2 lysate was prepared from embryos collected from 1 to 3-day old hermaphrodites. L1 and L4 are first and fourth larval stages, respectively, and contain no embryos. Gravid adults contain embryos. Tubulin is used here as a loading control.

B. Box plots showing the log₂ fold change in abundance for the indicated classes of sRNAs in *meg-3 meg-4*^{#1} animals compared to wild-type (Gu et al., 2009; Xu et al., 2018; Buckley et al., 2012; Claycomb et al., 2009; WormBase WS270). Boxes indicate the interquartile range; whiskers indicate the upper and lower quartiles; lines within the boxes indicate the median; notches display the confidence interval around the median. Parenthetical numbers indicate the number of sRNA-mapping genes represented by the respective box. Note that the WAGO-1 sRNA class as reported by Gu et al., 2009 only includes the ~80 highest ranked sRNAs that immunoprecipitated with WAGO-1. As such, the WAGO-1 class of sRNAs may be underrepresented in our analysis.

C-D. sRNA length distribution and 5' nucleotide preference of sRNAs in wild-type and *meg-3 meg-4*^{#1}.

E-G. Scatter plots comparing sRNA abundance in wild-type (X-axis) and *meg-3 meg-4* (Y-axis) hermaphrodites in the indicated *meg-3 meg-4* strains. Each dot represents an annotated locus in the *C. elegans* genome. Red dots represent loci with significantly upregulated or downregulated sRNAs as determined from analysis using two biological replicates for each genotype.

Figure S3

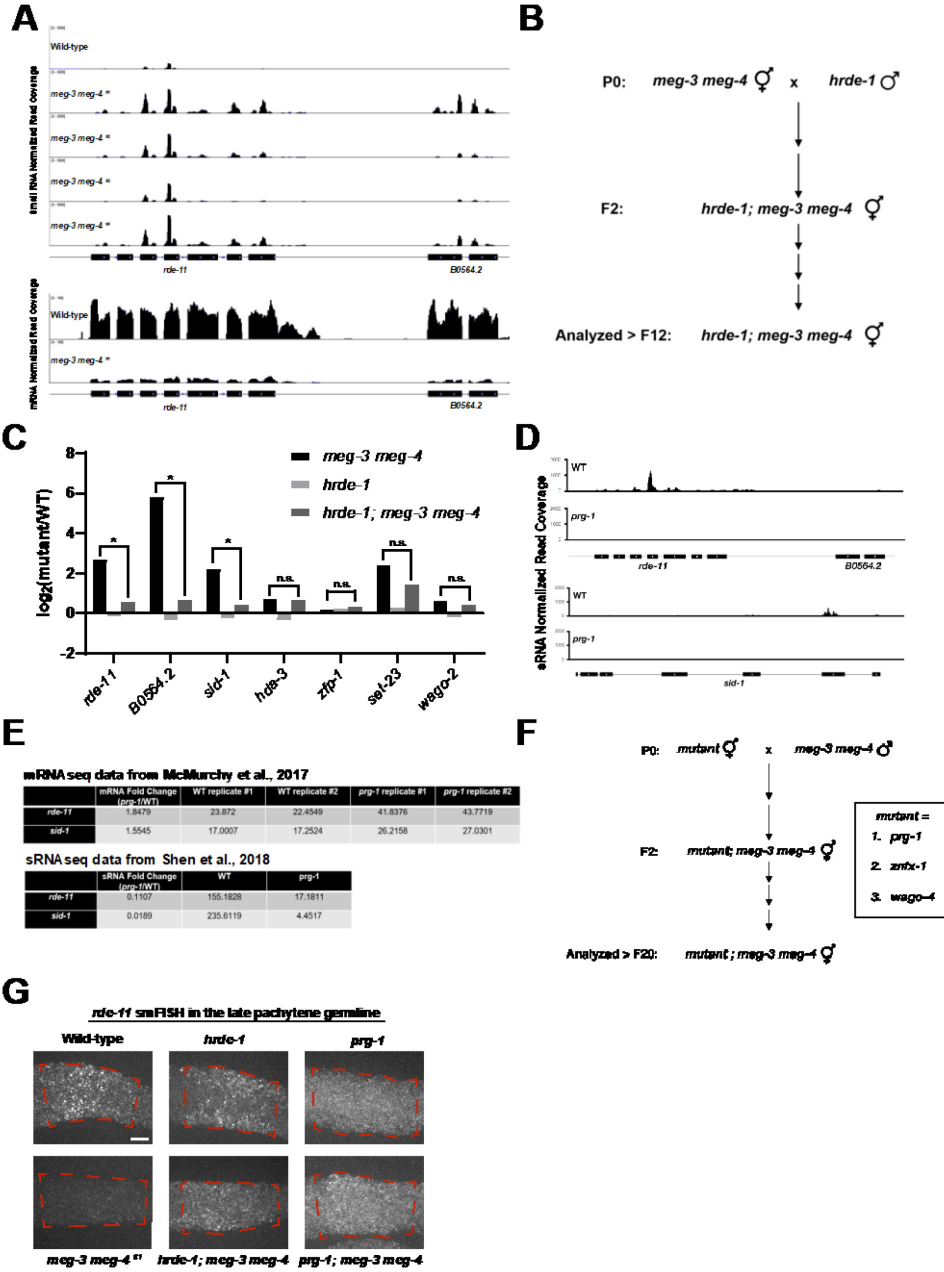


Fig. S3: related to Fig. 4

A. Browser view of the *rde-11/B0564.2* locus showing normalized sRNA reads in wild-type, *meg-3 meg-4^{#1}*, *meg-3 meg-4^{#2}*, *meg-3 meg-4^{#3}*, and *meg-3 meg-4^{#4}* mixed population. Lower panel shows mRNAseq data from *meg-3 meg-4^{#1}* adults. Note the increase in sRNA reads and decrease in mRNA reads at both loci in *meg-3 meg-4^{#1}* worms.

B. Crosses used to generate *hrde-1; meg-3 meg-4* triple mutant. Genotypes were determined by PCR.

C. Bar graph showing the log₂ fold change in sRNAs mapping to the indicated loci in the indicated genotypes compared to wild-type. The graphs represent the log₂ fold change from two biological replicates for each genotype. Stars indicate statistical significance in the comparison between *meg-3 meg-4* and *hrde-1; meg-3 meg-4* by DESeq2.

D. Browser view of the *rde-11/B0564.2* and *sid-1* loci showing normalized sRNA reads in the indicated genotypes. Data from Tang et al., 2018/Lee et al., 2012. At both loci, sRNAs decrease in *prg-1* mutants.

E. mRNA and sRNA fold changes and RPM values in *prg-1* compared to wild-type at the *sid-1*, *rde-11* loci from the indicated published studies.

F. Crosses used to generate *prg-1; meg-3 meg-4, znfx-1; meg-3 meg-4*, and *wago-4; meg-3 meg-4 strains*. Genotypes were determined by PCR.

G. Maximum projection photomicrographs of adult gonads of the indicated genotypes hybridized to fluorescent probes to visualize *rde-11* transcripts (quantified in Fig. 4C). Red stippled lines highlight the late pachytene region. Scale bar represents 10 μm.

Figure S4

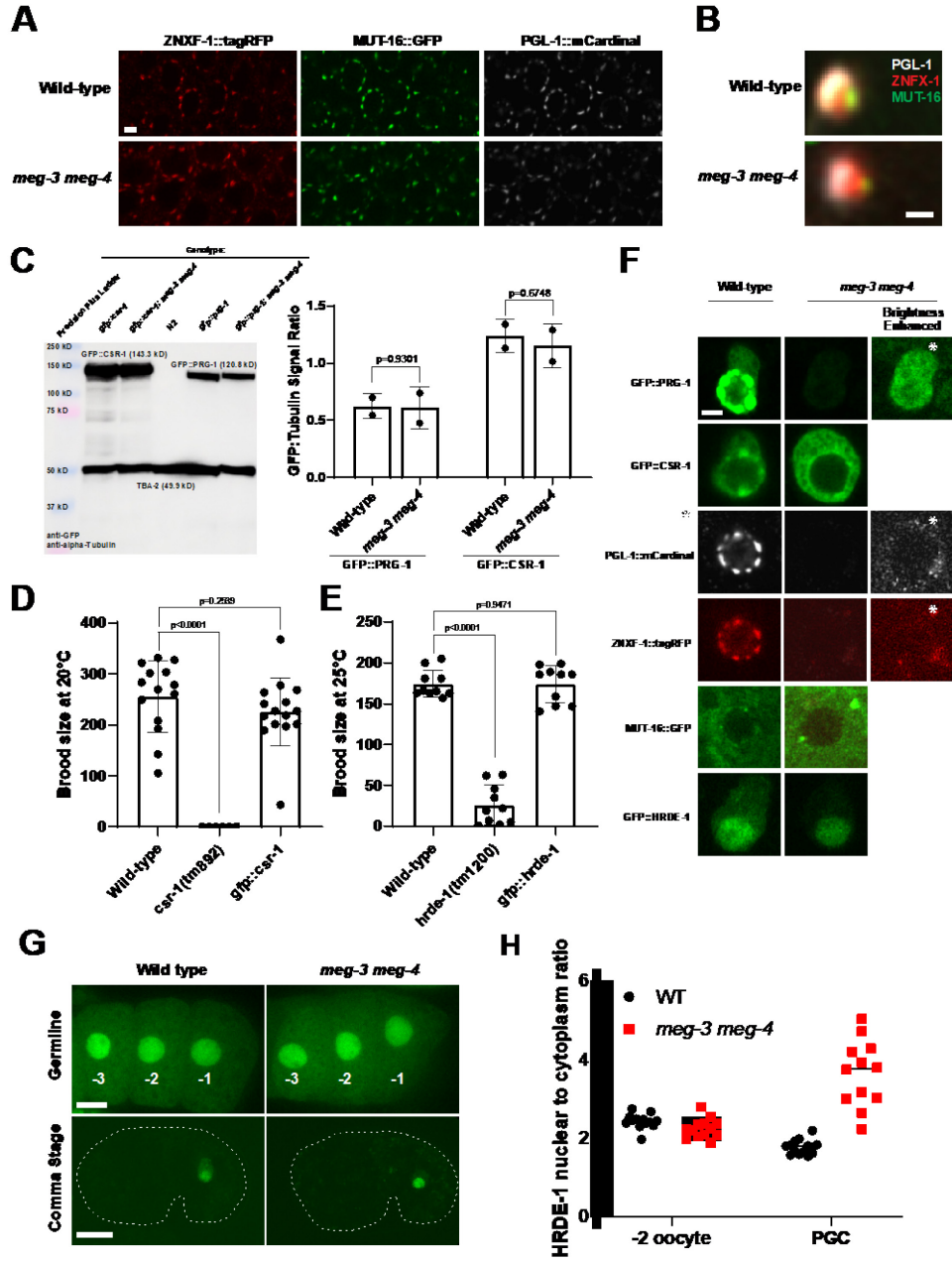


Fig. S4: related to Fig. 5

A. Photomicrographs showing germ cell nuclei (pachytene stage) in adult hermaphrodites of the indicated genotypes. No difference in the distribution in ZNFX-1, MUT-16 or PGL-1 are visible between wild-type and *meg-3 meg-4* at this stage. Scale bar is 2 μ m.

B. Same as A, but close-up showing the P granule - Z granule - Mutator pattern reported in Wan et al., 2018. Same pattern is visible in both wild-type and *meg-3 meg-4* strains. Scale bar is 500 nm.

C. Anti-GFP/anti- α -Tub western blot of the indicated strains to assess levels of GFP::PRG-1 and GFP::CSR-1 in wild-type vs *meg-3 meg-4* adults. The ratio of GFP:Tubulin signal was measured and plotted accordingly. Bar height indicates the mean value; error bars represent the standard deviation; p-values were calculated using an unpaired t-test. Only fertile *meg-3 meg-4* adult worms were used in this analysis. No significance differences in PRG-1 and CSR-1 levels were detected.

D-E. Functional validation of the *gfp::csr-1* and *gfp::hrde-1* lines. Strains were grown at 20° C and 25° C respectively and brood sizes were measured. Loss of function alleles for *csr-1* and *hrde-1* were included as a reference. Bar height indicates the mean value; error bars represent the standard deviation; p-values were calculated using an unpaired t-test.

F. Photomicrographs (also shown in Fig. 5A-B) of single primordial germ cells at comma-stage to show unadjusted *meg-3 meg-4* panels (last row). Acquisition and display parameters for panels in first and second rows are identical, and demonstrate the lower levels of PRG-1/ZNFX-1/PGL-1 in *meg-3 meg-4* compared to wild-type. Panels in the last row (asterisk) have been enhanced for brightness to reveal the distribution of the low levels of PRG-1/ZNFX-1/PGL-1 in *meg-3 meg-4* mutants. Scale bar is 2 μ m.

G. Photomicrographs showing GFP::HRDE-1 in oocytes of adult hermaphrodites (top row) and in primordial germ cells of comma-stage embryos (bottom row) comparing wild-type and *meg-3 meg-4*. White stippled lines indicate cell outline. Scale bar represents 10 μ m in both cases.

H. Quantitation of the nuclear-to-cytoplasmic ratio of GFP::HRDE-1. Note the higher ratio in *meg-3 meg-4* primordial germ cells (PGC). Each dot represents one oocyte or one embryo.

Figure S5

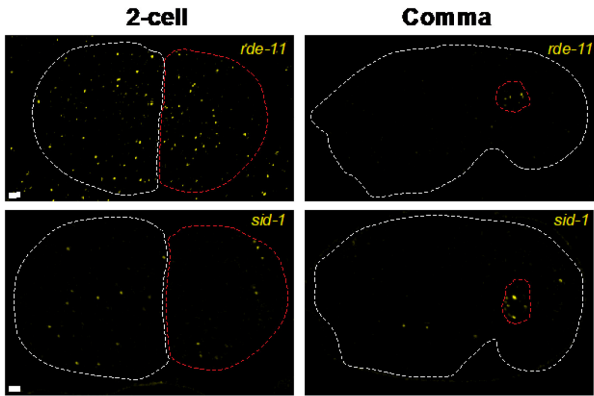


Fig. S5: related to Fig. 6

Photomicrographs of *pgl-1::gfp* embryos hybridized to fluorescent probes to visualize *rde-11* and *sid-1* transcripts (GFP not shown). Transcripts in 2-cell embryos represent maternal transcripts (white stippled cell is somatic blastomere AB, red stippled cell is germline blastomere P₁). Transcripts in later comma-stage embryos are likely zygotic transcripts. Stippled white lines indicate embryo outline, stippled red lines indicate germ cell outline. Scale bar is 2 μm .

List of supplementary tables

Refer to online document for table contents:

DOI: <https://doi.org/10.1016/j.devcel.2019.07.026>

Table S1. Genes with sRNAs up in all four *meg-3 meg-4* strains.

Table S2. Genes with sRNAs down in all four *meg-3 meg-4* strains.

Table S3. Genes involved in RNAi.

Table S4. Misregulated *meg-3 meg-4* sRNAs rescued in *hrde-1; meg-3 meg-4*.

Table S5. List of guides, repair templates, and oligos used in this study.

Table S6. List of high-throughput sequencing libraries used in this study.

Methods:

KEY RESOURCES TABLE

REAGENT or RESOURCE	SOURCE	IDENTIFIER
Antibodies		
anti-FLAG mouse IgG1	Sigma-Aldrich	Cat#: F1804
anti-OLLAS rat IgG1 Kappa HRP	Novus Biologicals	Cat#: NBP1-06713H
anti- α -Tubulin mouse IgG1	Sigma-Aldrich	Cat#: T6199
anti-GFP mouse IgG2a	Takara Bio Clontech	Cat#: 632380
goat anti-mouse IgG1 HRP	Jackson ImmunoResearch	Cat#: 115-035-205
goat anti-mouse IgG2a HRP	Jackson ImmunoResearch	Cat#: 115-035-206
Bacterial and Virus Strains		
<i>Escherichia coli</i> : OP50	Caenorhabditis Genetics Center	OP50
<i>Escherichia coli</i> : NA22	Caenorhabditis Genetics Center	NA22
<i>Escherichia coli</i> : HT115(DE3)	Caenorhabditis Genetics Center	HT115(DE3)
Chemicals, Peptides, and Recombinant Proteins		
LB media powder	Gentox	Cat#: 50-11.5
Ampicilin		
IPTG	GoldBio	Cat#: I2481C
KH ₂ PO ₄	Sigma-Aldrich	Cat#: P0662
Na ₂ HPO ₄	Fisher Scientific	Cat#: S374-3
NaCl	Fisher Scientific	Cat#: S271-3
MgSO ₄	Sigma-Aldrich	Cat#: M7506
cOmplete Mini, EDTA-free Protease Inhibitor Cocktail	Millipore Sigma	Cat#: 11836170001
PBS tablets	ThermoFisher Scientific	Cat#: 18912014
Dithiothreitol (DTT)	ThermoFisher Scientific	Cat#: R0861
Nestle Carnation Instant Nonfat Dry Milk	Amazon	Cat#: B004VDGXG2
Tween20	Sigma-Aldrich	Cat#: P7949
HyGLO Quick Spray Chemiluminescent HRP Antibody Detection Reagent	Denville Scientific Inc	Cat#: E2400
TRIzol	ThermoFisher Scientific	Cat#: 15596018
RNA 5' Polyphosphatase	Lucigen	Cat#: RP8092H
Phenol	VWR	Cat#: 97064-71
Chloroform	Fisher Scientific	Cat#: 02-002-584
Ethanol, 200 proof	Fisher Scientific	Cat#: BP2818100
Sodium Acetate (3 M), pH 5.5, RNase-free	ThermoFisher Scientific	Cat#: AM9740
Glycogen	ThermoFisher Scientific	Cat#: AM9510
Methanol	Fisher Scientific	Cat#: A412-4
Paraformaldehyde (PFA)	Electron Microscopy Sciences	Cat#: 15714

20x SCC Buffer	Thermo Fisher Scientific	Cat#: AM9770
Formamide	Sigma-Aldrich	Cat#: 221198
Ribonucleoside Vanadyl Complex	New England Biolabs	Cat#: S1402S
UltraPure™ BSA	Thermo Fisher Scientific	Cat#: AM2618
Dextran sulfate sodium salt from <i>Leuconostoc</i> spp.	Sigma-Aldrich	Cat#: D8906
Yeast total RNA	CustomBiotech (Roche)	Cat#: 10153320103
Critical Commercial Assays		
NNGM agar plates	N/A	N/A
Enriched peptone plates	N/A	N/A
Clontech In-Fusion HD Cloning Kit	Takara	Cat#: 638909
T7 RiboMAX Express Large Scale RNA Production System	Promega	Cat#: P1300
RNA Clean & Concentrator Kit	Zymo	Cat#: R1017
Novex™ TBE Gels, 6%, 10 well	Invitrogen	Cat#: EC6265BOX
NuPAGE LDS Sample Buffer	Invitrogen	Cat#: NP0008
Bolt 4-12% Bis-Tris Plus Gel	Invitrogen	Cat#: NW04120BOX
NuPAGE MOPS SDS Running Buffer	ThermoFisher Scientific	Cat#: NP0001
Immobilon-P PVDF Membrane	Sigma-Aldrich	Cat#: IPVH
KwikQuant™ Imager	Kindle Biosciences, LLC	Cat#: D1001
TruSeq Small RNA Library Preparation Kit	Illumina	Cat#: RS-200-0012
Ribo-Zero Gold rRNA Removal Kit, Epidemiology	Illumina	Cat#: MRZE706
ERCC RNA Spike-In Mix	Thermo Fisher Scientific	Cat#: 4456740
TruSeq RNA Library Prep Kit v2	Illumina	Cat#: RS-122-2001
VECTASHIELD Antifade Mounting Media with DAPI	Vector Laboratories	Cat#: H-1200
ProLong™ Diamond Antifade Mountant with DAPI	Thermo Fisher Scientific	Cat#: P36962
Precision Plus Protein Dual Color Standards	BoiRad	Cat#: 1610374
Deposited Data		
sRNAseq and mRNAseq from study	This study	NCBI GEO ID: GSE134638
<i>prg-1(n4357)</i> sRNAseq (Fig. S3D)	Lee et al., 2013	NCBI SRR ID: SRR513312
Wild-type sRNAseq (Fig. S3D)	Tang et al., 2013	NCBI SRR ID: SRR513311
Experimental Models: Organisms/Strains		
<i>C. elegans</i> strain: <i>meg-3(ax3055) meg-4(ax3052) X</i>	Smith et al., 2016	JH3475
<i>C. elegans</i> strain: <i>meg-3(ax3051[meg-3::ollas]) meg-4(ax2080[meg-4::3xflag]) X</i>	Smith et al., 2016	JH3474
<i>C. elegans</i> strain: <i>meg-3(ax3055) meg-4(ax2080[meg-4::3xflag]) X</i>	This study (CRISPR Paix et al., 2017)	JH3439
<i>C. elegans</i> strain: <i>meg-3(ax3055) meg-4(ax2080[meg-4::3xflag]) X</i>	This study	JH3669
<i>C. elegans</i> strain: <i>meg-3(ax3055) meg-4(ax2080[meg-4::3xflag]) X</i>	This study	JH3670

<i>C. elegans</i> strain: <i>meg-3(ax3055) meg-4(ax2080[meg-4::3xflag]) X</i>	This study	JH3671
<i>C. elegans</i> strain: <i>meg-3(ax3055) meg-4(ax4310) X</i>	This study (CRISPR Paix et al., 2017)	JH3672
<i>C. elegans</i> strain: <i>meg-3(ax3055) meg-4(ax4311) X</i>	This study (CRISPR Paix et al., 2017)	JH3673
<i>C. elegans</i> strain: <i>meg-3(ax3055) meg-4(ax4312) X</i>	This study (CRISPR Paix et al., 2017)	JH3674
<i>C. elegans</i> strain: <i>rde-11(hj37) IV</i>	Caenorhabditis Genetics Center	VS27
<i>C. elegans</i> strain: <i>hrde-1(tm1200) III</i>	Buckley et al., 2012	YY538
<i>C. elegans</i> strain: <i>prg-1(n4357) I</i>	Caenorhabditis Genetics Center	SX922
<i>C. elegans</i> strain: <i>mut-16(cmp3[mut-16::gfp::flag+loxP]) I; znfx-1(gg634[ha::tagrfp::znfx-1]) II; pgl-1(gg640[pgl-1::3xflag::mcardinal]) IV</i>	Wan et al., 2018	YY1492
<i>C. elegans</i> strain: <i>mut-16(cmp3[mut-16::gfp::flag+loxP]) I; znfx-1(gg634[ha::tagrfp::znfx-1]) II; pgl-1(gg640[pgl-1::3xflag::mcardinal]) IV; meg-3(ax3055) meg-4(ax3052) X</i>	This study	JH3676
<i>C. elegans</i> strain: <i>hrde-1(tm1200) III; meg-3(ax3055) meg-4(ax3052) X</i>	This study	JH3686
<i>C. elegans</i> strain: <i>prg-1(n4357) I; meg-3(ax3055) meg-4(ax3052) X</i>	This study	JH3687
<i>C. elegans</i> strain: <i>prg-1(ne4523[gfp::tev::flag::prg-1]) I</i>	Shen et al., 2018	WM527
<i>C. elegans</i> strain: <i>prg-1(ne4523) I; meg-3(ax3055) meg-4(ax3052) X</i>	This study	JH3689
<i>C. elegans</i> strain: <i>hrde-1(tor125[gfp::3xflag::hrde-1]) III</i>	This study (CRISPR Dickinson et al., 2015)	JMC231
<i>C. elegans</i> strain: <i>hrde-1(tor125[gfp::3xflag::hrde-1]) III; meg-3(ax3055) meg-4(ax3052) X</i>	This study	JH3682
<i>C. elegans</i> strain: <i>csr-1(tor67[gfp::3xflag::csr-1]) IV</i>	This study (CRISPR Dickinson et al., 2015)	JMC101
<i>C. elegans</i> strain: <i>csr-1(tor67[gfp::3xflag::csr-1]) IV; meg-3(ax3055) meg-4(ax3052) X</i>	This study	JH3684
<i>C. elegans</i> strain: <i>znfx-1(gg561); meg-3(ax3055) meg-4(ax3052) X</i>	This study	JH3690
<i>C. elegans</i> strain: <i>wago-4(tm1019); meg-3(ax3055) meg-4(ax3052) X</i>	This study	JH3691
<i>C. elegans</i> strain: <i>pgl-1(ax3122[pgl-1::gfp]) IV</i>	Putnam et al., 2019	JH3269
<i>C. elegans</i> strain: <i>csr-1(tm892) IV/nT1 [unc-(n754) let-?] (IV;V)</i>	Caenorhabditis Genetics Center	WM182
Oligonucleotides		
Oligonucleotides, guide RNAs, CRISPR repair templates	Integrated DNA Technologies	Table SX
Recombinant DNA		

L4440 RNAi vector	Source BioScience C. <i>elegans</i> RNAi Collection (Ahringer)	3318_Cel_RNAi_complete
<i>pos-1</i> 400nt L4440 RNAi vector	This study	
<i>pos-1</i> CDS L4440 RNAi vector	Dharmacon C. <i>elegans</i> RNAi collection	Cat#: RCE1181
<i>mex-5</i> L4440 RNAi vector	Source BioScience C. <i>elegans</i> RNAi Collection (Ahringer)	Cat#: 3318_Cel_RNAi_complete
<i>mex-6</i> L4440 RNAi vector	Source BioScience C. <i>elegans</i> RNAi Collection (Ahringer)	Cat#: 3318_Cel_RNAi_complete
Software and Algorithms		
Cutadapt	Martin, 2011	RRID:SCR_011841
Bowtie 2	Langmead and Salzberg, 2012	RRID:SCR_005476
SAMtools	Li et al., 2009	RRID:SCR_002105
HTSeq-count	Anders et al., 2015	RRID:SCR_011867
HISAT2	Kim et al., 2015	RRID:SCR_015530
Integrative Genomics Viewer	Robinson et al., 2011	RRID:SCR_011793
Fiji	https://imagej.net/Fiji/Downloads	RRID:SCR_002285
Imaris	https://imaris.oxinst.com/packages	RRID:SCR_007370
GraphPad Prism	http://www.graphpad.com/	RRID:SCR_002798
RStudio 3.4.1	https://www.rstudio.com/	RRID:SCR_000432
SlideBook	https://www.intelligent-imaging.com/slidebook	RRID:SCR_014300
Other		
Illumina HiSeq-2500 Sequencing System	N/A	N/A
Zeiss LSM 880-AiryScan	N/A	N/A
Zeiss Axio Imager with a Yokogawa spinning-disc confocal scanner	N/A	N/A

Lead Contact and Materials Availability:

Further information and requests for resources and reagents should be directed to Geraldine Seydoux (gseydoux@ihmi.edu). Plasmids generated in this study have been deposited to Addgene. Strains used in this study have been deposited at the Caenorhabditis Genetics Center (CGC). Unique reagents generated in this study are listed in the Key Resources Table.

Experimental Model and Subject Details:

All *C. elegans* strains used throughout this study were maintained at 20° C on NNGM growth media or Enriched Peptone media and fed OP50 or NA22 bacteria. Strains used in this study are listed in the Key Resources Table.

Methods Details:

Strain construction and validation:

CRISPR generated lines were created as in Paix et al., 2017 or Dickinson et al 2015 as indicated in the Key Resources Table. Guides and repair templates used for CRISPR are listed in Table S5. For functional validation of the *gfp::hrde-1* and *gfp::csr-1* strains, brood sizes were determined as follows: L4 stage worms were picked to separate plates and transferred every day until egg laying ceased. The progeny on each plate were counted 1-2 days after the mother was transferred. Experiments were conducted at 25° C and 20° C for *gfp::hrde-1* and *gfp::csr-1* respectively (Fig. S4D-E).

The following names were used throughout the paper to indicate the following strains:

- *meg-3 meg-4*^{#1} → JH3475
- *meg-3 meg-4*^{#2} → JH3672
- *meg-3 meg-4*^{#3} → JH3673
- *meg-3 meg-4*^{#4} → JH3674

RNA interference assays:

The *pos-1* 400 nt L4440 RNAi vector used for sRNA sequencing in Fig 2C, D was made using the Clontech In-Fusion HD Cloning Kit. The PCR oligos used for cloning are listed in Table S5. The *pos-1* segment cloned was amplified from the full CDS *pos-1* L4440 plasmid from the Dharmacon *C. elegans* RNAi collection and cloned into the L4440 vector.

All RNAi experiments were performed at 20°C. Feeding RNAi experiments were performed by placing worms on HT115 bacteria expressing dsRNA as previously described in Timmons and Fire, 1998. Briefly, HT115 cells were transformed with L4440 RNAi plasmids, and colonies were inoculated into 2 mLs 100 ug/mL ampicillin LB liquid media and grown for five

hours at 37° C. Cultures were then induced with IPTG for a final concentration of 5 mM and grown for 45 minutes. Bacteria were then plated on NNGM agar containing 100 ug/mL carbenicillin and 1 mM IPTG. Feeding was performed starting at the L1 or L4 stage (time of feeding is indicated in the figure legends for each experiment). For feeding at the L1 stage, worms were fed RNAi bacteria for ~72 hours before experimentation. For feeding at the L4 stage, experiments were performed ~36 hours after placement on RNAi.

For RNAi by injection, *pos-1* dsRNA was obtained using the T7 RiboMAX Express Large Scale RNA Production System and purified using Zymo's RNA Clean & Concentrator Kits. Young adults were injected with 200 ng/uL *pos-1* dsRNA and embryonic lethality was assessed for each injected mother 16 hours following injection.

For embryonic lethality calculations, single mothers or cohorts of 10-20 mothers were allowed to lay eggs for periods ranging from 1-2 hours. Embryos were then counted, and adults were scored four days later. *prg-1; meg-3 meg-4* hermaphrodites lay ~50% dead embryos even under non-RNAi conditions. For those experiments, embryonic lethality on *pos-1* RNAi was normalized to embryonic lethality on control L4440 RNAi.

Western Blots:

For the MEG-3::OLLAS/MEG-4::3X::FLAG western blot, a mixed population of worms was subjected to bleaching to obtain embryos for L1 synchronization by shaking in M9 (22.0 mM KH₂PO₄, 42.3 mM Na₂HPO₄, 85.6 mM NaCl, 1 mM MgSO₄) for 18-20 hours. L1 samples were then taken before plating on OP50 bacteria. Samples were then collected at different developmental stages. Embryo samples were collected from the synchronized gravid adult worms. Staged samples were resuspended in 1x PBS/cOmplete Mini, EDTA-free Protease Inhibitor Cocktail. 5.5 uL of dense worm volume was then combined with 2.5 uL of NuPAGE LDS Sample Buffer and 2 uL of 1 M DTT.

For GFP::PRG-1/GFP::CSR-1 western blots, 75-100 fertile adults were collected and placed in 20 uL of 1x PBS/ cOmplete Mini, EDTA-free Protease Inhibitor Cocktail. 9.09 uL of NuPAGE LDS Sample Buffer and 7.27 of 1 M DTT were added to each sample.

For sample preparation, all samples were lysed by four freeze thaw cycles. Following lysis, samples were heated at 85 C° for 10 minutes and then run on a Bolt 4-12% Bis-Tris Plus Gel in NuPAGE MOPS SDS Running Buffer. Samples were then transferred to an Immobilon-P PVDF Membrane, blocked in PBS+0.1%Tween20+5% nonfat dry milk and incubated with primary antibodies diluted in PBS+0.1%Tween20+5% milk. The blot was washed three times in PBS+0.1%Tween20 and visualized by treatment with HyGLO Quick Spray Chemiluminescent HRP Antibody Detection Reagent and imaging by the KwikQuant™ Imager. For samples requiring a secondary antibody, the blot was incubated with a secondary antibody diluted in PBS+0.1%Tween20+5% milk following the three washes after the primary antibody. The blot was washed thrice more in PBS+0.1%Tween20 and imaged as described above.

Antibody dilutions used were as follows:

- anti-FLAG M2 mouse IgG1: 1:500 dilution
- anti-OLLAS L2 rat IgG1 Kappa HRP: 1:1000
- anti- α -Tubulin mouse IgG1: 1:1000
- anti-GFP mouse IgG2a: 1:500
- goat anti-mouse IgG1 HRP: 1:2500
- goat anti-mouse IgG2a HRP: 2500

RNA extraction and high-throughput sequencing library preparation:

Mixed or adult staged (~55-60 hours following L1 synchronization) populations of worms were collected, and RNA was isolated using the TRIzol reagent and chloroform. RNA was then concentrated and purified using Zymo's RNA Clean & Concentrator Kits. For sRNA library preparation, RNA was either treated or untreated with RNA 5' polyphosphatase (20 U/ug of RNA). Samples were then incubated for 30 minutes at 37° C and purified via phenol/chloroform extraction and ethanol precipitation supplemented with sodium acetate and glycogen. sRNA libraries were then constructed using 1 ug of polyphosphatase-treated/untreated total RNA as input into the TruSeq Small RNA Library Preparation Kit with 11 cycles of PCR amplification. Libraries were then size selected on a Novex 6% TBE gel and purified.

For mRNA sequencing, 1 ug of total RNA was treated with Ribo-Zero Gold Epidemiology rRNA Removal Kit. A 1:100 dilution of ERCC RNA Spike-In Mix was added. Libraries were then prepared using the TruSeq RNA Library Prep Kit v2 with 13 cycles of PCR amplification.

All sequencing was performed using the Illumina HiSeq2500 at the Johns Hopkins University School of Medicine Genetic Resources Core Facility.

High-throughput sequencing analyses:

sRNA sequencing: 5' sequencing adapters were trimmed using Cutadapt with default settings (Martin, 2011). Reads longer than 30 nts and shorter than 18 nts were discarded. Reads were then aligned to the UCSC ce10 *C. elegans* reference genome using Bowtie 2 (Langmead and Salzberg, 2012). Reads mapping to genetic features were counted using HTSeq-count (Anders et al., 2015) and differential expression analysis was conducted using DESeq2 (Love et al., 2014). For all our sRNA analysis, reads were normalized based on library size.

For sRNA class analyses, piRNA and miRNA lists were downloaded from WormBase. All other sRNAs were placed in Argonaute classes based on the locus targeted and published lists of loci targeted by sRNAs immunoprecipitated with specific Argonautes from wild-type worm lysates [Gu et al., 2009 (WAGO-1 IP), Xu et al, 2018 (WAGO-4 IP), Buckley et al., 2012 (HRDE-1 IP), and Claycomb et al., 2009 (CSR-1 IP)].

mRNA sequencing: sequencing reads were aligned to the UCSC ce10 *C. elegans* reference genome using HISAT2 (Kim et al., 2015). Reads aligning to genetic features were then counted using HTSeq-count (Anders et al., 2015) and analyzed for differential expression analysis using DESeq2 (Love et al., 2014).

Genome browser views were adapted from IGV TDF file visualization with zoom levels set to 7, window function set to "Mean," and window size set to 5 (Robinson et al., 2011).

A list of high-throughput sequencing libraries generated in this study is listed in Table S6.

Single molecule fluorescence in situ hybridization (smFISH):

smFISH probes for *rde-11* and *sid-1* were designed using Biosearch Technologies's Stellaris Probe Designer. The fluorophores used in this study were Quasar570 and Quasar670.

For sample preparation, embryos or adult germlines were extruded from adults on poly-lysine slides and subjected to freeze-crack followed by methanol fixation. Samples were washed five times in PBS+0.1%Tween20 and fixed in 4% PFA for one hour at room temperature. Samples were again washed in PBS+0.1%Tween20 four times, twice in 2x SCC, and once in wash buffer (10% formamide, 2x SCC) before blocking in hybridization buffer (10% formamide, 2x SCC, 200 ug/mL BSA, 2mM Ribonucleoside Vanadyl Complex, 0.2 mg/mL yeast total RNA, 10% dextran sulfate) for 30 minutes at 37° C. Hybridization was then conducted by incubating samples with 50 nM probe solution diluted in hybridization buffer overnight at 37° C. Following hybridization, samples were washed twice in wash buffer at 37° C, twice in 2x SCC, once in PBS+0.1%Tween20, and twice in PBS. Lastly, samples were mounted using VECTASHIELD Antifade Mounting Media with DAPI or Prolong Diamond Antifade Mountant.

Microscopy:

Fluorescence confocal microscopy was performed using a Zeiss Axio Imager with a Yokogawa spinning-disc confocal scanner. Images were taken using Slidebook v6.0 software (Intelligent Imaging Innovations) using a 63x objective. For imaging of primordial germ cells, fluorescence super-resolution microscopy was performed using ZEISS LSM 880-AiryScan (Carl Zeiss) equipped with a 63X objective. Images were acquired and processed using ZEN imaging software (Carl Zeiss). Equally normalized images were exported via either Slidebook v6.0 or ZEN, and contrasts of images were equally adjusted between control and experimental sets using ImageJ.

Quantification and Statistical Analysis:

Statistical analysis used in Figs 2, 4, S4, and 6 were performed using an unpaired t-test. Statistics for differential expression analysis were done using DESeq2 (Love et al., 2014).

FIJI was used for western blot quantification, *rde-11* smFISH signal quantification in the germline, and quantification of GFP::HRDE-1's nuclear to cytoplasmic ratio. For western blot quantification, ROIs of constant area were placed over the GFP and tubulin bands and the integrated density values were measured. The ratios between GFP signal and tubulin signal was

then calculated. For the *rde-11* germline quantification, ROIs were drawn in the late pachytene region of the germline and mean intensity values were calculated using maximum projection images. Unstained germlines were then used for background calculation, which was then subtracted from the calculated mean intensity of the germlines with probes. These values were then normalized to the average of wild-type and plotted accordingly. For GFP::HRDE-1 nuclear to cytoplasmic ratio in the -2 oocyte, germlines were extruded and single plane images were taken of the -2 oocyte. ROIs were drawn in the nucleus and cytoplasm, and the ratio of the mean intensities was calculated for wild-type and *meg-3 meg-4*. For GFP::HRDE-1 nuclear to cytoplasmic ratio in the PGCs, single plane images were taken of wild-type and *meg-3 meg-4* embryos at comma-stage. In a similar manner to the adult germline, the mean intensities of the nucleus and cytoplasm were calculated and compared in a ratio.

smFISH quantification of PGC granule enrichment was conducted using Imaris Image Analysis Software visualization in 3D space. RNAs were counted manually, and the percentage localized in a GFP::PRG-1 granule was calculated.

Data and Code Availability:

Sequencing data has been deposited onto the Gene Expression Omnibus (GEO) and can be found using the following GEO SuperSeries accession: GSE134638.

The *prg-1* sRNA sequencing data from Fig. S3D was obtained from SRR513312 (Lee et al., 2012) and its corresponding wild-type from SRR6691711 (Tang et al., 2018).

References

- Anders, S., Pyl, P. T., & Huber, W. (2015). HTSeq—a Python framework to work with high-throughput sequencing data. *Bioinformatics*, 31(2), 166–169. <https://doi.org/10.1093/bioinformatics/btu638>
- Ashe, A., Sapetschnig, A., Weick, E.-M., Mitchell, J., Bagijn, M. P., Cording, A. C., ... Miska, E. A. (2012). piRNAs Can Trigger a Multigenerational Epigenetic Memory in the Germline of *C. elegans*. *Cell*, 150(1), 88–99. <https://doi.org/10.1016/j.cell.2012.06.018>
- Batista, P. J., Ruby, J. G., Claycomb, J. M., Chiang, R., Fahlgren, N., Kasschau, K. D., ... Mello, C. C. (2008). PRG-1 and 21U-RNAs Interact to Form the piRNA Complex Required for Fertility in *C. elegans*. *Molecular Cell*, 31(1), 67–78. <https://doi.org/10.1016/J.MOLCEL.2008.06.002>
- Belicard, T., Jareosettasin, P., & Sarkies, P. (2018). The piRNA pathway responds to environmental signals to establish intergenerational adaptation to stress. *BMC Biology*, 16(1), 103. <https://doi.org/10.1186/s12915-018-0571-y>
- Blumenthal, T., & Gleason, K. S. (2003). *Caenorhabditis elegans* operons: form and function. *Nature Reviews Genetics*, 4(2), 110–118. <https://doi.org/10.1038/nrg995>
- Brennecke, J., Malone, C. D., Aravin, A. A., Sachidanandam, R., Stark, A., & Hannon, G. J. (2008). An Epigenetic Role for Maternally Inherited piRNAs in Transposon Silencing. *Science*, 322(5906), 1387–1392. <https://doi.org/10.1126/science.1165171>
- Buckley, B. A., Burkhart, K. B., Gu, S. G., Spracklin, G., Kershner, A., Fritz, H., ... Kennedy, S. (2012). A nuclear Argonaute promotes multigenerational epigenetic inheritance and germline immortality. *Nature*, 489(7416), 447–451. <https://doi.org/10.1038/nature11352>
- Cecere, G., Hoersch, S., Jensen, M. B., Dixit, S., & Grishok, A. (2013). The ZFP-1(AF10)/DOT-1 complex opposes H2B ubiquitination to reduce Pol II transcription. *Molecular Cell*, 50(6), 894–907. <https://doi.org/10.1016/j.molcel.2013.06.002>

Cecere, G., Hoersch, S., O’Keeffe, S., Sachidanandam, R., & Grishok, A. (2014). Global effects of the CSR-1 RNA interference pathway on the transcriptional landscape. *Nature Structural & Molecular Biology*, 21(4), 358–365. <https://doi.org/10.1038/nsmb.2801>

Claycomb, J. M., Batista, P. J., Pang, K. M., Gu, W., Vasale, J. J., van Wolfswinkel, J. C., ... Mello, C. C. (2009). The Argonaute CSR-1 and Its 22G-RNA Cofactors Are Required for Holocentric Chromosome Segregation. *Cell*, 139(1), 123–134. <https://doi.org/10.1016/j.cell.2009.09.014>

de Albuquerque, B. F. M., Placentino, M., & Ketting, R. F. (2015). Maternal piRNAs Are Essential for Germline Development following De Novo Establishment of Endo-siRNAs in *Caenorhabditis elegans*. *Developmental Cell*, 34(4), 448–456. <https://doi.org/10.1016/j.devcel.2015.07.010>

Dickinson, D. J., Pani, A. M., Heppert, J. K., Higgins, C. D., & Goldstein, B. (2015). Streamlined Genome Engineering with a Self-Excising Drug Selection Cassette. *Genetics*, 200(4), 1035–1049. <https://doi.org/10.1534/genetics.115.178335>

Dodson, A. E. and Kennedy, S. (2019). Germ Granules Coordinate RNA-based Epigenetic Inheritance Pathways. *Dev Cell*.

Feinberg, E. H., & Hunter, C. P. (2003). Transport of dsRNA into Cells by the Transmembrane Protein SID-1. *Science*, 301(5639), 1545–1547. <https://doi.org/10.1126/science.1087117>

Folkmann, A. W., & Seydoux, G. (2019). Spatial regulation of the polarity kinase PAR-1 by parallel inhibitory mechanisms. *Development (Cambridge, England)*, 146(6), dev.171116. <https://doi.org/10.1242/dev.171116>

Gu, W., Shirayama, M., Conte, D., Vasale, J., Batista, P. J., Claycomb, J. M., ... Mello, C. C. (2009). Distinct Argonaute-Mediated 22G-RNA Pathways Direct Genome Surveillance in the *C. elegans* Germline. *Molecular Cell*, 36(2), 231–244. <https://doi.org/10.1016/j.molcel.2009.09.020>

Guang, S., Bochner, A. F., Pavelec, D. M., Burkhart, K. B., Harding, S., Lachowiec, J., & Kennedy, S. (2008). An Argonaute Transports siRNAs from the Cytoplasm to the Nucleus. *Science*, 321(5888), 537–541. <https://doi.org/10.1126/science.1157647>

Houri-Ze'evi, L., Korem, Y., Sheftel, H., Faigenbloom, L., Toker, I. A., Dagan, Y., ... Rechavi, O. (2016). A Tunable Mechanism Determines the Duration of the Transgenerational Small RNA Inheritance in *C. elegans*. *Cell*, 165(1), 88–99. <https://doi.org/10.1016/J.CELL.2016.02.057>

Huang, X., Fejes Tóth, K., & Aravin, A. A. (2017). piRNA Biogenesis in *Drosophila melanogaster*. *Trends in Genetics*, 33(11), 882–894. <https://doi.org/10.1016/j.tig.2017.09.002>

Ishidate, T., Ozturk, A. R., Durning, D. J., Seth, M., Shirayama, M., Mello Correspondence, C. C., ... Mello, C. C. (2018). ZNFX-1 Functions within Perinuclear Nuage to Balance Epigenetic Signals Article ZNFX-1 Functions within Perinuclear Nuage to Balance Epigenetic Signals. *Molecular Cell*, 70, 639–649. <https://doi.org/10.1016/j.molcel.2018.04.009>

Kawasaki, I., Shim, Y. H., Kirchner, J., Kaminker, J., Wood, W. B., & Strome, S. (1998). PGL-1, a predicted RNA-binding component of germ granules, is essential for fertility in *C. elegans*. *Cell*, 94(5), 635–645. [https://doi.org/10.1016/S0092-8674\(00\)81605-0](https://doi.org/10.1016/S0092-8674(00)81605-0)

Kim, D., Langmead, B., & Salzberg, S. L. (2015). HISAT: a fast spliced aligner with low memory requirements. *Nature Methods*, 12(4), 357–360. <https://doi.org/10.1038/nmeth.3317>

Kim, J. K., Gabel, H. W., Kamath, R. S., Tewari, M., Pasquinelli, A., Rual, J.-F., ... Ruvkun, G. (2005). Functional Genomic Analysis of RNA Interference in *C. elegans*. *Science*, 308(5725), 1164–1167. <https://doi.org/10.1126/science.1109267>

Langmead, B., & Salzberg, S. L. (2012). Fast gapped-read alignment with Bowtie 2. *Nature Methods*, 9(4), 357–359. <https://doi.org/10.1038/nmeth.1923>

Lee, H.-C., Gu, W., Shirayama, M., Youngman, E., Conte, D., & Mello, C. C. (2012). *C. elegans* piRNAs Mediate the Genome-wide Surveillance of Germline Transcripts. *Cell*, 150(1), 78–87. <https://doi.org/10.1016/J.CELL.2012.06.016>

Lev, I., Toker, I. A., Mor, Y., Nitzan, A., Weintraub, G., Bhonkar, O., ... Rechavi, O. (2019). Germ Granules Functions are Memorized by Transgenerationally Inherited Small RNAs. *BioRxiv*, 576934. <https://doi.org/10.1101/576934>

Li, H., Handsaker, B., Wysoker, A., Fennell, T., Ruan, J., Homer, N., ... 1000 Genome Project Data Processing Subgroup. (2009). The Sequence Alignment/Map format and SAMtools. *Bioinformatics*, 25(16), 2078–2079. <https://doi.org/10.1093/bioinformatics/btp352>

Love, M. I., Huber, W., & Anders, S. (2014). Moderated estimation of fold change and dispersion for RNA-seq data with DESeq2. *Genome Biology*, 15(12), 550. <https://doi.org/10.1186/s13059-014-0550-8>

Martin, M. (2011). Cutadapt removes adapter sequences from high-throughput sequencing reads. *EMBnet.Journal*, 17(1), 10. <https://doi.org/10.14806/ej.17.1.200>

Mainpal, R., Nance, J., & Yanowitz, J. L. (2015). A germ cell determinant reveals parallel pathways for germ line development in *Caenorhabditis elegans*. *Development (Cambridge, England)*, 142(20), 3571–3582. <https://doi.org/10.1242/dev.125732>

McMurphy, A. N., Stempor, P., Gaarenstroom, T., Wysolmerski, B., Dong, Y., Aussianikava, D., ... Ahringer, J. (2017). Correction: A team of heterochromatin factors collaborates with small RNA pathways to combat repetitive elements and germline stress. *ELife*, 6. <https://doi.org/10.7554/eLife.32516>

Minkina, O., & Hunter, C. P. (2017). Stable Heritable Germline Silencing Directs Somatic Silencing at an Endogenous Locus. *Molecular Cell*, 65(4), 659-670.e5. <https://doi.org/10.1016/j.molcel.2017.01.034>

Paix, A., Folkmann, A., & Seydoux, G. (2017). Precision genome editing using CRISPR-Cas9 and linear repair templates in *C. elegans*. *Methods*, 121–122, 86–93. <https://doi.org/10.1016/j.ymeth.2017.03.023>

Pak, J., & Fire, A. (2007). Distinct Populations of Primary and Secondary Effectors During RNAi in *C. elegans*. *Science*, 315(5809), 241–244. <https://doi.org/10.1126/science.1132839>

Phillips, C. M., Montgomery, T. A., Breen, P. C., & Ruvkun, G. (2012). MUT-16 promotes formation of perinuclear Mutator foci required for RNA silencing in the *C. elegans* germline. *Genes & Development*, 26(13), 1433–1444. <https://doi.org/10.1101/gad.193904.112>

Phillips, C. M., Brown, K. C., Montgomery, B. E., Ruvkun, G., & Montgomery, T. A. (2015). piRNAs and piRNA-Dependent siRNAs Protect Conserved and Essential *C. elegans* Genes from Misrouting into the RNAi Pathway. *Developmental Cell*, 34(4), 457–465.

<https://doi.org/10.1016/j.devcel.2015.07.009>

Putnam, A., Cassani, M., Smith, J., & Seydoux, G. (2019). A gel phase promotes condensation of liquid P granules in *Caenorhabditis elegans* embryos. *Nature Structural & Molecular Biology*, 26(3), 220–226. <https://doi.org/10.1038/s41594-019-0193-2>

Robinson, J. T., Thorvaldsdóttir, H., Winckler, W., Guttman, M., Lander, E. S., Getz, G., & Mesirov, J. P. (2011). Integrative genomics viewer. *Nature Biotechnology*, 29(1), 24–26.

<https://doi.org/10.1038/nbt.1754>

Robinson, J. T., Thorvaldsdóttir, H., Winckler, W., Guttman, M., Lander, E. S., Getz, G., & Mesirov, J. P. (2011). Integrative genomics viewer. *Nature Biotechnology*, 29(1), 24–26.

<https://doi.org/10.1038/nbt.1754>

Schaner, C. E., Deshpande, G., Schedl, P. D., & Kelly, W. G. (2003). A conserved chromatin architecture marks and maintains the restricted germ cell lineage in worms and flies.

Developmental Cell, 5(5), 747–757. Retrieved from

<http://www.ncbi.nlm.nih.gov/pubmed/14602075>

Schubert, C. M., Lin, R., de Vries, C. J., Plasterk, R. H., & Priess, J. R. (2000). MEX-5 and MEX-6 function to establish soma/germline asymmetry in early *C. elegans* embryos. *Molecular Cell*, 5(4), 671–682. Retrieved from <http://www.ncbi.nlm.nih.gov/pubmed/10882103>

Seth, M., Shirayama, M., Gu, W., Ishidate, T., Conte, D., & Mello, C. C. (2013). The *C. elegans* CSR-1 Argonaute Pathway Counteracts Epigenetic Silencing to Promote Germline Gene Expression. *Developmental Cell*, 27(6), 656–663. <https://doi.org/10.1016/J.DEVCEL.2013.11.014>

Shen, E.-Z., Chen, H., Ozturk, A. R., Tu, S., Shirayama, M., Tang, W., ... Mello, C. C. (2018). Identification of piRNA Binding Sites Reveals the Argonaute Regulatory Landscape of the *C. elegans* Germline. *Cell*, 172(5), 937-951.e18. <https://doi.org/10.1016/j.cell.2018.02.002>

- Shirayama, M., Seth, M., Lee, H.-C., Gu, W., Ishidate, T., Conte, D., & Mello, C. C. (2012). piRNAs initiate an epigenetic memory of nonself RNA in the *C. elegans* germline. *Cell*, 150(1), 65–77. <https://doi.org/10.1016/j.cell.2012.06.015>
- Sijen, T., Steiner, F. A., Thijssen, K. L., & Plasterk, R. H. A. (2007). Secondary siRNAs Result from Unprimed RNA Synthesis and Form a Distinct Class. *Science*, 315(5809), 244–247. <https://doi.org/10.1126/science.1136699>
- Subramaniam, K., & Seydoux, G. (1999). *nos-1* and *nos-2*, two genes related to *Drosophila nanos*, regulate primordial germ cell development and survival in *Caenorhabditis elegans*. *Development (Cambridge, England)*, 126, 4861–4871. Retrieved from <http://www.ncbi.nlm.nih.gov/pubmed/8787767>
- Tabara, H., Hill, R. J., Mello, C. C., Priess, J. R., & Kohara, Y. (1999). *pos-1* encodes a cytoplasmic zinc-finger protein essential for germline specification in *C. elegans*. *Development (Cambridge, England)*, 126(1), 1–11. Retrieved from <http://www.ncbi.nlm.nih.gov/pubmed/9834181>
- Wan, G., Fields, B. D., Spracklin, G., Shukla, A., Phillips, C. M., & Kennedy, S. (2018). Spatiotemporal regulation of liquid-like condensates in epigenetic inheritance. *Nature*, 557(7707), 679–683. <https://doi.org/10.1038/s41586-018-0132-0>
- Wang, G., & Reinke, V. (2008). A *C. elegans* Piwi, PRG-1, Regulates 21U-RNAs during Spermatogenesis. *Current Biology*, 18(12), 861–867. <https://doi.org/10.1016/J.CUB.2008.05.009>
- Wang, J. T., & Seydoux, G. (2013). Germ Cell Specification. In *Advances in experimental medicine and biology* (Vol. 757, pp. 17–39). https://doi.org/10.1007/978-1-4614-4015-4_2
- Wang, J. T., Smith, J., Chen, B.-C., Schmidt, H., Rasoloson, D., Paix, A., ... Seydoux, G. (2014). Regulation of RNA granule dynamics by phosphorylation of serine-rich, intrinsically disordered proteins in *C. elegans*. *ELife*, 3. <https://doi.org/10.7554/eLife.04591>

Wang, E., & Hunter, C. P. (2017). SID-1 Functions in Multiple Roles To Support Parental RNAi in *Caenorhabditis elegans*. *Genetics*, 207(2), 547–557.

<https://doi.org/10.1534/genetics.117.300067>

Winston, W. M., Molodowitch, C., & Hunter, C. P. (2002). Systemic RNAi in *C. elegans* Requires the Putative Transmembrane Protein SID-1. *Science*, 295(5564), 2456–2459.

<https://doi.org/10.1126/science.1068836>

Yang, H., Zhang, Y., Vallandingham, J., Li, H., Li, H., Florens, L., & Mak, H. Y. (2012). The RDE-10/RDE-11 complex triggers RNAi-induced mRNA degradation by association with target mRNA in *C. elegans*. *Genes & Development*, 26(8), 846–856. <https://doi.org/10.1101/gad.180679.111>

Yigit, E., Batista, P. J., Bei, Y., Pang, K. M., Chen, C.-C. G., Tolia, N. H., ... Mello, C. C. (2006). Analysis of the *C. elegans* Argonaute family reveals that distinct Argonautes act sequentially during RNAi. *Cell*, 127(4), 747–757. <https://doi.org/10.1016/j.cell.2006.09.033>

Zhang, C., Montgomery, T. A., Gabel, H. W., Fischer, S. E. J., Phillips, C. M., Fahlgren, N., ... Ruvkun, G. (n.d.). *mut-16* and other mutator class genes modulate 22G and 26G siRNA pathways in *Caenorhabditis elegans*. <https://doi.org/10.1073/pnas.1018695108>

Zhang, C., Montgomery, T. A., Fischer, S. E. J., Garcia, S. M. D. A., Riedel, C. G., Fahlgren, N., ... Ruvkun, G. (2012). The *Caenorhabditis elegans* RDE-10/RDE-11 Complex Regulates RNAi by Promoting Secondary siRNA Amplification. *Current Biology*, 22(10), 881–890. <https://doi.org/10.1016/j.cub.2012.04.011>

Zhang, D., Tu, S., Stubna, M., Wu, W.-S., Huang, W.-C., Weng, Z., & Lee, H.-C. (2018). The piRNA targeting rules and the resistance to piRNA silencing in endogenous genes. *Science*, 359(6375), 587–592. <https://doi.org/10.1126/science.aao2840>

Zhang, Y., Yan, L., Zhou, Z., Yang, P., Tian, E., Zhang, K., ... Zhang, H. (2009). SEPA-1 Mediates the Specific Recognition and Degradation of P Granule Components by Autophagy in *C. elegans*. *Cell*, 136(2), 308–321. <https://doi.org/10.1016/J.CELL.2008.12.022>

Chapter 3: Two parallel sRNA amplification cycles contribute to transgenerational RNAi in *C. elegans*

Authors: John Paul T. Ouyang¹, Lucy Zhang¹, and Geraldine Seydoux^{1,2}.

1. HHMI and Dept. of Molecular Biology and Genetics, Johns Hopkins University School of Medicine, Baltimore MD USA

2. Corresponding author: gseydoux@jhmi.edu

Key Words: RNA-mediated interference, transgenerational epigenetic inheritance, small RNA amplification, Argonautes, nuage.

Abstract:

RNA-mediated interference (RNAi) is a conserved mechanism that uses small RNAs (sRNAs) to tune gene expression. In *C. elegans*, exposure to dsRNA induces the production of gene-specific sRNAs that are propagated to progeny not exposed to the dsRNA trigger. We present evidence that RNAi inheritance is mediated by two parallel sRNA amplification loops. The first loop, dependent on the nuclear Argonaute HRDE-1, targets nascent transcripts, and reduces but does not eliminate productive transcription at the locus. The second loop, dependent on the conserved helicase ZNFX-1, targets mature transcripts and concentrates them in perinuclear condensates (nuage). Each amplification loop generates a distinct class of sRNAs that perpetuate silencing into the next generation, with the ZNFX-1 loop responsible for the bulk of sRNA production. We speculate that nuage is a germline adaptation that allows for cytoplasmic transcripts to be used as templates for robust sRNA amplification in the absence of the original trigger.

Introduction:

RNA-mediated interference (RNAi) is a wide-spread mechanism that employs small RNAs (sRNAs) to modulate gene expression. First discovered as a response to exogenously provided dsRNA in *C. elegans* (Fire et al., 1998), RNAi-like mechanisms have been described in a broad range of organisms, from yeast to mammals. At the core of the RNAi machinery are RNA-induced silencing complexes (RISC) consisting of ~20-base single stranded RNAs complexed with Argonaute proteins. RISC recognizes complementary RNAs via base pairing with the sRNA guide and effects silencing by reducing RNA stability and/or translation efficiency (Bartel, 2018; Billi et al., 2014; Carthew & Sontheimer, 2009). Certain RISC complexes also recognize nascent transcripts and interfere with productive transcription by stalling RNA polymerase, RNA processing and/or recruiting chromatin modifiers to the locus (Billi et al., 2014; Castel & Martienssen, 2013; Weiser & Kim, 2019). In many organisms, sRNA pathways depend on cycles that amplify the production of sRNAs to achieve maximal silencing (Billi et al., 2014; Czech & Hannon, 2016). In *Drosophila*, a complex “ping pong” cycle in perinuclear condensates amplifies the processing of genomically-encoded precursor transcripts containing sRNAs that target active transposable elements (piRNAs; Czech and Hannon, 2016). In *S. pombe*, the nuclear RISC-like complex (RITS) recruits an RNA-dependent RNA polymerase (RdRP) to the targeted locus (Martienssen & Moazed, 2015). The RdRP uses nascent transcripts as templates for continued synthesis of sRNAs that feed back into RITS (Martienssen & Moazed, 2015). In both cases, the sRNA amplification loops depend on transcription of the locus targeted for silencing to supply the template necessary to stimulate the processing (*Drosophila*) or the *de novo* synthesis (*S. pombe*) of the relevant sRNAs.

As in *S. pombe*, sRNA amplification in *C. elegans* involves the activity of RdRPs that synthesize new sRNAs on transcripts recognized by RISC complexes. Two sRNA amplification mechanisms have been described. A first mechanism involves “primary” sRNAs derived from genomically encoded loci (e.g. piRNAs) or from dsRNA processed by the RNA endonuclease Dicer (Billi et al., 2014). Recognition of complementary transcripts by primary sRNAs, complexed with primary Argonautes (e.g. RDE-1), leads to their cleavage by the endonuclease RDE-8 and tailing of the 5' fragment by the poly(UG) polymerase MUT-2/RDE-3 (Shukla et al., 2020; Tsai et al.,

2015). The “pUG” tail recruits RdRPs that synthesize “secondary” sRNAs near the cleavage site (Shukla et al., 2020). Secondary sRNAs in turn associate with secondary Argonautes (WAGOs) to trigger the degradation of complementary transcripts in the cytoplasm by an unknown mechanism (Yigit et al., 2006). A second cycle depends on the Argonaute HRDE-1, which shuttles between the cytoplasm and nucleus (Ashe et al., 2012; Buckley et al., 2012; Shirayama et al., 2012; Sapetschnig et al., 2015). This cycle is less well understood but is thought to function similarly to RITS in *S. pombe*, coordinating heterochromatin deposition and sRNA synthesis by binding to nascent transcripts (Billi et al., 2014; Martienssen & Moazed, 2015 ; Weiser and Kim, 2019).

A fascinating aspect of RNAi-induced silencing in *C. elegans* is the ability for the silenced state to be passed on to progeny even in the absence of the initial trigger (Fire et al., 1998; Grishok et al., 2000; Alcazar et al., 2008; Lev et al., 2017; Weiser and Kim, 2019). pUGylated transcripts have been observed in the progeny of worms exposed to dsRNA, raising the possibility that a pUGylation-dependent sRNA amplification cycle may be heritable (Shukla et al., 2020, 2021). An early study examining RNAi in somatic tissues of *C. elegans* suggested, however, that only primary Argonautes can initiate sRNA amplification (Pak et al., 2012); secondary Argonautes, in contrast, only target cognate mRNAs for degradation (Pak et al., 2012). Subsequent studies showed that production of “tertiary” sRNAs is allowed in the germline and depends on HRDE-1 and other nuclear RNAi factors (Sapetschnig et al., 2015). Unlike secondary sRNAs which map near the site of the primary sRNA trigger, tertiary sRNAs generated through the nuclear RNAi pathway map throughout the transcript possibly because they are synthesized by a nuclear RdRP that uses nascent transcripts as templates (Sapetschnig et al., 2015). Cytoplasmic factors have also been implicated in transgenerational inheritance including the Argonaute WAGO-4 and the helicase ZNFX-1 (Ishidate et al., 2018; Wan et al., 2018; Xu et al., 2018). Whether these factors function in the HRDE-1 cycle or a different sRNA amplification cycle was not known.

In germ cells, several components of the RNAi machinery are concentrated in condensates at the nuclear periphery. Five condensate types have been described so far, including P granules (Strome & Wood, 1982), Mutator foci (Phillips et al., 2012), R2 bodies (Yang et al., 2014), Z granules (Wan et al., 2018), and SIMR foci (Manage et al., 2020). In this study, we

refer to these condensates collectively as “nuage” following the convention for perinuclear condensates in *Drosophila* and mammalian systems (Dodson and Kennedy, 2020). Nuage condensates often overlay nucleopores and have been proposed to serve as compartments specialized in transcript surveillance and sRNA amplification (Voronina et al., 2011; Gao and Arkov, 2013; Dodson and Kennedy, 2020; Sundby et al., 2021). What specific functions these compartments play in RNAi and transgenerational inheritance is not known.

In this study, we examined the fate of germline mRNAs in animals exposed (by feeding) to a gene-specific dsRNA trigger. Our findings indicate that the HRDE-1 cycle, although sufficient to partially silence the locus, is not sufficient for robust inheritance of the silenced state. A second cycle involving the Z granule component ZNFX-1 is also required in parallel. We find that ZNFX-1 is responsible for localization of targeted mRNAs to nuage, and for transgenerational pUGylation and sRNA amplification. Together, our findings suggest that nuage condensates represent privileged compartments where non-primary sRNAs are permitted to initiate new rounds of pUGylation and sRNA amplification on mature transcripts exported from the nucleus.

Results:

Changes in the abundance of nascent and cytoplasmic transcripts appear within hours of exposure to the dsRNA trigger

To examine the consequences of RNAi-induced gene silencing, we first used fluorescent *in situ* hybridization (FISH) to examine changes in the level and localization of a targeted transcript. We chose *mex-6* as a model transcript because 1) *mex-6* is expressed in the pachytene region of the adult germline, where nuage condensates are prominent (Fig 1A, 1B, 1C), 2) *mex-6* is minimally targeted by endogenous sRNAs under non-RNAi conditions (Fig S1A), and 3) *mex-6* is a non-essential maternal-effect gene (redundant with *mex-5*), whose silencing does not affect germline development or morphology (Schubert et al., 2000).

The germline of adult *C. elegans* hermaphrodites is a syncytial tissue organized in two tubes folded into distal and proximal arms. Germ cells are arranged in order of maturation with mitotic stem cells at the distal-most end, followed by germ cells that have initiated meiosis (pachytene), and growing oocytes in the proximal arm (Fig. 1A). Like other maternal transcripts,

mex-6 RNA is transcribed in nuclei in the pachytene region and accumulates in the cytoplasm shared by pachytene nuclei (rachis of the distal arm) and growing oocytes (Chi and Reinke, 2006). As expected, by FISH, we detected *mex-6* transcripts diffuse in the rachis and cytoplasm of growing oocytes and concentrated in bright nuclear puncta within pachytene nuclei (but not in oocyte nuclei; Fig 1B, 1C). At high magnification, the nuclear puncta overlapped with DAPI staining and occasionally resolved into twin or triplet dots (Fig. 1C), consistent with tight pairing of replicated homologous chromosomes in pachytene nuclei (Lui & Colaiácovo, 2013). Two-color RNA FISH against *mex-6* and a transcript expressed from a linked locus (*puf-5*) revealed closely linked puncta in pachytene nuclei, confirming that the nuclear puncta correspond to nascent transcripts at the *mex-6* and *puf-5* loci.

To silence the *mex-6* gene, we designed a 600bp double-stranded RNA trigger targeting the 3' most region of the *mex-6* transcript, including the 3' UTR. The *mex-6* trigger was designed to avoid overlap with the FISH probes used to visualize the *mex-6* transcript (Fig S2A). Synchronized first-day adult hermaphrodites were plated onto bacteria expressing the *mex-6* trigger (*mex-6* RNAi) or a control vector trigger (no-RNAi). Animals were collected for FISH after 2, 4, 6, 8, and 24 hours of feeding and nuclear and cytoplasmic *mex-6* FISH signals were quantified (Methods). We first detected a reduction in FISH signal in the cytoplasm of oocytes after 4 hours of treatment, culminating in > 90% decrease by 24 hours (Fig 2A, 2B), confirming the efficacy of our RNAi feeding protocol. Starting at the 6-hour time point, we also detected an increase in the intensity distribution of nuclear puncta in the pachytene region (Fig 2A, 2C, 2D). The intensity distribution remained elevated through the 8-hour time point (Fig 2C, 2D), before diminishing slightly by the 24-hour time-point (Fig 2A, 2C). We conclude that, in the first 24 hours of exposure to the dsRNA trigger, RNAi induces a transient increase in the accumulation of nascent transcripts at the locus and a steady decrease in cytoplasmic transcripts.

Targeted transcripts accumulate in nuage

Beginning at the 4-hour time point, we also noticed accumulation of *mex-6* transcripts in micron-sized clusters in the cytoplasm of growing oocytes (Fig 2A, 2E, 2F). Colocalization with nuage markers ZNFX-1 and PRG-1 revealed that the clusters coincide with nuage (Fig 2E, S2B). At

the 6 and 8-hour time points, we also detected *mex-6* accumulation in nuage in the loop and pachytene region (Fig 2A). At the 24-hour time point, *mex-6* accumulation in nuage in oocytes was strongly diminished, mirroring the strong depletion of *mex-6* transcripts in the cytoplasm (Fig 2A, 2B). However, *mex-6* signal could still be detected in nuage in the pachytene region where the *mex-6* locus is transcribed (Fig S2C). We conclude that *mex-6* transcripts accumulate in nuage throughout the RNAi response. Note that the resolution of our *in situ* protocol did not allow us to distinguish whether targeted RNAs localized to all or a subset of condensate types in nuage.

RNAi-induced changes in nascent and cytoplasmic transcripts require *rde-1* and *mut-16* activity

To determine whether the changes observed were dependent on the RNAi machinery, we examined *rde-1* and *mut-16* mutants. RDE-1 is the Argonaute that recognize primary sRNAs derived from exogenous triggers (Tabara et al., 1999; Yigit et al., 2006), and MUT-16 is required for amplification of secondary sRNAs (Zhang et al., 2011). We found that *rde-1* and *mut-16* mutants were completely defective in the RNAi response (Fig S2D, S2E). *rde-1* and *mut-16* animals exposed to the *mex-6* trigger resembled animals exposed to the no-RNAi control trigger at both the 8 and 24-hour time points and showed none of the changes observed in wild-type animals exposed to the dsRNA trigger (Fig S2D, S2E). We conclude that changes in the level and localization of nascent and cytoplasmic transcripts depend on initiation of the RNAi response by RDE-1 and synthesis of secondary sRNAs.

RNAi-induced changes in nascent and cytoplasmic transcripts are inherited transgenerationally

To examine inheritance of the RNAi response, we performed FISH analysis on the progeny (F1) of hermaphrodites fed the dsRNA trigger (P0). P0 hermaphrodites at the 24-hour time point were bleached, and F1 embryos were synchronized and plated onto non-RNAi plates starting at the L1 stage. The F1s were raised to the adult stage (in the absence of the RNAi trigger) and processed for FISH. We observed a strong reduction in *mex-6* RNA throughout the germline of F1 animals compared to non-RNAi controls (Fig. 3A, S3A). The average intensity of nuclear signals in the pachytene region was reduced by ~50% compared to no-RNAi controls (Fig 3B). Despite this strong reduction, we still detected transcripts in perinuclear dots overlapping with nuage

markers in the pachytene region (Fig 3C, S3B). In contrast, little to no nuage accumulation was evident in oocytes (Fig 3A, S3C). Similar observations were made in the F2 generation (Fig S3C). These observations suggest that, despite a reduction in nascent transcripts, some *mex-6* transcripts are still exported from the nucleus and allowed to accumulate at least transiently in nuage in the pachytene region in F1 and F2 animals.

***hrde-1* is required for nascent transcripts to respond to RNAi in P0 and F1 animals**

HRDE-1/WAGO-9 is a germline-specific nuclear Argonaute required for trans-generational inheritance of the RNAi-induced silenced state (Ashe et al., 2012; Buckley et al., 2012; Shirayama et al., 2012). We found that *hrde-1* mutants mounted a normal RNAi response in oocytes of P0 hermaphrodites: we observed loss of *mex-6* RNA in the cytoplasm and accumulation in nuage in *hrde-1* mutants as in wild-type (Fig 4A, S4A). We observed, however, no change in the intensity distribution of nuclear puncta in the pachytene region (Fig 4A, 4B, 4C), consistent with a failure to silence the *mex-6* locus. To explore this possibility further, we examined the accumulation of *mex-6* transcripts in the rachis, the shared cytoplasm immediately adjacent to pachytene nuclei. In wild-type animals, *mex-6* levels in the rachis declined by >90% at the 24-hour time point (Fig 4D, 4E). In contrast, in *hrde-1* mutants, *mex-6* levels in the rachis were reduced only by ~50% at the 24-hour time point (Fig 4D, 4E). These observations suggest that *hrde-1* mutants fail to interfere with the production of *mex-6* transcripts in P0 hermaphrodites. We obtained similar results in a strain mutated for another component of the nuclear RNAi machinery, *nrde-2* (Fig S4B).

Failure to silence the *mex-6* locus was also observed in *hrde-1* F1 progeny. The distribution of nuclear puncta intensity was similar in *hrde-1* F1s and no-RNAi controls (Fig 4A, 4C). As in wild-type, however, *hrde-1* F1 progeny accumulated *mex-6* transcripts in nuage in the pachytene region (Fig S4C). *mex-6* RNA levels in the pachytene rachis were higher in *hrde-1* F1 progeny than in wild-type F1s but averaged only 50% of that observed in the no-RNAi controls (Fig S4D). We conclude that *hrde-1* is required for silencing of the locus in P0 and F1 animals (nuclear response) but is not essential for RNA degradation in the cytoplasm and accumulation in nuage in P0 and F1 animals (cytoplasmic response).

***znfx-1* is required for accumulation of targeted transcripts in nuage in P0 and F1 animals**

ZNFX-1 is an SF1 helicase-domain containing zinc finger protein that, like HRDE-1, is required for trans-generational inheritance of the RNAi-induced silenced state (Ishidate et al., 2018; Wan et al., 2018). Unlike HRDE-1, which is primarily nuclear, ZNFX-1 localizes to specific condensates in nuage called Z granules (Wan et al., 2018). We found that, in *znfx-1* P0 animals, *mex-6* transcripts were rapidly degraded as in wild-type (Fig S5A). *mex-6* transcripts, however, failed to accumulate in nuage (Fig 5A, 5B).

We detected an increase in the intensity distribution of *mex-6* nuclear puncta in *znfx-1* mutants at the 4-hour time point, earlier than in wild-type (8 hour) (Fig S5A,SB). This premature peak in nuclear signals was followed by a subsequent decrease to levels lower than the non-RNAi condition by the 24-hour time point in *znfx-1* mutants (Fig S5A,B). No changes in nuclear signal were observed in *znfx-1; hrde-1* double mutant animals, indicating that the nuclear response in *znfx-1* mutants was dependent on *hrde-1*, as in wild-type (Fig S5C,S5D). We conclude that *znfx-1* is required for robust recruitment of *mex-6* transcripts to nuage in P0 animals but is not required for RNA degradation in the cytoplasm or for engagement of the nuclear RNAi machinery in P0 animals. Despite a failure to silence the *mex-6* locus and to enrich *mex-6* transcripts in nuage, *znfx-1; hrde-1* P0s still showed rapid loss of cytoplasmic *mex-6* RNA throughout the germline, confirming that neither ZNFX-1 nor HRDE-1 is required for RNA turn over in the cytoplasm of P0 animals (Fig S5C).

In *znfx-1* F1 animals, we observed a partial (~50%) reduction in cytoplasmic accumulation of *mex-6* transcripts in the pachytene rachis and no accumulation in nuage in the pachytene region (Fig 5D,5E,S5E). The intensity distribution of nuclear puncta was reduced as observed in wild-type F1s (Fig S5B). This reduction was dependent on *hrde-1*, as nuclear puncta intensities of *znfx-1; hrde-1* F1s matched that of the no-RNAi controls (Fig S5C, S5D). We conclude that *znfx-1* is not required for silencing of the locus in P0 and F1 animals (nuclear response) but is required for the accumulation of targeted transcripts in nuage in P0 and F1 animals (cytoplasmic response).

***hrde-1* and *znfx-1* are required additively for maximal silencing in F1 animals**

Unlike in P0 animals, cytoplasmic *mex-6* RNA levels in *znfx-1; hrde-1* F1s were indistinguishable from no-RNAi controls, indicating that *znfx-1* and *hrde-1* are both required for maximal silencing in F1 animals (Fig 5C, 5D). To examine this further, we compared *mex-6* RNA levels using RT-PCR in wild-type, *znfx-1*, *hrde-1*, and *znfx-1; hrde-1* double mutants F1 animals (Fig S6A). These experiments confirmed partial silencing of *mex-6* transcripts in the single mutants, and complete loss of silencing in the double mutant (Fig S6A). We obtained similar results when targeting two other germline-expressed genes by RNAi (*oma-1* and *puf-5*) (Fig S6B, S6B). We conclude that *hrde-1* and *znfx-1* contribute independently to silencing in F1s and are required additively for maximal silencing.

***hrde-1* and *znfx-1* are responsible for distinct populations of sRNAs in F1 progeny**

The additive phenotype of the *znfx-1; hrde-1* double mutant suggested that *hrde-1* and *znfx-1* function in separate mechanisms to maintain nuclear and cytoplasmic silenced states. To examine this possibility further, we sequenced sRNAs in wild-type, *hrde-1*, *znfx-1* and *znfx-1; hrde-1* F1 adult progeny of *mex-6* fed P0s. As expected, wild-type F1s exhibited a 23-fold increase in sRNAs mapping to the *mex-6* locus compared to no-RNAi controls, with a dominant peak corresponding to the location targeted by the dsRNA trigger fed to the P0 generation (Fig 6A, 6B). A similar pattern was observed in *hrde-1* mutants, although the overall increase was roughly only 83% that observed in wild-type (Fig 6A, 6B). In contrast, *znfx-1* mutants only showed a modest increase in sRNAs corresponding to 6% that of wild-type (Fig 6A, 6B). Strikingly, the distribution of sRNAs in *znfx-1* mutants showed no preference for the region targeted by the trigger (Fig 6A). Instead sRNAs appeared distributed throughout the *mex-6* locus, with a slight bias for the 5' end of the transcript. Consistent with the complete lack of inherited RNAi response, *znfx-1; hrde-1* double mutants exhibited no significant differences in sRNAs across the *mex-6* locus in *mex-6* RNAi vs. control RNAi conditions (Fig 6A, 6B). These observations suggest that *hrde-1* and *znfx-1* are required for the amplification of distinct pools of sRNAs across the *mex-6* locus, with *znfx-1* being required for the majority of sRNA generation, especially around the sequence targeted by the original trigger. We noticed that the number of sRNA reads mapping to the *mex-6* locus in

znfx-1 and *hrde-1* single mutants added up to only 89% of the reads observed in wild-type F1s (Fig S6G; see Methods). This observation confirms that the ZNFX-1 and HRDE-1 amplification cycles function mostly independently, with possibly some synergy between the two cycles accounting for ~10% of sRNAs observed in wild-type.

To determine whether *znfx-1* is also required for sRNA amplification in P0 animals, we sequenced sRNAs in wild-type and *znfx-1* hermaphrodites at different time points following feeding onset. We observed ~200-fold increase in sRNA accumulation at the *mex-6* locus in wild-type and *znfx-1* P0 animals compared to no-RNAi conditions (Fig S6D). sRNAs levels in *znfx-1* mutants were slightly lower than in wild-type (~16% reduction), suggesting that *znfx-1*, although not essential, contributes modestly to sRNA amplification in P0s. In contrast, in F1 progeny, *znfx-1* is required for the majority of sRNA production (Fig. 6A-B), especially within the region corresponding to the trigger.

***znfx-1*, but not *hrde-1*, is required for sustained accumulation of pUGylated transcripts in F1 progeny**

sRNAs mapping to the trigger region can be derived directly by Dicer cleavage of the dsRNA trigger (1° sRNAs) or from RdRPs that use pUGylated transcripts as templates to generate 2° sRNAs (Shukla et al., 2020, 2021). To determine whether *hrde-1* or *znfx-1* are required for pUGylation of the *mex-6* RNA, we amplified pUGylated *mex-6* transcripts from RNA extracted from wild-type, *hrde-1*, *znfx-1*, and *znfx-1; hrde-1* F1 animals. As expected, wild-type F1 animals exhibited abundant pUGylated *mex-6* transcripts (Fig 6C). pUGylated *mex-6* transcripts were also observed in *hrde-1* F1 animals (Fig 6C). In contrast no pUGylated *mex-6* transcripts were observed in *znfx-1* or *znfx-1; hrde-1* F1 adult animals (Fig 6C), indicating that ZNFX-1 is required for accumulation of pUGylated mRNAs in F1 adult progeny. Similar results were observed in the F1 progeny of *puf-5* and *oma-1* RNAi-ed P0s (Fig S6E, S6F).

To determine whether *znfx-1* is also required for pUGylation in animals exposed to the dsRNA trigger, we repeated the pUGylation assays on *znfx-1* P0 worms at 8 and 24 hours after RNAi exposure. We observed robust accumulation of pUGylated *mex-6* transcripts, indicating that *znfx-1* is not required for the initial production of pUGylated RNAs in animals exposed to the

dsRNA trigger (Fig 6D). We also detected pUGylated mRNAs in *znfx-1* F1 embryos (Fig 6E). We conclude that *znfx-1* is not required for pUGylation in P0 animals or for transfer of pUGylated transcripts to F1 embryos. ZNFX-1, however, is required for sustained production of pUGylated RNAs in adult F1 animals.

ZNFX-1 associates with pUGylated *mex-6* transcripts and is required for accumulation of pUGylated RNAs in germ granules

ZNFX-1 immunoprecipitates with transcripts targeted by RNAi (Wan et al., 2018). To determine whether ZNFX-1 interacts with pUGylated transcripts, we immunoprecipitated FLAG-tagged ZNFX-1 in animals exposed to *puf-5* or *mex-6* RNAi triggers following 12 hours of RNAi. We performed reverse transcription reactions on the immunoprecipitates using a poly(UG) specific RT primer to amplify pUGylated RNAs (Shukla et al., 2020, 2021). We found that ZNFX-1 co-immunoprecipitated with *mex-6* pUGylated transcripts in animals exposed to the *mex-6* trigger and with *puf-5* pUGylated transcripts in animals exposed to the *puf-5* trigger (Fig 7A, S7A, S7B). We conclude that ZNFX-1 associates with pUGylated RNAs.

Animals not exposed to exogenous RNAi triggers naturally contain pUGylated transcripts, due to targeting by endogenous sRNAs (Shukla et al., 2020). Endogenous pUGylated transcripts can be visualized by FISH using a poly(AC) probe and have been reported to accumulate in nuage (Shukla et al., 2020). Consistent with this report, we detected endogenous pUGylated transcripts in nuage in the pachytene region and in oocytes (Fig 7B, S7C, S7D). Remarkably, in *znfx-1* mutant germlines, accumulation of pUGylated transcripts in nuage was strongly reduced in both the pachytene region and in oocytes (Fig 7B, S7C, S7D). We conclude that ZNFX-1 is required for accumulation (and/or possibly synthesis) of endogenous pUGylated RNAs in nuage.

Discussion:

In this study, we have used fluorescent *in situ* hybridization, small RNA sequencing and pUGylation assays to examine the fate of mRNAs targeted for silencing by feeding RNAi. Together with prior studies, our findings suggest the following model for silencing by an exogenous dsRNA trigger (Fig. 7C). Primary siRNAs derived from the double-stranded RNA trigger load onto the

primary Argonaute RDE-1. RDE-1 recognize complementary transcripts and marks them for cleavage, pUGylation, and synthesis of secondary sRNAs by RNA-dependent RNA polymerases (Tabara et al., 1999; Sijen et al., 2001; Yigit et al., 2006; Sijen et al., 2007; Pak et al., 2007; Tsai et al., 2015; Shukla et al., 2020). Secondary sRNAs are loaded onto secondary Argonautes (HRDE-1 and WAGOs) that, in turn, activate three parallel silencing pathways. In the first pathway, WAGOs target transcripts in the cytoplasm for rapid degradation by an unknown mechanism. In the second pathway, HRDE-1 shuttles into the nucleus to initiate “nuclear RNAi”, a silencing program that suppresses but does not eliminate transcription of the locus. In the third pathway, WAGOs that associate with ZNFX-1 recruit a subset of targeted transcripts to germ granules and initiate a new cycle of pUGylation and sRNA amplification. Only the HRDE-1 and ZNFX-1 cycles generate “tertiary” sRNAs that feedback into their respective cycles to generate parallel, self-reinforcing sRNA amplification loops. The HRDE-1 and ZNFX-1 amplification loops are transmitted to the next generation independently of each other and both are required for maximum silencing in F1 progeny. In the following sections, we summarize evidence supporting the three silencing pathways and discuss remaining open questions.

Pathway 1: RDE-1 and MUT-16 dependent amplification of secondary sRNAs induces RNA degradation in the cytoplasm

Under our feeding RNAi conditions, we detected a reduction in transcript levels in the cytoplasm after 4 hours of feeding, eventually reaching 95% reduction by 24 hours. Loss of transcripts was most rapid in growing oocytes, consistent with prior reports showing that trigger RNAs enter the germline in a manner dependent on the oocyte yolk receptor RME-2 (Marré et al., 2016; Wang & Hunter, 2017). As expected (Tabara et al., 1999; Zhang et al., 2011; Phillips et al., 2012), mRNA degradation was dependent on the primary Argonaute RDE-1 and on MUT-16, a scaffolding protein required for amplification of secondary sRNAs.

mRNAs targeted by miRNAs for degradation have been reported to enrich in P bodies (Liu et al., 2005; Shih et al., 2011), RNA granules in the cytoplasm that contain components of the RNA degradation machinery (Luo et al., 2018). In our feeding experiments, we observed enrichment of targeted mRNAs in clusters that overlapped with nuage components, but this

enrichment did not appear linked to degradation. Most strikingly, no nuage enrichment was observed in *znfx-1* mutants despite normal RNA degradation in these animals. We conclude that, unlike miRNA-induced RNA degradation, RNAi-induced RNA degradation does not require visible enrichment of RNA in cytoplasmic granules. The robust sRNA amplification observed in *znfx-1* P0 animals also suggests that secondary sRNA amplification initiated by primary sRNAs occurs in bulk cytoplasm or at a minimum does not require accumulation of targeted transcripts in granules. We cannot exclude, however, that transit through nuage or some other RNA granules, in the absence of visible accumulation, is required for secondary sRNA amplification and/or RNA degradation. The RDE-1-initiated cycle of pUGylation and sRNA amplification is sufficient to eliminate most cytoplasmic transcripts in animals exposed to the dsRNA trigger. This cycle is not self-perpetuating, however, and on its own will eventually self-extinguish leaving no memory of the RNAi response.

Pathway II: HRDE-1-dependent silencing targets nascent transcripts within hours of dsRNA exposure and reduces, but does not eliminate, transcription of the targeted locus

Quantification of FISH signals at the targeted locus revealed a transient increase in nascent transcripts starting at 6 hours of feeding, followed by a subsequent decrease in signal at 24 hours in P0 animals, and even lower levels in F1 animals. This response requires the Argonaute HRDE-1, a component of the nuclear RNAi pathway. We speculate that the initial increase in FISH signal reflects stalling of RNA polymerase II and/or stalling of pre-mRNA processing causing nascent transcripts to accumulate at the locus. Stalling of RNA polymerase has previously been implicated in nuclear RNAi (Guang et al., 2010; Liao et al., 2020). Additionally, several lines of evidence have suggested a close connection between RNAi and splicing, including apparent co-evolution of the RNAi and splicing machineries (Tabach et al., 2013), splicing factors identified as HRDE-1 interactors (Akay et al., 2017; Tyc et al., 2017), sRNA defects associated with mutations or knock down of spliceosome components (Kim et al., 2005; Newman et al., 2018), and insensitivity to nuclear RNAi of an endogenous transcript whose introns were removed by genome editing (Wan et al., 2020). It will be interesting to determine which components of the nuclear RNAi machinery in addition to HRDE-1 are required for the transient increase in nascent

transcripts at the locus and whether a slow-down in RNA polymerase elongation or splicing is primarily responsible.

A recent study (Yang et al., 2021) also reported a transient increase in RNA signal in the pachytene region early in the RNAi response but interpreted this observation differently. In their analysis, using *oma-1* as a gene model, they reported that the bright RNA foci overlapped with a single enlarged perinuclear nuage condensate (P granule) outside each pachytene nucleus. Although we did observe targeted transcripts in nuage (see below), they did not concentrate in just one condensate, nor did we observe enlargement of a single P granule per nucleus under live or fixed conditions (Fig. S8A, S8B). In our hands, the bright foci did not correspond to P granules but rather overlapped with DAPI at the nuclear periphery and often could be resolved in two or more closely apposed dots (<150nm; Fig S8C), consistent with nascent transcripts at the locus, which at this stage of germline development is present in four tightly synapsed copies. In their analyses, Yang et al. reported that the *oma-1* locus and associated nascent transcripts appear as two well-separated (~0.5um) foci in the center of pachytene nuclei that eventually move to the periphery and merge near the enlarged P granule during the RNAi response. These observations were based on a new DNA/RNA hybridization protocol and contrast with several studies using standard DNA *in situ* methods that have demonstrated that, throughout the pachytene region, homologous chromosomes are tightly synapsed at the nuclear periphery and excluded from a central, DNA-depleted zone occupied by the nucleolus (Phillips and Dernburg, 2006; Dernburg et al., 1998; Lui & Colaiácovo, 2013; Macqueen et al., 2002; Zalevsky et al., 1999).

At 24 hours post-feeding, we observed a decrease in the accumulation of nascent transcripts in the pachytene region, which became even more acute in F1 animals. We speculate that the decrease reflects a reduction in transcription initiation at the locus. The nuclear RNAi machinery deposits chromatin marks at the locus predicted to decrease transcription (Burkhart et al., 2011; Burton et al., 2011; Gu et al., 2012; Mao et al., 2015; Schwartz-Orbach et al., 2020). We note, however, that despite the apparent decrease in transcriptional output, we continued to observe transcripts in perinuclear nuage even in F1 animals, indicating that a baseline level of transcription and export is maintained at the silenced locus. In *S. pombe*, transcription is also maintained at the silent locus, but export is blocked and replaced by rapid degradation of nuclear

transcripts (Martienssen & Moazed, 2015). We speculate that this difference reflects a *C. elegans*-specific adaptation that allows mature transcripts to be used as templates for sRNA amplification in perinuclear condensates (see Pathway III).

sRNA sequencing analyses suggest that the HRDE-1 cycle generates sRNAs that map throughout the locus without preference for the trigger area. Interestingly, HRDE-1-dependent sRNAs exhibit a slight preference for the 5' end of the transcript. A similar pattern was described previously in the context of transgenes and endogenous transcripts targeted by endogenous sRNA pathways and also was found to be dependent on the nuclear RNAi machinery (Sapetschnig et al., 2015). One hypothesis is that the 5' bias is due to RNA-dependent RNA polymerases that use nascent transcripts as templates for sRNA synthesis as described in *S. pombe*. Consistent with this hypothesis, the nuclear RNAi machinery has been shown to interact with pre-mRNAs at the locus, which naturally exhibit a 5' bias (Burkhart et al., 2011; Guang et al., 2010). We suggest that HRDE-1, initially loaded with secondary sRNAs templated in the cytoplasm, initiates a nuclear cycle of sRNA amplification by recruiting an RdRP to nascent transcripts. The HRDE-1 cycle generates "tertiary" sRNAs which in turn become complexed with HRDE-1 to perpetuate the cycle. The RNA-dependent RNA polymerase (RdRP) EGO-1 has been reported to localize within nuclei (Claycomb et al., 2009), but a specific molecular interaction between EGO-1 and HRDE-1 has not been reported. Analyses of silencing in operons, however, has provided indirect evidence for an RdRP activity in nuclei. Operons are loci that generate long primary transcripts that are cleaved in the nucleus into multiple transcripts by trans-splicing (Agabian, 1990). Several studies have documented that sRNA production initiated on a specific transcript spreads to other transcripts in the same operon, implying that nascent transcripts are used as templates for sRNA production before trans-splicing (Bosher et al., 1999; S. Guang et al., 2008; Ouyang et al., 2019; Sapetschnig et al., 2015). Although we favor a model where HRDE-1 and associated machinery use nascent transcripts to direct sRNA synthesis (Fig. 7C), we cannot exclude the possibility that HRDE-1-dependent sRNA amplification actually occurs outside of the nucleus. For example, HRDE-1 could deposit marks on nascent transcripts that target them for sRNA amplification after export into the cytoplasm. Investigation into the factors that support HRDE-1-dependent sRNA production is an important future goal.

Pathway III: ZNFX-1 memorializes the dsRNA trigger by initiating a self-perpetuating pUGylation/sRNA amplification cycle, likely within nuage

Our genetic analyses indicate that the HRDE-1 amplification cycle is not sufficient for maximum silencing in F1 progeny. A second cycle dependent on the nuage protein ZNFX-1 is also required. Unlike the HRDE-1 cycle, the ZNFX-1 cycle generates sRNAs focused primarily on the area of the transcript targeted by the original trigger. Consistent with that observation, ZNFX-1 (but not HRDE-1) is required to maintain the production of pUGylated transcripts in adult F1s. Interestingly, ZNFX-1 is NOT required for the initial production of pUGylated transcripts in P0 animals exposed to the trigger. These observations suggest that ZNFX-1 becomes essential for pUGylation when the dsRNA trigger and primary sRNAs become limiting. One possibility is that ZNFX-1 extends the half-life of pUGylated mRNAs by protecting them from being targeted for degradation by secondary Argonautes. Additionally, ZNFX-1 could also function as a bridge between secondary Argonautes and the pUGylation machinery, allowing secondary Argonautes to generate new pUGylated transcripts for synthesis of “tertiary” sRNAs. Consistent with this model, ZNFX-1 has been reported to immunoprecipitate in complexes that also contain the secondary Argonautes WAGO-1 and WAGO-4 and the RNA-dependent RNA polymerase EGO-1 (Barucci et al., 2020; Ishidate et al., 2018; Wan et al., 2018). We suggest that tertiary sRNAs generated in the ZNFX-1 loop feedback into additional cycles of pUGylation and sRNA amplification to ensure trans-generational propagation of sRNA amplification. Because this self-perpetuating cycle is initiated by secondary sRNAs that target the trigger region, the ZNFX-1 cycle “memorializes” the position of the trigger. A role for ZNFX-1 in a self-propagating sRNA amplification cycle is consistent with the role proposed for Hrr1, the *S. pombe* ortholog of ZNFX-1, which functions in a nuclear complex with an RNA-dependent RNA polymerase to amplify sRNAs off nascent transcripts (Motamedi et al., 2004). Unlike Hrr1 which has been shown to be nuclear (Motamedi et al., 2004), ZNFX-1 is prominent in nuage (Ishidate et al., 2018; Wan et al., 2018) and is required to concentrate targeted transcripts (and pUGylated RNAs) to nuage (this work). We speculate therefore that *C. elegans* ZNFX-1 functions outside of the nucleus on mature transcripts exported from the nucleus into nuage.

It has been suggested that, in *C. elegans*, initiation of sRNA amplification by non-primary sRNA/Argonaute complexes is limited *in vivo* to prevent dangerous run-away loops (Pak et al., 2012). We speculate that enrichment of ZNFX-1 in nuage serves to place the ZNFX-1 amplification loop under tight regulation by competing sRNA pathways (such as the piRNA pathway) that protect transcripts from permanent silencing (Shukla et al., 2021). Consistent with this, loss of the nuage component PRG-1 causes indefinite silencing and pUGylation of RNAi-silenced transcripts (Shukla et al., 2021). Enrichment of pUGylated transcripts in nuage may also serve to protect them from degradation in the cytoplasm. By maintaining a transcript pool in nuage, ZNFX-1 prevents self-extinction of the RNAi response that might arise as a consequence of rapid transcript turn over in the cytoplasm. ZNFX-1 homologs in mice and humans function in the primary immune response against RNA viruses and bacteria (Wang et al., 2019; Le Voyer et al., 2021; Vavassori et al., 2021). We do not yet know how these functions relate to those described here for *C. elegans* ZNFX-1 and described previously for *S. pombe* Hrr1 (Motamedi et al., 2004). We speculate that a common function for ZNFX-1 homologs across eukarya may be to memorialize transcripts for long-term silencing.

The HRDE-1 and ZNFX-1-dependent amplification loops contribute mostly additively to RNAi inheritance

Our findings suggest that inheritance of the silenced state by F1 progeny not exposed to the trigger involves two pathways: 1) the HRDE-1 “nuclear” sRNA amplification pathway that generates sRNAs across the locus and does not appear to require pUGylation, and 2) the ZNFX-1 “nuage” pathway that uses cycles of pUGylation and sRNA amplification to memorialize the dsRNA trigger. In contrast to RDE-1-initiated sRNA amplification and RNA degradation in P0 animals exposed to the trigger, the HRDE-1 and ZNFX-1 programs are self-sustaining cycles that maintain a pool of targeted transcripts for use as templates for sRNA amplification. Our analyses suggest that both the HRDE-1 and ZNFX-1 programs are required for full silencing in F1 animals. Because our analyses were restricted to feeding RNAi against three loci with similar expression patterns in the germline (*mex-6*, *puf-5* and *oma-1*), it is possible that reliance on the HRDE-1 or ZNFX-1 programs will vary between different loci and in response to different silencing triggers,

such as endogenous sRNAs. Consistent with this hypothesis, different genetic requirements for transgenerational inheritance have been documented for *oma-1* and a germline expressed *gfp::H2B* transgene (Kalinava et al., 2017; Lev et al., 2019).

Although our genetic analyses suggest that the HRDE-1 and ZNFX-1 pathways function primarily independently of each other, two lines of evidence hint at possible cross-talk. First, we found that the sum of *mex-6* sRNAs induced by RNAi in *hrde-1* and *znfx-1* F1s adds up to only 89% of what is observed in wild-type. While this observation will need to be repeated in different contexts to ensure reproducibility, it raises the possibility that sRNAs produced by one amplification cycle extend sRNA production in the other cycle. Second, we observed an accelerated nuclear RNAi response in *znfx-1* P0 animals compared to wild-type, suggestive of competition between the ZNFX-1 and HRDE-1 pathways. One possibility is that in the absence of ZNFX-1, more secondary sRNAs and/or RdRPs are available to fuel the nuclear pathway in the early stages of the RNAi response. Alternatively, ZNFX-1 may antagonize HRDE-1-initiated transcriptional silencing to ensure sufficient production of mature mRNAs for use in the ZNFX-1 cycle. More complex interplays involving Argonautes that participate in multiple sRNA amplification mechanisms are also possible. How the RDE-1, HRDE-1, and ZNFX-1-driven sRNA amplification mechanisms (Fig. 7C) are coordinated in cells and across generations will be an important focus for future investigations.

Figure 1

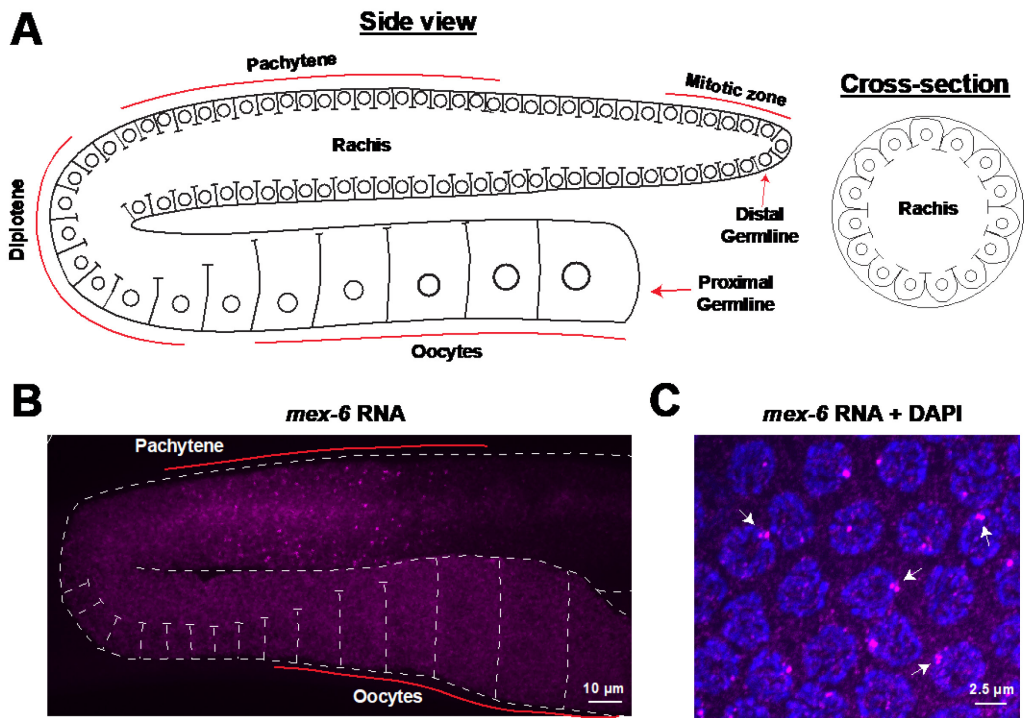
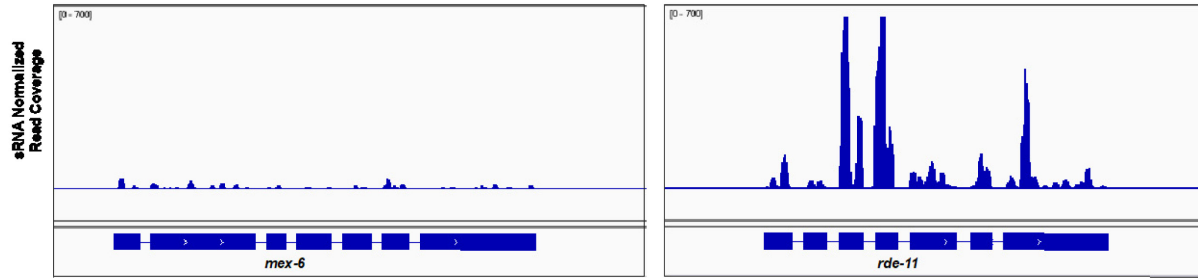


Figure 1. *mex-6* RNA expression in the *C. elegans* germline.

- A) Schematic diagrams (adapted from Gartner et al., 2008) of adult hermaphrodite gonads from a side or cross-sectional view. Circles indicate germline nuclei; lines indicate plasma membranes. Distal nuclei are in mitosis and progress through the different stages of meiosis and oogenesis as they move towards the proximal end of the germline. A common cytoplasm (rachis) runs through the entire germline, excluding the most distal (mature) oocyte which is completely cellularized.
- B) Maximum projection photomicrograph of an adult *C. elegans* germline oriented as in A and with *mex-6* RNA visualized by fluorescent *in situ* hybridization (magenta).
- C) High resolution photomicrograph showing pachytene nuclei (blue, stained with DAPI) and *mex-6* RNA (magenta). Arrows point to nuclei where nascent transcripts at the *mex-6* locus resolve into two or three closely apposed foci, as expected for tightly synapsed, replicated homologous chromosomes in the pachytene stage of meiosis.

Figure S1

A



B

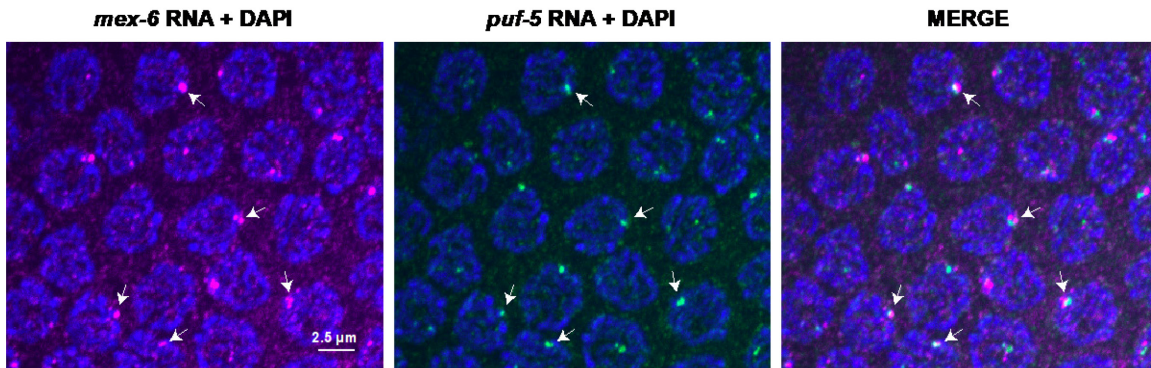


Figure S1. Related to Figure 1.

A) IGV genome browser views of wild-type sRNAseq data showing the minimally sRNA-targeted *mex-6* locus (left) as compared to the highly sRNA-targeted *rde-11* locus (right).

B) Maximum projection photomicrographs of pachytene nuclei showing DNA (blue, stained with DAPI), *mex-6* RNA (magenta), and *puf-5* RNA (green). Arrows indicate pronounced instances *mex-6* and *puf-5* RNA adjacency. The genes for *mex-6* and *puf-5* are located on Chromosome II less than 1 centimorgan apart.

Figure 2

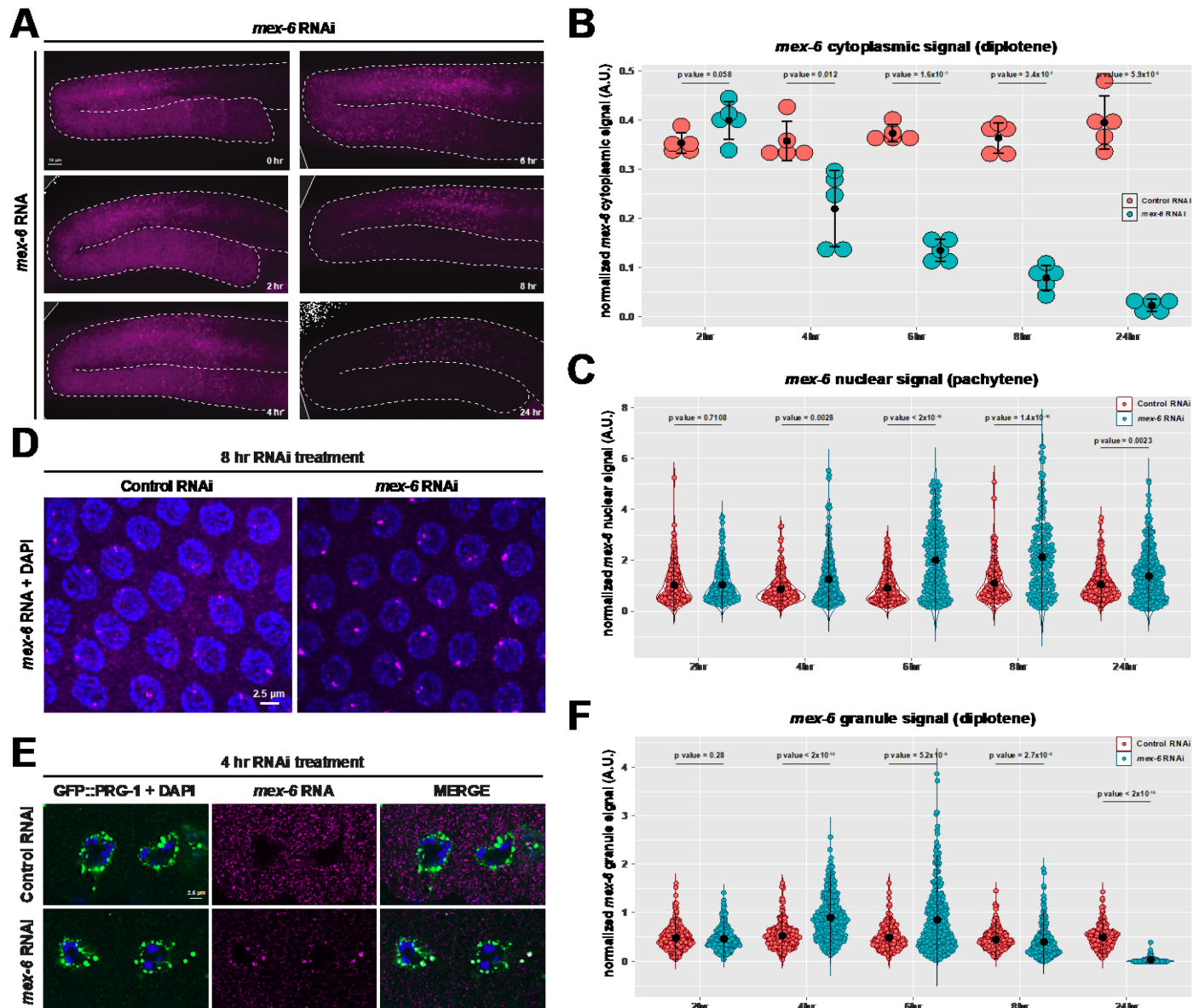


Figure 2. Evolution of *mex-6* RNA during 24-hour RNAi treatment (P0 generation).

A) Maximum projection photomicrograph of germlines oriented as in Figure 1 with *mex-6* RNA (magenta) at indicated times post onset of feeding RNAi.

B) Graph comparing mean cytoplasmic *mex-6* RNA FISH signals (diplotene region) in control (red) and *mex-6* (blue) RNAi conditions at the indicated time points of RNAi treatment. Each dot represents a single germline. Values (arbitrary units) were normalized to *puf-5* RNA FISH signals visualized in same germline (Methods). Central black dot and error bars represent the mean and standard deviation, respectively. P values were calculated using an unpaired t-test.

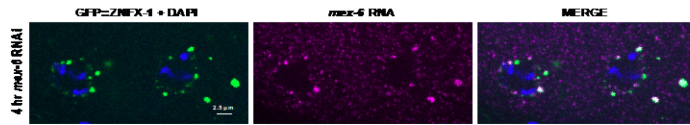
C) Graph comparing maximum nuclear *mex-6* RNA FISH signals (pachytene region) in control (red) vs *mex-6* (blue) RNAi conditions at the indicated time points of RNAi treatment. Each dot represents one nucleus. Nuclei in three worms were quantified for each time point and condition. Values (arbitrary units) were normalized to *puf-5* RNA FISH signals visualized in same nuclei (Methods). Central black dot and error bars represent the mean and standard deviation respectively. P values were calculated using an unpaired Wilcoxon test.

Figure S2

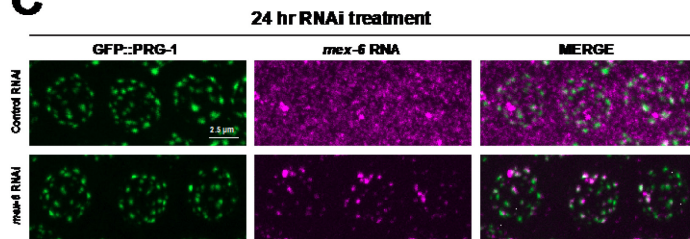
A



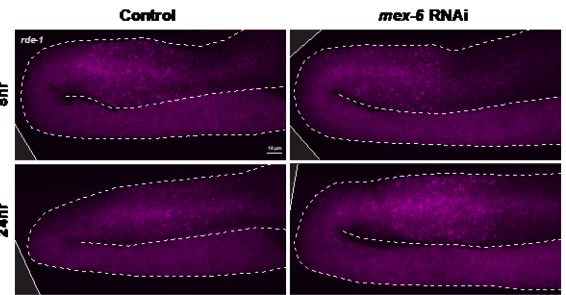
B



C



C



D

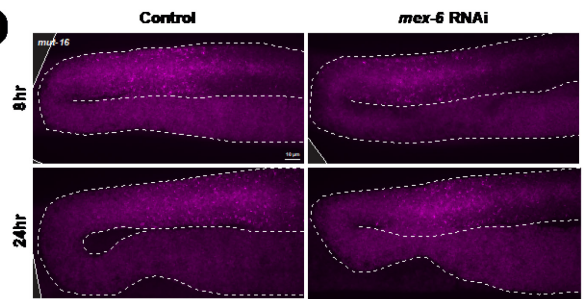


Figure S2. Related to Figure 2.

A) Schematic representation of the *mex-6* mRNA with the mutually exclusive positioning of the smFISH probes (purple) and the dsRNA trigger (red) targeting the 3' 600 nts of the transcript.

B) Photomicrographs of oocytes showing the Z granule marker GFP::ZNFX-1 (green), DNA (blue, stained with DAPI), and *mex-6* RNA (magenta) following 4 hours of *mex-6* RNAi treatment.

C) Maximum projection photomicrographs of pachytene nuclei showing the germ granule marker GFP::PRG-1 (green) and *mex-6* RNA (magenta) following 24 hours of either control (top) or *mex-6* (bottom) RNAi treatment.

D) Maximum projection photomicrographs of *rde-1* mutant germlines showing *mex-6* RNA (magenta) in either control (left) or *mex-6* (right) RNAi conditions at 8 (top) and 24 (bottom) hours of RNAi treatment.

E) Maximum projection photomicrographs of *mut-16* mutant germlines showing *mex-6* RNA (magenta) in either control (left) or *mex-6* (right) RNAi conditions at 8 (top) and 24 (bottom) hours of RNAi treatment.

Figure 3

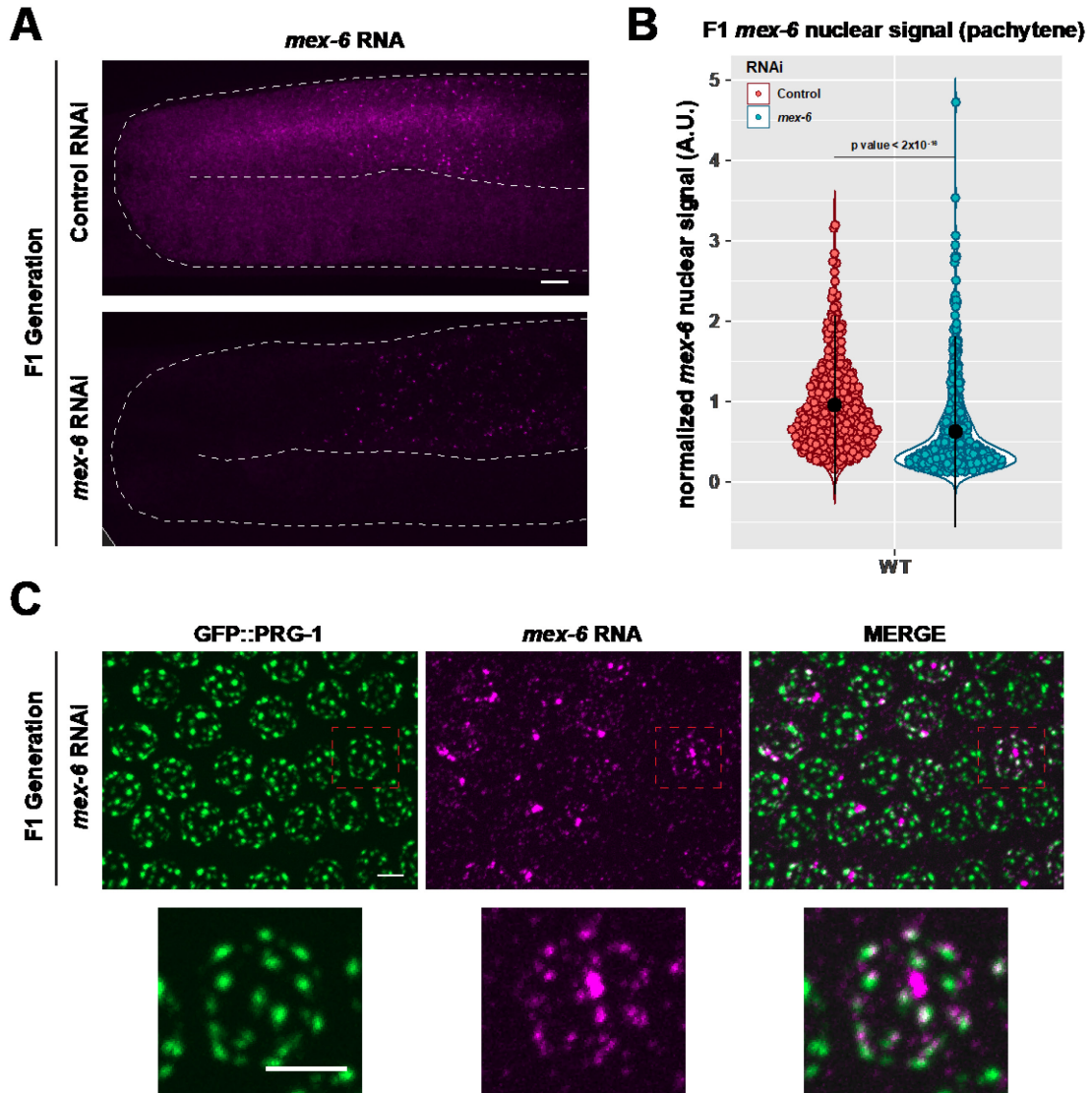


Figure 3. *mex-6* RNA in adult progeny (F1 generation) of animals exposed to *mex-6* dsRNA.

A) Maximum projection photomicrographs of germlines showing *mex-6* RNA (magenta) in adult F1 progeny of animals exposed to control or *mex-6* RNAi (Methods).

B) Maximum projection photomicrographs of pachytene nuclei showing the germ granule marker GFP::*PRG-1* (green) and *mex-6* RNA (magenta) in F1 progeny of animals exposed to *mex-6* RNAi. See Fig. S3B for photomicrographs of the control condition.

C) Graph comparing maximum nuclear *mex-6* RNA FISH signals (pachytene region) in F1 progeny of animals exposed to control (red) or *mex-6* (blue) RNAi. Each dot represents one nucleus. Nuclei in three worms were quantified for each time point and condition. Values (arbitrary units) were normalized to *puf-5* RNA FISH signals visualized in same nuclei (Methods). Central black dot and error bars represent the mean and standard deviation respectively. P values were calculated using an unpaired Wilcoxon test.

Figure S3

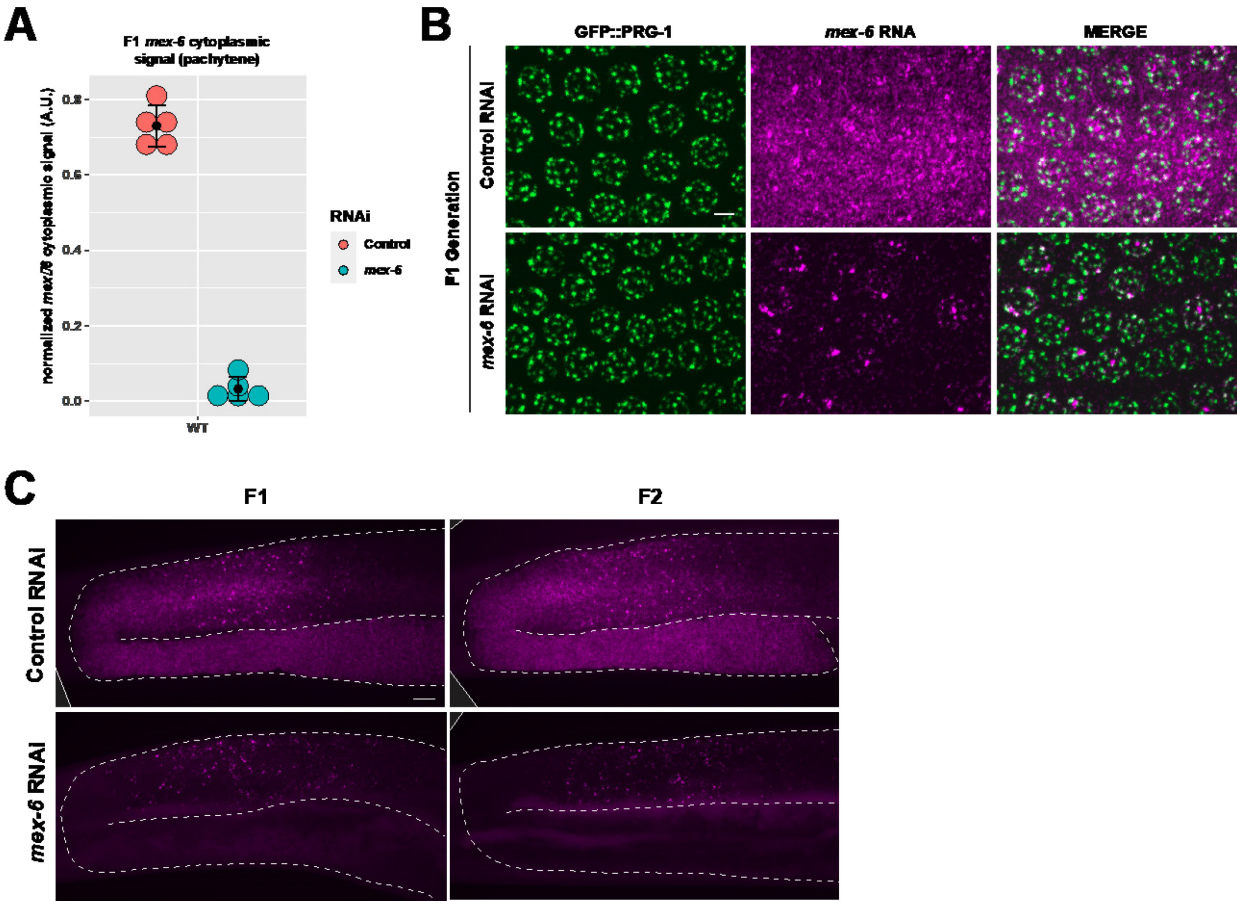


Figure S3. Related to Figure 3.

A) Graph comparing the mean *mex-6* RNA FISH signal from the pachytene rachis in wild-type F1 progeny of P0s administered either control (red) or *mex-6* (blue) RNAi. Each dot represents a single worm. Central black dot and error bars represent the mean and standard deviation, respectively. Values (arbitrary units) were normalized to *puf-5* RNA FISH signals visualized in same region (Methods)

B) Maximum projection photomicrographs of F1 pachytene nuclei showing the germ granule marker GFP::*PRG-1* (green) and *mex-6* RNA (magenta) following administration of either control or *mex-6* RNAi in the P0 generation. Images of the *mex-6* RNAi condition are the same as the ones shown in Fig 3B.

C) Maximum projection photomicrographs of F1 and F2 wild-type germlines showing *mex-6* RNA following administration of either control (left) or *mex-6* (right) RNAi in the P0 generation.

Figure 4

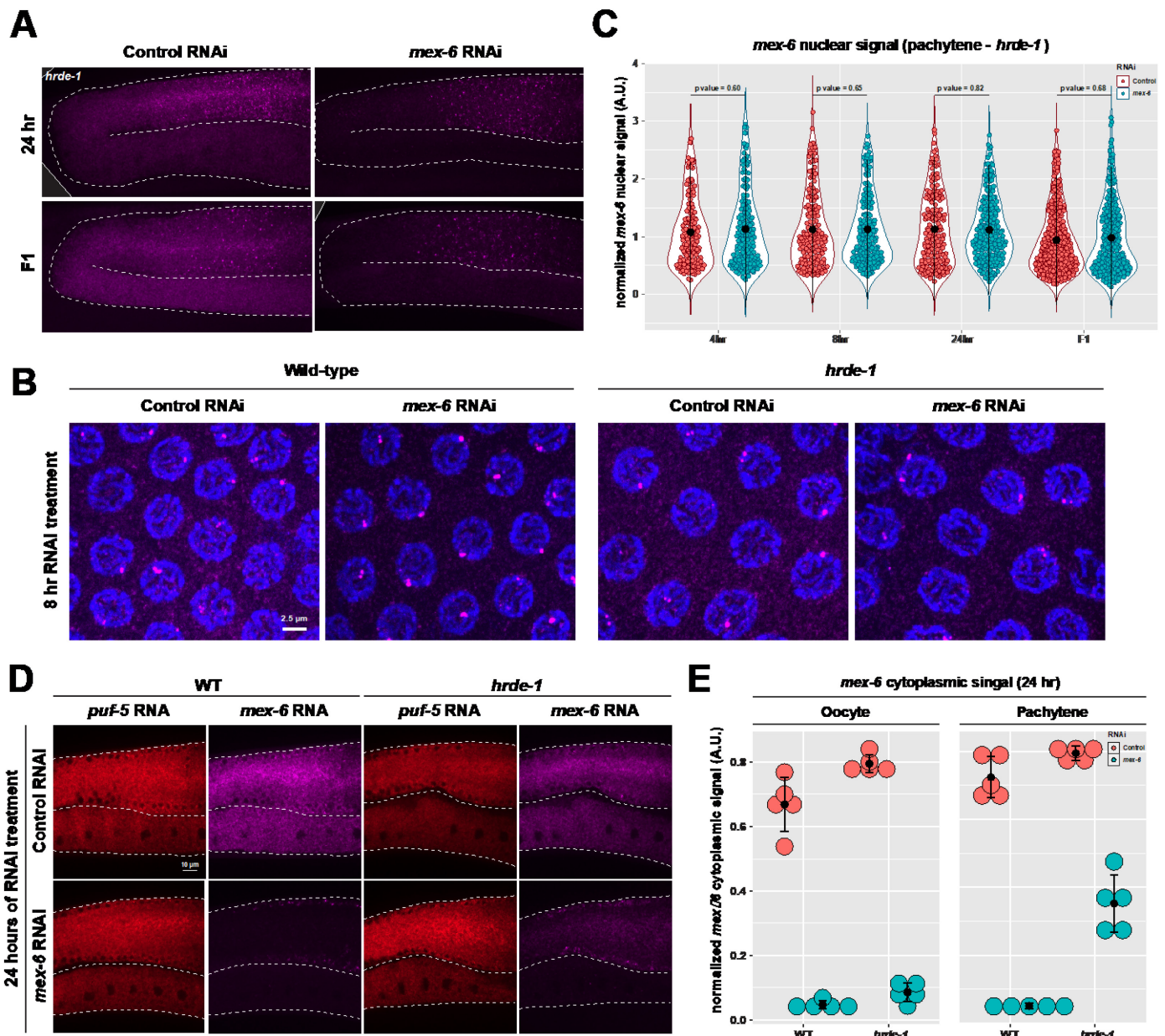


Figure 4. HRDE-1 is required for RNAi-induced changes in nascent transcripts

A) Maximum projection photomicrographs of germlines showing *mex-6* RNA (magenta) in P0 (24 hr RNAi exposure) and F1 *hrde-1* mutants under control or *mex-6* RNAi conditions.

B) Maximum projection photomicrographs of pachytene nuclei in P0 wild-type and *hrde-1* mutant animals showing *mex-6* RNA (magenta) and DNA (blue, stained with DAPI) following 8 hours of either control or *mex-6* RNAi treatment.

C) Graph comparing maximum nuclear *mex-6* RNA FISH signals (pachytene region) in P0 *hrde-1* mutants following either control (red) or *mex-6* (blue) RNAi at the indicated timepoints. Each dot represents one nucleus. Three worms were quantified for each stage and condition. Central black dot and error bars represent the mean and standard deviation, respectively. Values (arbitrary units) were normalized to *puf-5* RNA FISH signals visualized in same nuclei (Methods). P values were calculated using an unpaired Wilcoxon test.

D) Single z-plane photomicrographs showing *mex-6* RNA (magenta) and control *puf-5* RNA (red) in the cytoplasm in the pachytene and oocyte regions comparing wild-type and *hrde-1* mutants at 24 hours of RNAi treatment. *mex-6* RNA is depleted in both regions in wild-type but is only partially depleted in the pachytene region of *hrde-1* mutants consistent with a failure to silence the locus.

E) Graph comparing mean *mex-6* RNA levels in the cytoplasm of oocytes and pachytene region in wild-type and *hrde-1* mutant at 24 hours of RNAi treatment. Each dot represents an individual animal. Values (arbitrary units) were normalized to *puf-5* RNA FISH signals visualized in the same areas (Methods).

Figure S4

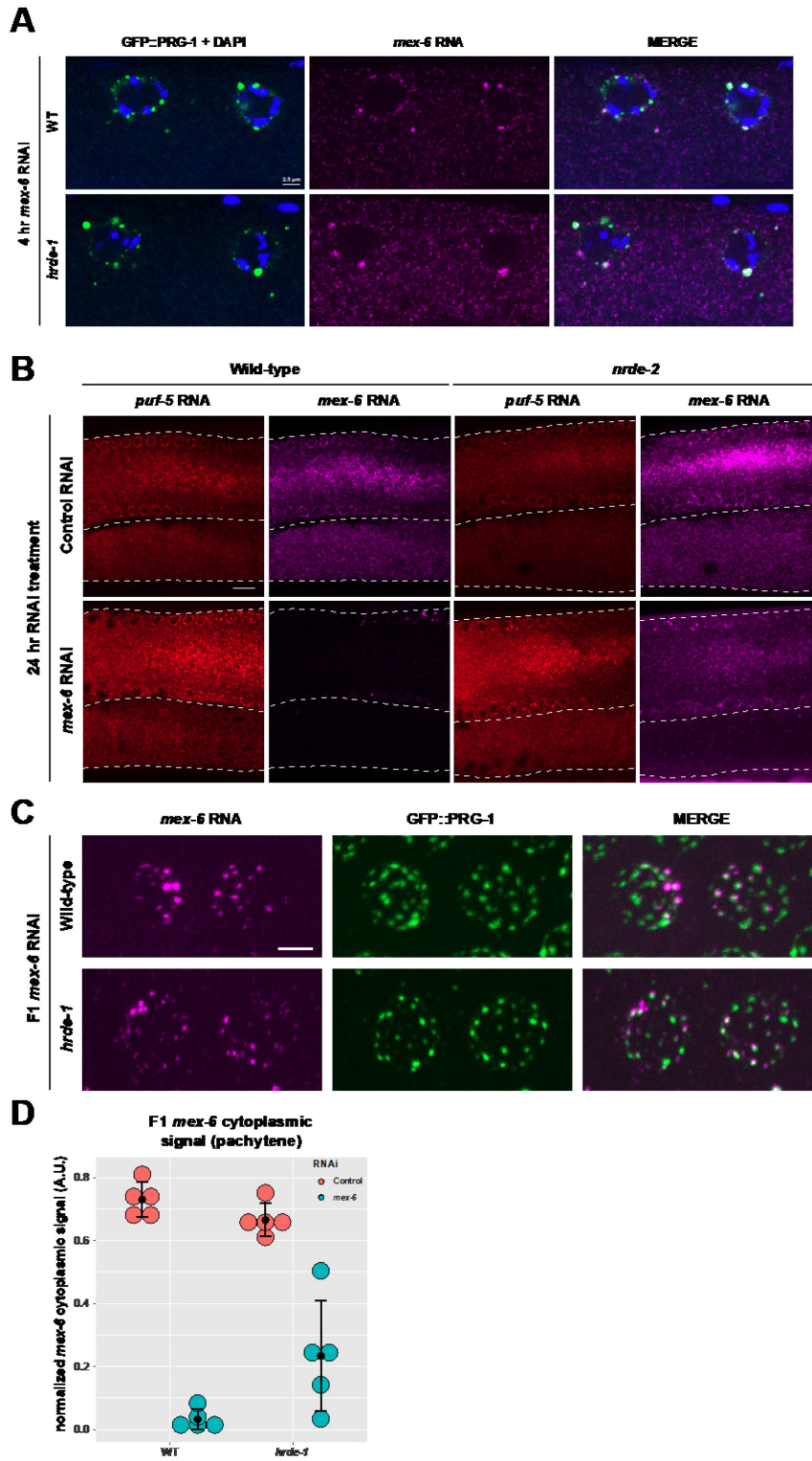


Figure S4. Related to Figure 4.

A) Photomicrographs of P0 wild-type (top) and *hrde-1* mutant (bottom) oocytes showing the germ granule marker GFP::PRG-1 (green), DNA (blue, stained with DAPI), and *mex-6* RNA (magenta) following 4 hours of *mex-6* RNAi treatment

B) Single z-plane photomicrographs of P0 wild-type and *nrde-2* mutant germlines (showing both the pachytene region and oocytes) at 24 hours after control or *mex-6* RNAi administration. *mex-6* RNA FISH is shown in magenta. *puf-5* RNA FISH is shown in red (used as an *in situ* control).

C) Maximum projection photomicrographs of F1 wild-type or *hrde-1* mutant pachytene nuclei showing the germ granule marker GFP::PRG-1 (green) and *mex-6* RNA (magenta) following administration of either control or *mex-6* RNAi in the P0 generation.

D) Graph comparing the mean *mex-6* RNA FISH signal from the pachytene rachis in wild-type and *hrde-1* mutant F1 progeny of P0s administered either control (red) or *mex-6* (blue) RNAi. Each dot represents a single worm. Central black dot and error bars represent the mean and standard deviation, respectively. Values (arbitrary units) were normalized to *puf-5* RNA FISH signals visualized in same nuclei (Methods). WT values are the same as shown in Fig. S3A.

Figure 5

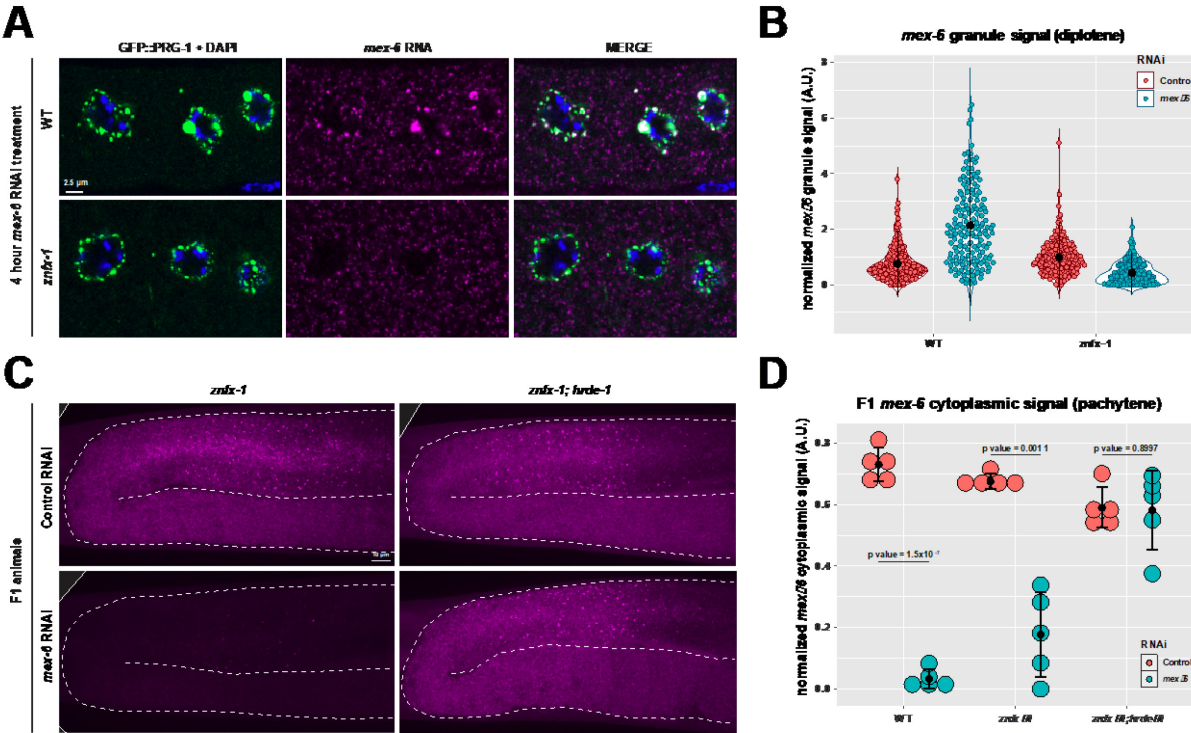


Figure 5. ZNFX-1 is required for enrichment of RNAi-targeted transcripts in germ granules.

A) Photomicrographs of oocytes in wild-type and *znfx-1* mutant animals after 4 hours of RNAi treatment showing the germ granule marker GFP::PRG-1 (green), DNA stained with DAPI (blue), and *mex-6* RNA (magenta).

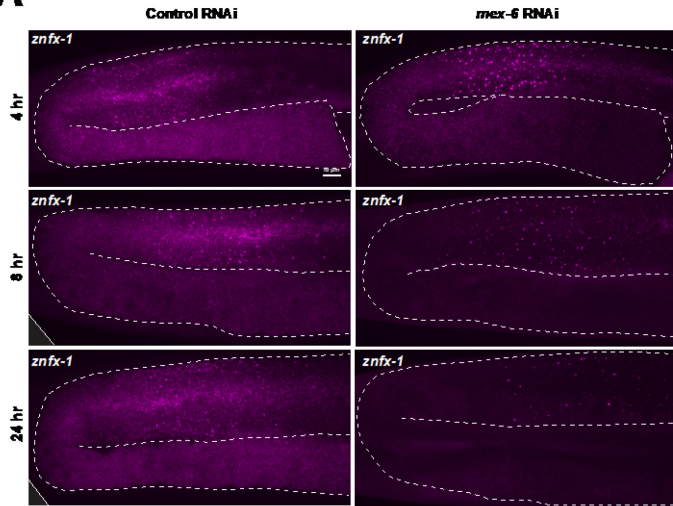
B) Graph comparing the mean *mex-6* RNA FISH signal in germ granules in wild-type and *znfx-1* mutant animals after 4 hours of RNAi treatment. Each dot represents an individual granule. Five worms were quantified for each condition. Values (arbitrary units) were normalized to *puf-5* RNA FISH signals visualized in the same granules (Methods).

C) Maximum projection photomicrographs of germlines showing *mex-6* RNA (magenta) in F1 progeny of animals with the indicated RNAi treatment.

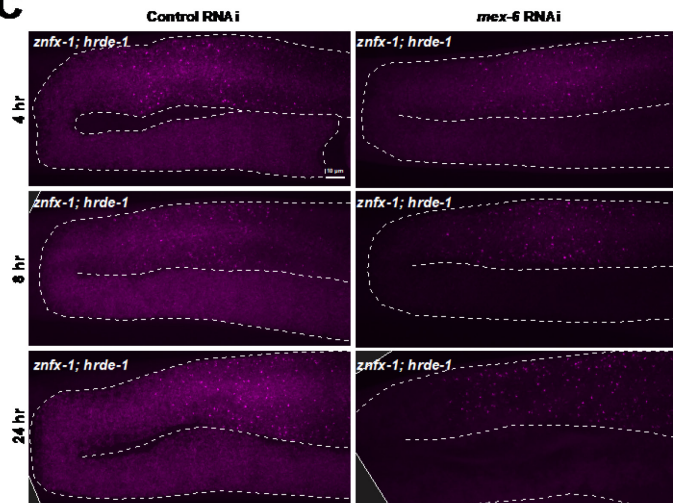
D) Graph comparing the mean *mex-6* RNA FISH signal in germ granules in the pachytene region of *znfx-1* and *znfx-1; hrde-1* F1 progeny derived from animals with the indicated RNAi treatment. Each dot represents a single worm. Central black dot and error bars represent the mean and standard deviation, respectively. Values (arbitrary units) were normalized to *puf-5* RNA FISH signals visualized in the germlines (Methods). P values were calculated using an unpaired t-test.

Figure S5

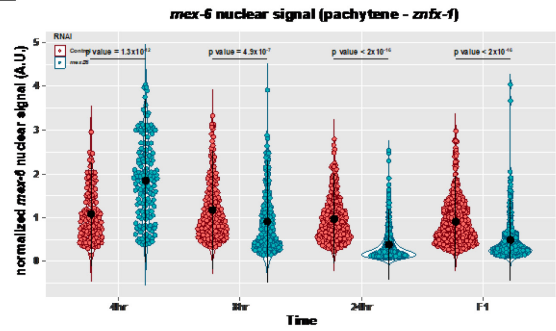
A



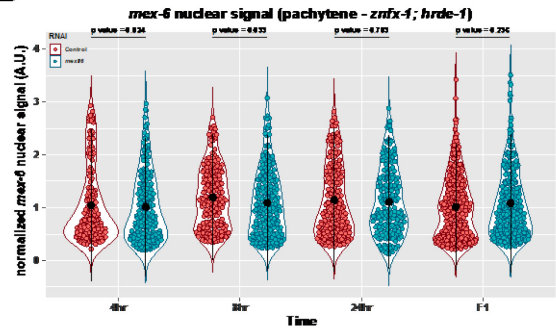
C



B



D



E

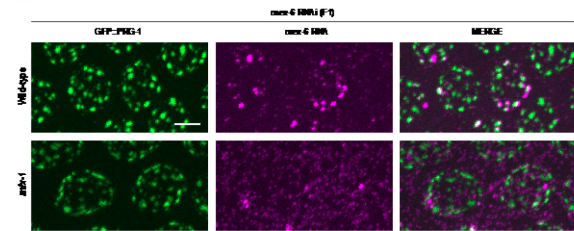


Figure S5. Related to Figure 5.

A) Maximum projection photomicrographs of *znfx-1* mutant germlines showing *mex-6* RNA at the indicated timepoints following either control or *mex-6* RNAi.

B) Graph comparing the maximum *mex-6* nuclear FISH signal in control (red) vs *mex-6* (blue) RNAi at the indicated time points following RNAi in *znfx-1* mutant animals. Each dot of the violin plot represents one nucleus. Nuclei in three worms were quantified for each time point and condition. Values (arbitrary units) were normalized to *puf-5* RNA FISH signals visualized in same nuclei (Methods). Central black dot and error bars represent the mean and standard deviation, respectively. P values were calculated using an unpaired Wilcoxon test.

C) Maximum projection photomicrographs of *znfx-1; hrde-1* mutant germlines showing *mex-6* RNA at the indicated timepoints following either control or *mex-6* RNAi.

D) Graph comparing the maximum *mex-6* nuclear FISH signal in control (red) vs *mex-6* (blue) RNAi at the indicated time points following RNAi in *znfx-1; hrde-1* mutant. Each dot of the violin plot represents one nucleus. Nuclei in three worms were quantified for each time point and condition. Values (arbitrary units) were normalized to *puf-5* RNA FISH signals visualized in same nuclei (Methods). Central black dot and error bars represent the mean and standard deviation, respectively. P values were calculated using an unpaired Wilcoxon test.

E) Maximum projection photomicrographs of F1 wild-type and *znfx-1* mutant pachytene nuclei showing the germ granule marker GFP::PRG-1 (green) and *mex-6* RNA (magenta) following administration of *mex-6* RNAi in the P0 generation.

Figure 6

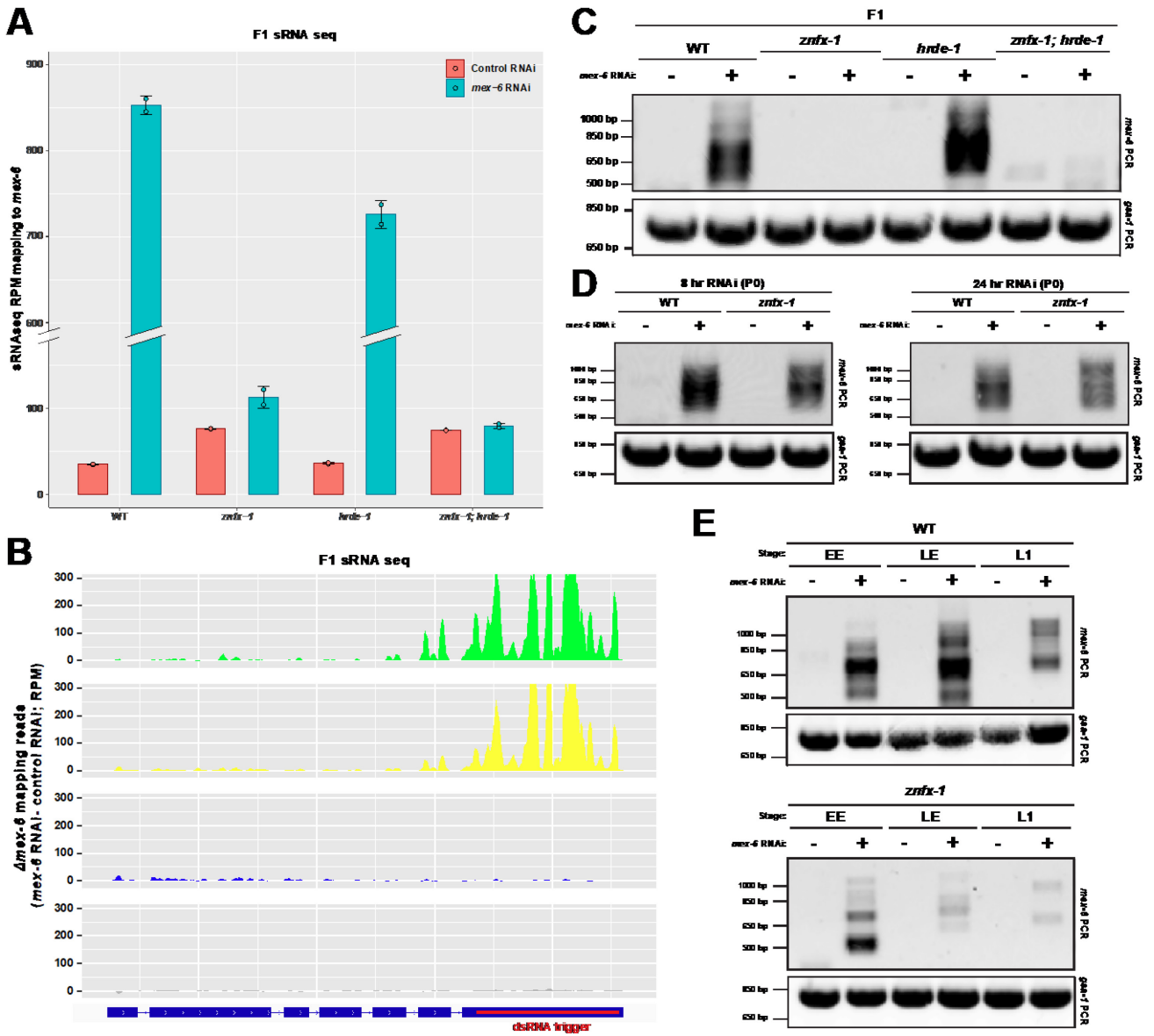


Figure 6. ZNFX-1 and HRDE-1 function in separate pathways contributing to transgenerational RNAi.

A) Bar graph depicting the number of sRNAseq reads (normalized per million) mapping to the *mex-6* transcript in wild-type, *znfx-1*, *hrde-1*, and *znfx-1; hrde-1* mutant F1 progeny derived from animals with the indicated RNAi treatment.

B) Genome browser view of the sRNAseq reads mapping to the *mex-6* locus in wild-type, *znfx-1*, *hrde-1*, and *znfx-1; hrde-1* mutant F1 progeny of animals treated with *mex-6* RNAi. sRNA reads were binned across the *mex-6* gene, and the number of reads in each bin under the *mex-6* RNAi condition were subtracted from the number of reads in each respective bin under the control condition. Positioning of the dsRNA trigger administered in the P0 generation is indicated in red.

C) Gel showing PCR amplification of pUGylated *mex-6* RNA from lysates derived from F1 progeny from animals of the indicated genotype treated with control ("-") or *mex-6* ("+") RNAi (top panel). The *gsa-1* transcript has a genomically-encoded 18-nucleotide poly(UG) stretch and is used here as a positive control for pUG amplification (bottom panel; Shukla et al., 2020).

D) Gel showing PCR amplification of pUGylated *mex-6* RNA from lysates derived from P0 animals of the indicated genotype and treated for 8 hours with control ("-") or *mex-6* ("+") RNAi (top panel). *gsa-1* is the pUG amplification control (bottom panels).

E) Gel showing PCR amplification of pUGylated *mex-6* RNA from lysates derived from early embryos (EE), late embryos (LE), and first larval stage F1 progeny from animals of the indicated genotype treated with control ("-") or *mex-6* ("+") RNAi. *gsa-1* is the pUG amplification control (bottom panels).

Figure S6

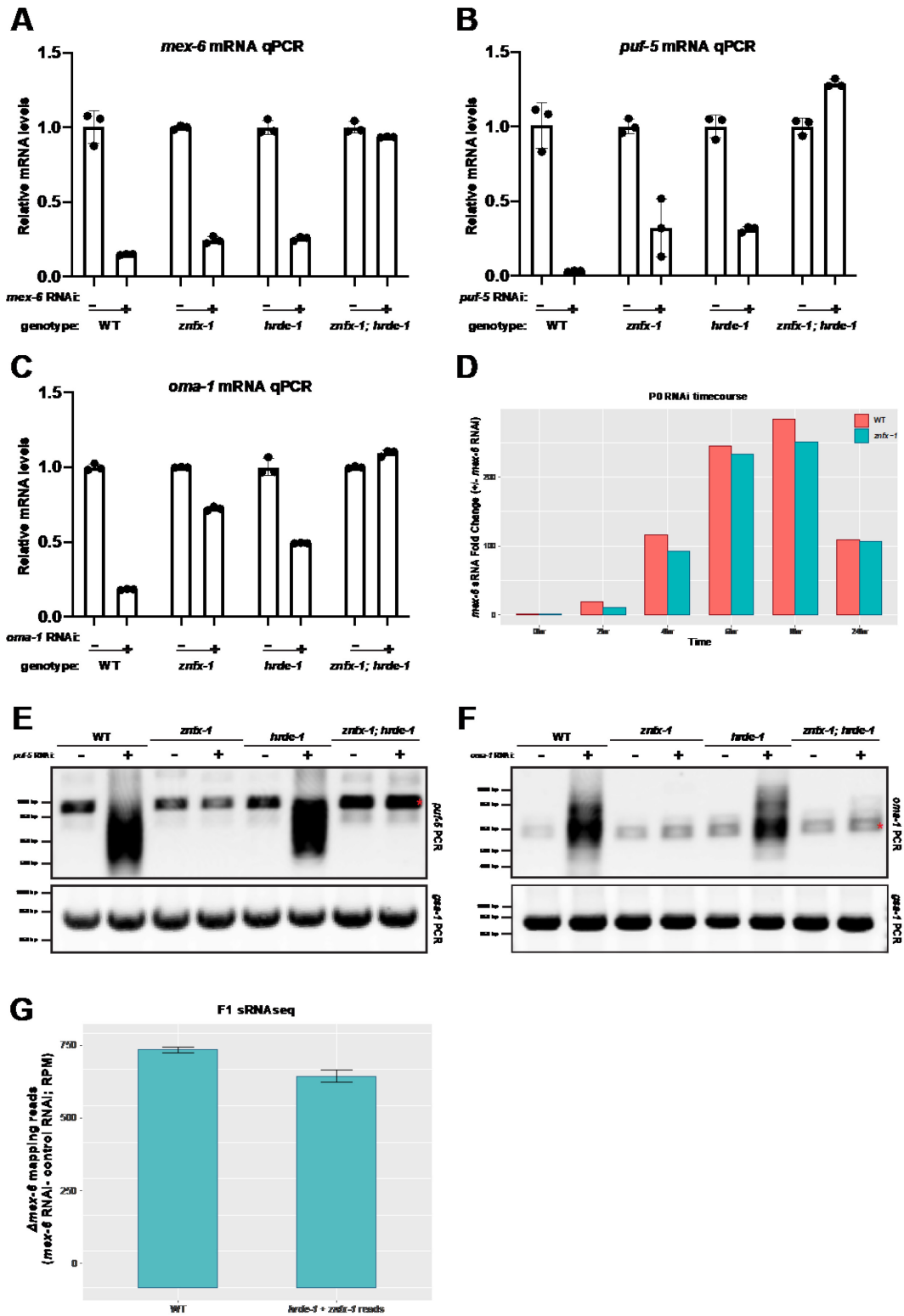


Figure S6. Related to Figure 6.

A-C) *mex-6* (A), *puf-5* (B), and *oma-1* (C) RT-qPCR from RNA derived from wild-type, *znfx-1*, *hrde-1*, and *znfx-1; hrde-1* F1 progeny of P0 worms administered either control, *mex-6* (A), *puf-5* (B), or *oma-1* (C) RNAi. Respective RT-qPCR Ct values are normalized to *tbb-2* RT-qPCR Ct values. The control RNAi condition for each genotype was normalized to 1 and the respective RNAi condition was compared to that (see Methods).

D) Bar graph depicting the number of sRNAseq reads (normalized per million) mapping to the *mex-6* transcript in wild-type and *znfx-1* mutant P0s at the indicated timepoints following either control (red) or *mex-6* (blue) RNAi.

E-F) *puf-5* (E) and *oma-1* (F) specific PCRs of pUG cDNA generated from wild-type, *znfx-1*, *hrde-1*, and *znfx-1; hrde-1* mutant F1s following either control (“-”) or *puf-5/oma-1* (“+”; Figure S6E/S6F, respectively) RNAi in the P0 (top panel). *gsa-1* was used as a pUG RT-PCR control (bottom panels).

G) Graph depicting the change in *mex-6* mapping sRNA reads (*mex-6* RNAi – control RNAi) in wild-type as compared to the summed change in *mex-6* mapping sRNA reads of the *hrde-1* and *znfx-1* single mutants.

Figure 7

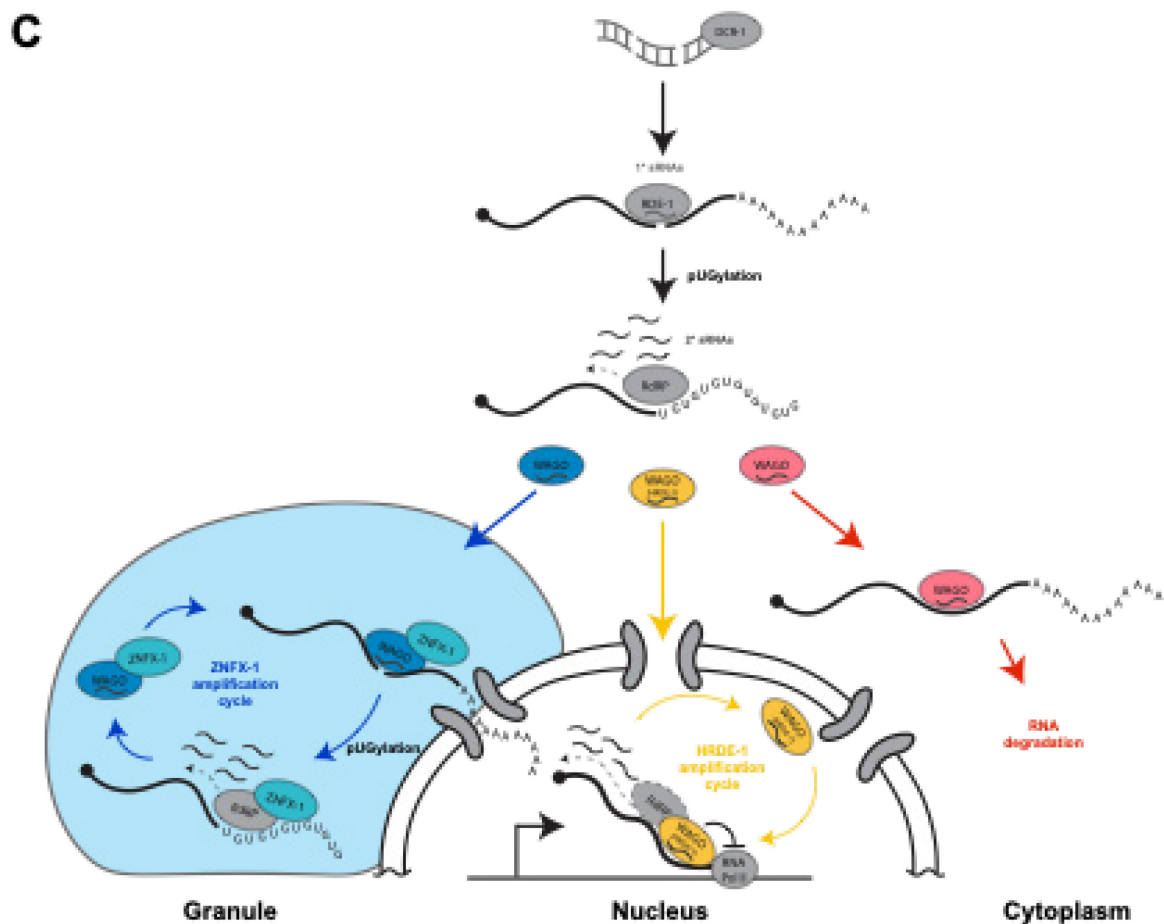
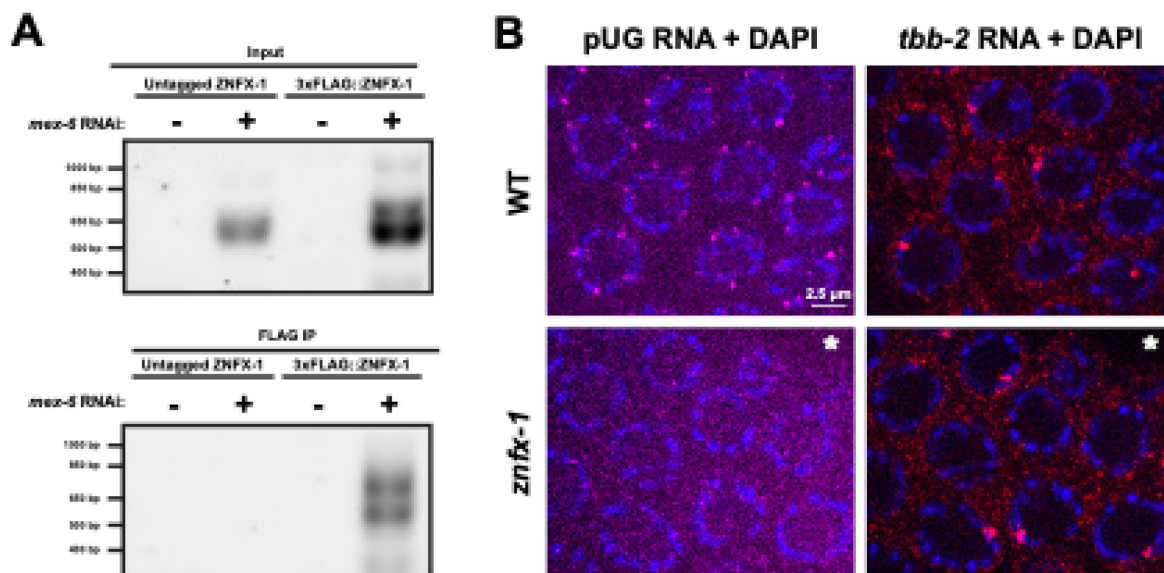


Figure 7. ZNFX-1 is required for pUG RNA localization to germ granules.

A) Gel showing PCR amplification of pUGylated *mex-6* RNA from input (top panel) or FLAG immunoprecipitates (bottom panel) from animals where the *znfx-1* locus is under untagged or tagged with 3xFLAG. Lysates were collected from adult worms grown for 12 hours on either *mex-6* (“+”) or *puf-5* (“-”) RNAi.

B) Photomicrographs of pachytene nuclei in dissected germline from wild-type or *znfx-1* mutant animals showing endogenous pUGylated RNAs (magenta), control *tbb-2* RNA (red), and DNA stained with DAPI (blue). Images marked with asterisks were enhanced for contrast for visualization purposes. See Fig. S7C for evenly contrasted images.

C) Model for exogenous RNAi. dsRNA is processed into primary sRNAs that load with RDE-1 to target complementary transcripts for pUGylation. pUGylated transcripts recruit RdRPs to generate secondary sRNAs in the cytoplasm. Secondary sRNAs bind to secondary Argonautes (“WAGOs”), which initiate three distinct pathways. A first pathway leads to degradation of cytoplasmic transcripts with no further sRNA amplification. On its own, this pathway is sufficient to silence gene expression in animals exposed to dsRNA triggers but is not sufficient to propagate the RNAi response transgenerationally. A second pathway dependent on the nuclear Argonaute HRDE-1 partially silences the locus and uses nascent transcript as templates for the production of “tertiary” sRNAs. A third pathway dependent on the nuage helicase ZNFX-1 enriches targeted transcripts in nuage where they are pUGylated and used as templates for further “tertiary” sRNAs amplification. Tertiary sRNAs feedback into their respective cycles ensuring transgenerational inheritance of the silenced state. Possible cross talk between the HRDE-1 and ZNFX-1 cycles is not shown, see Discussion for further considerations.

Figure S7

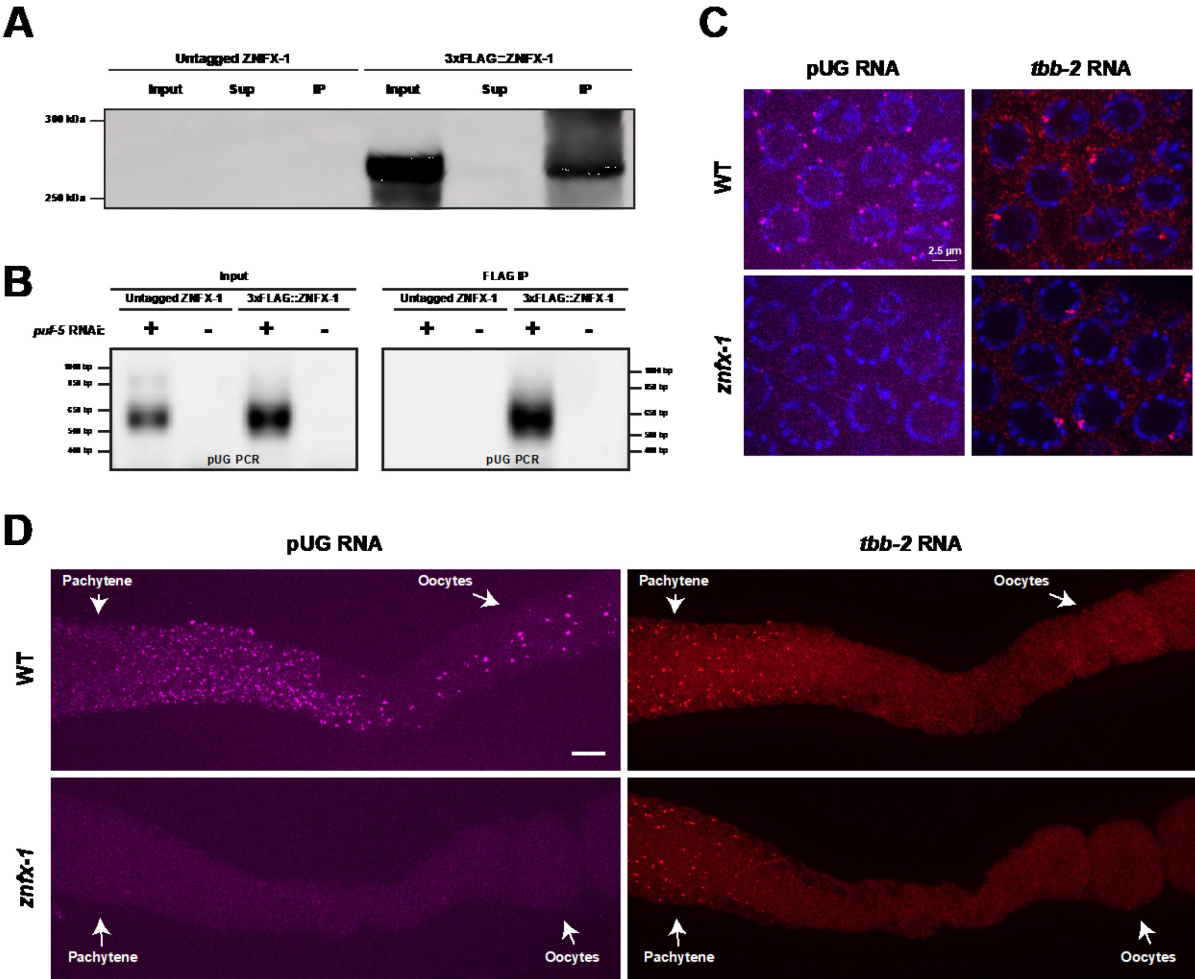


Figure S7. Related to Figure 7.

A) anti-FLAG western blot of FLAG immunoprecipitation experiments from untagged and 3xFLAG-tagged ZNFX-1 lysis. “Input” represents 1% of the input sample prior to immunoprecipitation; “Sup” represents 1% of the supernatant following immunoprecipitation; “IP” represents 1% of the immunoprecipitation sample following FLAG elution.

B) *puf-5*-specific PCRs of pUG cDNA generated from input (left panel) or FLAG immunoprecipitations (right panel) of untagged or 3xFLAG-tagged ZNFX-1 lysis. Lysis was obtained from adult worms grown for 12 hours on either *puf-5* (“+”) or *mex-6* (“-”) RNAi. PCRs were generated from the same pUG cDNA used in Fig 7A.

C) Photomicrographs of pachytene nuclei from dissected wild-type and *znfx-1* mutant germlines showing pUG RNA FISH (magenta), DNA (blue, stained with DAPI), and *tbb-2* RNA (red; used as an *in situ* control). Same images as in Fig. 7B, but equally contrasted.

D) Maximum projection photomicrographs of dissected wild-type and *znfx-1* mutant germlines showing pUG RNA FISH (magenta) and *tbb-2* RNA (red, used as an *in situ* control). The pachytene region and oocytes are indicated with arrows.

Figure S8

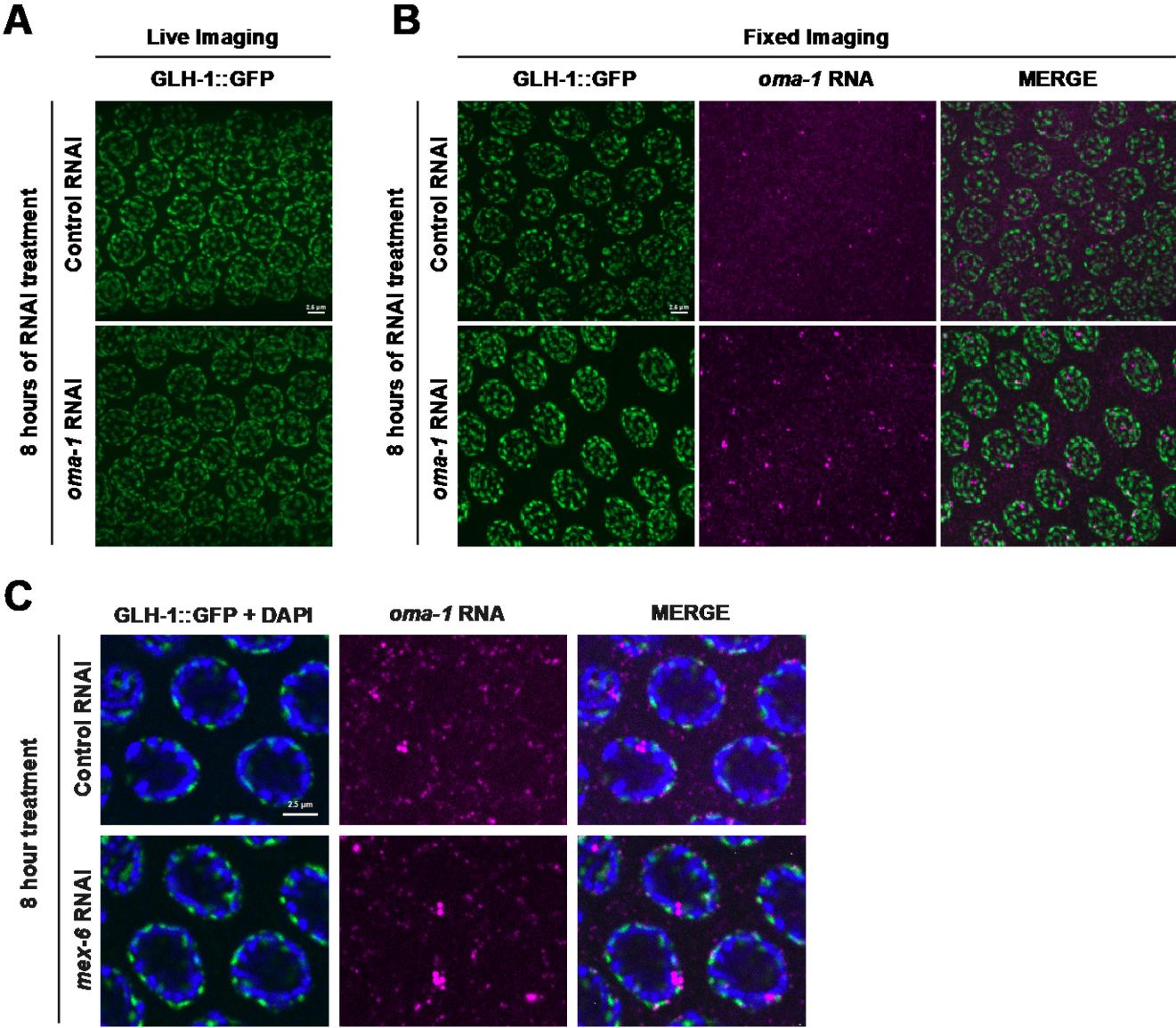


Figure S8. Related to Discussion.

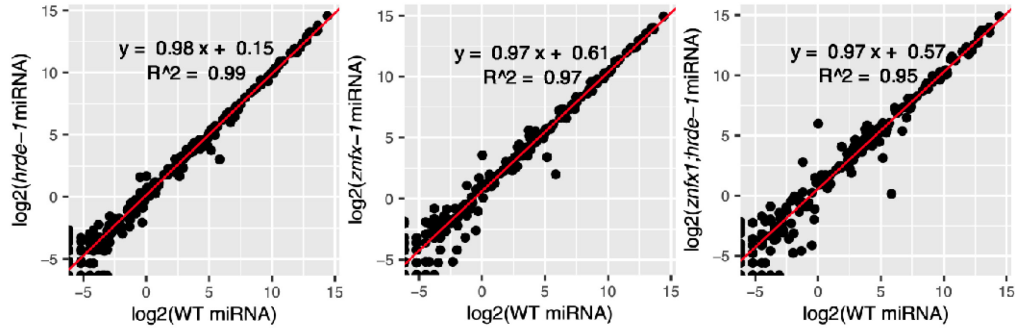
A) Maximum projection photomicrographs of live-imaged pachytene nuclei showing GLH-1::GFP after 8 hours of either control or *oma-1* RNAi treatment.

B) Maximum projection photomicrographs of fixed-imaged pachytene nuclei showing GLH-1::GFP (green) and *oma-1* RNA (magenta) after 8 hours of either control or *oma-1* RNAi treatment.

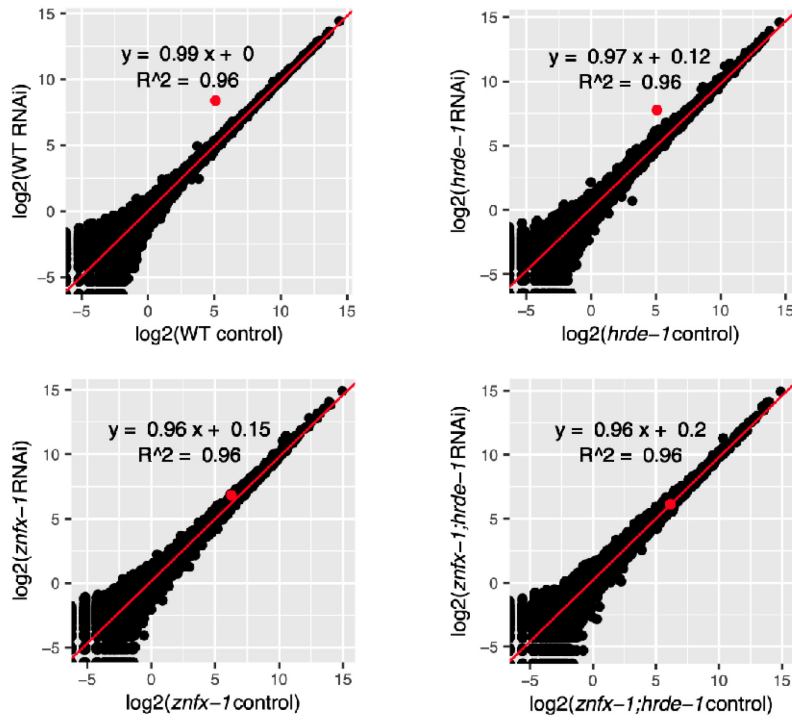
C) Single Z-plane photomicrographs of fixed-imaged pachytene nuclei showing GLH-1::GFP (green), DNA (blue, stained with DAPI) and *oma-1* RNA (magenta) after 8 hours of either control or *oma-1* RNAi treatment.

Figure S9

A



B



C

	WT F1 (control RNAi)	WT F1 (mex-6 RNAi)	hrde-1 F1 (control RNAi)	hrde-1 F1 (mex-6 RNAi)
slope	0.94	0.97	0.98	0.99
intercept	0.2	0.05	0.04	-0.02
R2	0.96	0.96	0.96	0.96

	znfx-1 F1 (control RNAi)	znfx-1 F1 (mex-6 RNAi)	znfx-1; hrde-1 F1 (control RNAi)	znfx-1; hrde-1 F1 (mex-6 RNAi)
slope	0.97	0.98	1	0.99
intercept	0.09	0	-0.06	0
R2	0.96	0.96	0.96	0.96

Figure S9. Related to Methods.

A) Scatter plots comparing miRNA RPMs in wild-type (X-axis) and mutants (Y-axis) under control RNAi conditions (*hrde-1* on the left; *znfx-1* in the center; *znfx-1; hrde-1* on the right). Linear regression is used to fit the data. miRNA counts in each condition are averaged across two replicates.

B) Scatter plots comparing sRNA RPMs in the F1 progeny of control and *mex-6* RNAi fed P0 worms for the indicated genotypes. Each dot represents the level of sRNA reads mapping to an annotated locus in the *C. elegans* genome. The red dot represents sRNA reads mapping to the *mex-6* transcript. Linear regression is calculated without *mex-6* sRNA counts. sRNA counts in each condition were averaged across two replicates.

C) Linear regression statistics modeling the relationship between the two sRNAseq replicates for each genotype in both control and *mex-6* RNAi conditions.

Methods:

Strains and maintenance:

All strains were cultured/maintained at 20° C on either OP50 bacteria plated on NNGM media or NA22 bacteria plated on Enriched Peptone (EP) media. The following strains were used in this study: N2 (JH1), *znfx-1(gg561) II* (YY996; Wan et al., 2018), *hrde-1(tm1200) III* (YY538; Buckley et al., 2012), *znfx-1(gg561) II*; *hrde-1(tm1200) III* (JH4054; this study), *prg-1(ne4523[gfp::tev::flag::prg-1]) I* (WM527; Shen et al., 2018), *znfx-1(gg544[3xflag::gfp::znfx-1])* (YY916; Wan et al., 2018), *prg-1(ne4523) I*; *znfx-1(gg561) II* (JH4055; this study), *prg-1(ne4523) I*; *hrde-1(tm1200) III* (JH4056; this study), *prg-1(ne4523) I*; *znfx-1(gg561) II*; *hrde-1(tm1200) III* (JH4057; this study), *prg-1(ne4523) I*; *rde-1(ne219) V* (JH4058; this study), *prg-1(ne4523) mut-16(pk710) I* (JH4059; this study), *ego-1(ne4518[gfp::ego-1]) I*; *znfx-1(ne4355[3Xflag::tev::znfx-1])II* (WM514; Ishidate et al., 2018), *ego-1(ne4518[gfp::ego-1]) I* (WM522; Ishidate et al., 2018), *glh-1(ax3843[glh-1::eGFP]) I* (JH4022; Paix et al., 2016).

RNA extraction and purification:

RNA extraction was performed on up to 100 uL of worms flash frozen in liquid nitrogen and stored at -80° C. First, frozen samples were resuspended in 1 mL of Trizol (ThermoFisher; Cat #: 15596026) and subjected to three freeze-thaw cycles. Samples were then shaken at 1500 RPM for five minutes at RT in a benchtop shaker (Benchmark Scientific; Model #: H5000-HC). Samples were then incubated for 5 minutes at RT with no shaking. 200 uL of chloroform was then added to each tube, and the samples were then shaken by hand for 15 seconds, followed by a 2-3 minute incubation at RT. Tubes were then spun at 4° C at 12,000xg for 15 minutes. The upper aqueous phase was then removed and an equal volume of 95-100% ethanol was added and mixed. These samples were then input into the Zymo RNA Clean & Concentrator Kit columns (Zymo; Cat #: R1017) and purified according to the kit manual. On-column DNase I digestions with MgCl₂ buffer (ThermoFisher; Cat # EN0521) were used for each RNA prep to remove contaminating DNA. Samples were eluted in water.

Plasmid construction:

RNAi plasmids were constructed using the In-Fusion® HD Cloning Kit (Takara Bio; Cat #: 639650) and the L4440 vector. Primers for cloning the 3' portion of *mex-6* (600 nt), *puf-5* (500 nt), and *oma-1* (600 nt) were designed using the Takara Bio In-Fusion Cloning online design tool and are listed in Table SY. NEB Phusion PCRs (NEB; Cat #: M0531S) were conducted from reverse transcriptase reactions generated from the SuperScript™ VILO™ cDNA Synthesis Kit (ThermoFisher; Cat #: 11754050) and RNA extracted from adult animals (see RNA extraction). The L4440 plasmid was digested using XbaI and NcoI, gel purified, and added to the In-Fusion® HD Cloning reaction along with the amplified PCR products. Reactions were then transformed into Stellar™ competent cells (Takara Bio; Cat #: 636766), and plasmids were subsequently isolated using Qiagen mini-prep kits (Qiagen; Cat #: 27104).

RNAi assays:

RNAi plates were made as follows: RNAi constructs were transformed into HT115 bacteria, and overnight starter cultures were then grown from the HT115 transformants in 100 ug/mL ampicillin LB liquid media culture at 37° C with vigorous shaking. The starter culture was then used to inoculate a fresh LB/ampicillin culture at a ratio of 1:100 (e.g. 10 mLs starter culture into 990 mLs LB), and grown for 6 hours with vigorous shaking at 37° C. RNAi cultures were then induced with IPTG for a final concentration of 500 uM and shaken for 30 more minutes at 37° C. Cultures were then spun down and resuspended in 1/20 of the culture volume with 100 ug/mL ampicillin/500 uM IPTG LB (e.g. 50 mLs for 1000 mLs of culture) and densely plated onto NNGM agar containing 100 ug/mL carbenicillin and 1 mM IPTG. Plates were then allowed to dry, and then subsequently used for RNAi.

RNAi assays were conducted as follows: embryos were isolated from gravid mothers through bleaching and placed in M9 overnight at 20° C and 110 RPM shaking. Synchronized L1s were then plated onto NA22 bacteria grown on EP media. Worms were then collected at the adult stage approximately 60 hours after plating and washed and collected using a filter. Worms were then plated onto either control or gene-specific RNAi plates for the specified lengths of time, and then washed and collected for fixation (see FISH assays) or RNA collection (see RNA collection).

For transgenerational RNAi assays, synchronized P0 L1s were plated onto NA22 plates for approximately 60 hours and were collected as adults with a filter. Worms were then put onto either control or *mex-6* RNAi plates for 24 hours. After 24 hours, adult worms were collected, and embryos were isolated through bleaching. Embryos were further synchronized by shaking overnight (110 RPM) at 20° C. The worms were then plated onto NA22 plates and collected for fixation/RNA extraction ~72 hours later. For examining the F2 generation, F1 adult worms were bleached, and embryos were isolated. F2 adults were collected ~72 hours after plating synchronized L1s onto NA22 plates.

For experiments examining late vs early F1 embryos, adult worms fed RNAi for 24 hours were isolated. Embryos extracted from bleaching mothers were considered “early embryos.” Embryos collected from the plate were considered “late embryos.” Late embryo samples were bleached to avoid any hatched L1s also being collected.

FISH protocol:

For whole worm (undissected) FISH, 1000 uL of freshly prepared fixation buffer (1xPBS; 3.7% formaldehyde) was added to up to 100 uL of live worms collected in an eppendorf tube. Samples were rotated at RT for 45 minutes, spun down at 3000xg in a table top centrifuge, and washed twice with 1000 uL 1xPBS. Following removal of the supernatant, 1000 uL of 75% ethanol was added to each sample, and stored at 4° C for at least 4 hours. Following ethanol permeabilization, samples were then washed once with 1000 uL of freshly prepared Stellaris® Buffer A Mixture (10% deionized formamide; 20% Stellaris® RNA FISH Wash Buffer A (Biosearch Technologies; Cat #: SMF-WA1-60); 70% RNase-free water). Following removal of the supernatant, 100 uL of freshly prepared Hybe Buffer Mixture was added (for two color *in situs*: 85.5 uL of Stellaris® RNA FISH Hybridization Buffer (Biosearch Technologies; Cat #: SMF-HB1-10); 9.5 uL deionized formamide; 2.5 uL of 5 uM probe #1 suspended in TE; 2.5 uL of 5 uM probe #2 suspended in TE) and samples were incubated at 37° C overnight. Following incubation, 1000 uL of freshly prepared Stellaris® Buffer A Mixture was added to the samples and incubated at 37° C for 30 minutes. Buffer was then removed and 1000 uL of Stellaris® Buffer A Mixture with 5 ng/mL DAPI was added, and samples were again incubated at 37° C for 30 minutes. Buffer was then

removed, and samples were subsequently incubated with Stellaris® RNA FISH Wash Buffer B (Biosearch Technologies; Cat #: SMF-WB1-20) as prepared through manufacturers protocol for 5 minutes at RT. Stellaris® RNA FISH Wash Buffer B was removed and samples were resuspended in Vectashield Antifade Mounting Medium with DAPI (VWR; Cat #: H-1200-10). Samples were then placed on a slide and sealed with a coverslip and nail polish.

For FISH on dissected germlines, worms were first placed on poly-L-lysine coated slides in a solution of M9 with 10 mM levamisole to induce paralysis. Germlines were dissected with needles, and coverslips were subsequently placed over slides. Slides were then immediately frozen on dry ice, and freeze-cracked, and placed immediately into -20° C methanol for fixation. Samples were washed three times in PBS+0.1%Tween20 and fixed in 4% PFA for one hour at room temperature. Samples were then washed on the slide with 500 uL of freshly prepared Stellaris® Buffer A Mixture, followed by a brief incubation with 100 uL of Stellaris® Buffer A Mixture placed directly on the slide. Excess buffer was removed and 100 uL of freshly prepared Hybe Buffer Mixture was added (for two color *in situs*: 85.5 uL of Stellaris® RNA FISH Hybridization Buffer (Biosearch Technologies; Cat #: SMF-HB1-10); 9.5 uL deionized formamide; 2.5 uL of 5 uM probe #1 suspended in TE; 2.5 uL of 5 uM probe #2 suspended in TE) onto each slide and incubated at 37° C overnight. Following incubation, the Hybe Buffer Mixture was removed and slides were first washed with 500 uL of freshly prepared Stellaris® Buffer A Mixture and then incubated with 100 uL of Stellaris® Buffer A Mixture for 30 minutes at 37° C. Excess buffer was removed and slides were washed with 500 uL of freshly prepared Stellaris® Buffer A Mixture containing 5 ng/mL DAPI and then incubated with 100 uL of 5 ng/mL DAPI containing Stellaris® Buffer A Mixture for 30 minutes at 37° C. Following this incubation, buffer was removed, and samples were subsequently washed with 500 uL of Stellaris® RNA FISH Wash Buffer B (Biosearch Technologies; Cat #: SMF-WB1-20) as prepared through manufacturers and incubated with 100 uL of Stellaris® RNA FISH Wash Buffer B protocol for 5 minutes at RT. Stellaris® RNA FISH Wash Buffer B was removed and Vectashield was added to each sample before sealing with a coverslip and nail polish. smFISH probes were designed using the Stellaris Probe Designer (v4.2) and were purchased with Quasar670 and Quasar570 dyes.

sRNA sequencing:

Small RNA libraries were prepared as follows: 5 ug of extracted total RNA was treated with 5' polyphosphatase (20 U/ug of RNA) for 30 minutes at 37 C. RNA then was purified using the Zymo RNA Clean & Concentrator Kit columns (Zymo; Cat #: R1017). 1 ug of treated RNA was then input into the Illumina TruSeq Small RNA Library Preparation Kit (Illumina; Cat #: RS-200-0012) with 11 cycles of PCR amplification. Libraries were then run on either a 6% Novex TBE gel or a 5% Criterion TBE gel and size selected according to the illumine protocol. Purified samples were then sequenced on the Illumina HiSeq2500 at the Johns Hopkins University School of Medicine Genetic Resources Core Facility.

High-throughput sequencing analyses:

5' Illumina adapter sequences were removed using the default settings of Cutadapt (Martin, 2011), and reads with lengths longer than 30 nts or shorter than 18 nts were discarded. Libraries were then aligned to the UCSC ce10 reference genome using HISAT2 (Kim et al., 2015). For assessing the number of reads mapping to the *mex-6* gene, the total number of reads aligning to *mex-6* were counted and normalized to the number of singly aligned reads mapping to the genome (library size) per 1 million reads (RPM).

In order to determine if the sRNAseq libraries from our different genotypes were comparable, we compared the number of miRNA mapping reads from each mutant genotype to wild-type (Fig. S9). No drastic change in miRNA mapping reads was detected, suggesting that that there is not a global change that could affect comparisons of siRNA levels between genotypes (Fig. S9). We therefore concluded that are libraries can be accurately compared.

For sRNA read coverage analysis, mapped sRNA reads across the *mex-6* gene were placed into 5-bp bins. The number of nucleotides per bin were normalized based on library size and averaged across two technical replicates. sRNAs present in the control RNAi condition (L4440 RNAi vector) were then subtracted from the RNAi condition. All scripts are available upon request.

pUGylation assays:

pUG cDNA was synthesized using the SuperScript™ III First-Strand Synthesis System (ThermoFisher; Cat # 18080051) according to the manufacturers instruction. Briefly, 1 ug of isolated total RNA was combined with 1 uL of the 2 uM pUG specific RT primer (Shukla et al., 2020), 1 uL of 10 mM dNTP mix, and filled up to 10 uL with RNase-free water. Mixtures were then incubated at 65 C for 5 minutes then placed on ice for at least 1 minute. 10 uL of the cDNA Synthesis Mix (2 uL of 10x RT buffer, 4 uL of 25 mM MgCl₂, 2 uL of 0,1 M DTT, 1 uL of 40 U/uL RNaseOUT™, 1 uL of 200 U/uL SuperScript III RT) was then added to each reaction and then incubated for 50 min at 50 C followed by 5 min at 85 C. Reactions were then chilled on ice, and 1 uL of RNase H was subsequently added. Reactions were then incubated at 37 C for 20 min. cDNA was then stored at -20 C.

For pUGylation assays following the 3xFLAG::ZNFX-1 IP, 8 uL of the eluted 20 uL of RNA from the IP RNA extraction was used for the pUG cDNA synthesis (representative of approximately 40% of the IPed RNA). 5 ug of RNA was used for the IP input pUG cDNA synthesis (representative of approximately 0.25% of the input RNA).

Immunoprecipitation:

Adult worms were collected with a filter and washed in sonication buffer (20 mM Tris-HCl pH 7.5, 200 mM NaCl, 2.5 mM MgCl₂, 10% glycerol, 0.5% NP-40, 1 mM DTT) with cComplete™, Mini, EDTA-free Protease Inhibitor Cocktail (Millipore Sigma; Cat #: 11836170001; 1 tablet/10 mLs). Worms were flash frozen in sonication buffer and stored at -80 C. For sonication, samples were thawed on ice, and SUPERase•In™ RNase Inhibitor (ThermoFisher; Cat #: AM2694) was added for a final concentration of 80 U/mL. Samples were sonicated with a Branson Digital Sonifier SFX 250 with a microtip (15s on, 45s off, 20% power, 3 min for total on time) and cleared by centrifugation at 4 C for 15 minutes at 18,400xg. Lysate concentration was found with the Pierce BCA assay (ThermoFisher; Cat # 23225). For the IP, Anti-FLAG M2 magnetic beads (Millipore Sigma; Cat #: M8823-1ML) were prepared by vigorous vortexing. 20 uL of bead slurry was washed three times in 200 uL of sonication buffer + 80 U/mL SUPERase•In™ RNase Inhibitor, and 400 uL of 500 ug/uL lysate was added to the beads. An equivalent of 1% input lysate was used for analysis of the IP by western blot (see Western blotting). An additional equivalent of

50% of input lysate was saved for RNA extraction (see RNA extraction and purification). Samples were rotated at 4 C for 2 hours. Samples were cleared with a magnetic stand, and 4.2 uL of the supernatant (~1%) was saved for western analysis (see Western blotting). The supernatant was removed and beads were washed 5x with 500 uL of sonication buffer + 80 U/mL SUPERase•In™ RNase Inhibitor. After final wash, beads were eluted with 4 uL of 5000 ug/mL 3xFLAG peptide (resuspended in TBS; Millipore Sigma; Cat #: F4799-4MG) + 96 uL of sonication buffer + 80 U/mL SUPERase•In™ RNase Inhibitor for 30 minutes at 4 C (final FLAG peptide concentration of 200 ug/mL). Beads were placed on a magnetic stand, and 1 uL of the elution was saved for western analysis (see Western blotting). Trizol was added to the rest of the elution/bead solution for RNA extraction (see RNA extraction and purification).

Western blotting:

For western blotting, DTT and Tris-Glyc SDS 2x sample buffer (ThermoFisher; Cat #: LC2676) were added to samples for a final concentration of 200 mM DTT and 1x Tris-Glyc SDS sample buffer. Samples were then flash frozen and stored at -80 C. Samples were then thawed and heated at 95 C for 10 minutes. Samples were run in Novex™ Tris-Glycine SDS Running Buffer (ThermoFisher; Cat #: LC2675) on a Novex™ WedgeWell™ 6%, Tris-Glycine, 1.0 mm, Mini Protein Gel, 12-well gel (ThermoFisher; Cat #: XP00062BOX) with a Spectra™ Multicolor High Range Protein Ladder (ThermoFisher; Cat #: 26625). Samples were transferred to an Immobilon-P PVDF Membrane (Sigma-Aldrich; Cat #: IPVH) and blocked in PBS/0.1%Tween20/5% Blotting-Grade Blocker (BioRad; Cat #: 1706404) for 30 minutes. The membrane was then incubated with anti-FLAG M2 primary antibody (1:500 dilution; Millipore Sigma; Cat #: MF1804) in PBS/0.1%Tween20/5% Blotting-Grade Blocker overnight. The membrane was washed three times for 5-10 minutes in PBS/0.1%Tween20 and incubated for 30 minutes with the Goat Anti-Mouse IgG1 HRP-conjugated secondary antibody (1:2500 dilution; JacksonImmuno; Cat #: 115-035-205) in PBS/0.1%Tween20/5% Blotting-Grade Blocker at RT. Following the secondary incubation, the membrane was washed thrice more in PBS/0.1%Tween20 and visualized with HyGLO Quick Spray Chemiluminescent HRP Antibody Detection Reagent (Denville Scientific Inc; Cat #: E2400) and the KwikQuant™ Imager (Kindle Biosciences, LLC; Cat#: D1001).

RT-qPCR Analysis:

500 ng of isolated total RNA was used as input into a 10 uL reaction of the SuperScript™ VILO™ cDNA Synthesis Kit (ThermoFisher; Cat #: 11754050), and samples were incubated according to the manufactures instructions. 3 uL of a 1:20 dilution of the cDNA was used as input into each 10 uL qPCR reaction using the SsoAdvanced™ Universal SYBR® Green Supermix (BioRad; Cat #: 1725271). *mex-6*, *puf-5*, and *oma-1* gene-specific primers were used in each reaction (final primer concentration of 250 nM for each primer). Parallel *tbb-2* qPCR reactions were run for each sample for normalization. Reactions were run on a QuantStudio™ 6 Flex Real-Time PCR System (ThermoFisher; Cat #: 4485691). Fold change calculations were done based on the $\Delta\Delta Ct$ method. Briefly, mean *tbb-2* Ct values were subtracted from the respective *mex-6*, *puf-5*, and *oma-1* Ct values (ΔCt). Average ΔCt values from the control condition of each genotype were then subtracted from the control and gene-specific RNAi condition of the same genotype ($\Delta\Delta Ct$). Fold change with respect to the control condition was calculated using $2^{(-\Delta\Delta Ct)}$.

Microscopy:

Fluorescence confocal microscopy was performed using two microscopes: 1) an inverted Zeiss Axio Observer with CSU-W1 Sora spinning disk scan head (Yokogawa), 1X/2.8x relay lens (Yokogawa), fast piezo z-drive (Applied Scientific Instrumentation), a iXon Life 888 EMCCD camera (Andor), and a 405/488/561/637nm solid-state laser (Coherent) with a 405/488/561/640 transmitting dichroic (Semrock) and 624-40/692-40/525-30/445-45nm bandpass filter (Semrock) respectively. Slidebook v6.0 software (Intelligent Imaging Innovations) was used for image capture, and a 63X-1.4NA objective (Zeiss) was used; 2) an inverted ZEISS LSM 880-AiryScan (Carl Zeiss) equipped with a 63X objective. ZEN imaging software (Carl Zeiss) was used for image capture, and images were subsequently processed by the ZEN Airyscan Processing method.

Image analysis and quantification:

Images were processed in Fiji (<https://imagej.net/software/fiji/downloads>). For *in situ* quantification of cytoplasmic RNA level, images containing both the RNA of interest (*mex-6*) and

a control RNA (*puf-5*) were processed. Regions of interest (ROIs) were drawn in single Z planes corresponding to the indicated germline area, and the ROI mean intensity was calculated for both the *mex-6* and *puf-5* channels. Background mean intensity values were measured in adjacent soma tissues for both channels and subtracted from the measured values in the germline. The background-subtracted mean *mex-6* germline measurement was then normalized to the background-subtracted mean *puf-5* germline measurement, and values were plotted. Five individual worms were used for each condition.

For *in situ* quantification of pachytene nuclear signal, maximum projections were taken from half of the *C. elegans* germline and individual ROIs were drawn around 10 rows of pachytene nuclei starting in the center of the *mex-6* expression region. The maximum, mean, and median value for each ROI was measured for each channel. The median *mex-6* value for each nuclei was subtracted from its respective *mex-6* maximum value. The *mex-6* maximum value was then normalized by dividing it by the mean *puf-5* value measured for the respective ROI, and values were plotted. Three individual worms were used for each condition.

For *in situ* quantification of granule signal, ROIs for individual granules were drawn by masking in FIJI, and the mean *mex-6* and *puf-5* values were measured for each granule. Background mean intensity values were measured in adjacent soma tissues for both channels and subtracted from the measured values in the germline. The background-subtracted mean *mex-6* germline measurement was then normalized to the background-subtracted mean *puf-5* germline measurement, and values were plotted. Five individual worms were used for each condition.

References:

Agabian, N. (1990). Trans splicing of nuclear pre-mRNAs. *Cell* 61, 1157–1160.

Akay, A., Di Domenico, T., Suen, K.M., Nabih, A., Parada, G.E., Larance, M., Medhi, R., Berkyurek, A.C., Zhang, X., Wedeles, C.J., et al. (2017). The Helicase Aquarius/EMB-4 Is Required to Overcome Intronic Barriers to Allow Nuclear RNAi Pathways to Heritably Silence Transcription. *Dev. Cell* 42, 241-255.e6.

Alcazar, R.M., Lin, R., and Fire, A.Z. (2008). Transmission Dynamics of Heritable Silencing Induced by Double-Stranded RNA in *Caenorhabditis elegans*. *Genetics* 180, 1275–1288.

Ashe, A., Sapetschnig, A., Weick, E.-M., Mitchell, J., Bagijn, M.P., Cording, A.C., Doebley, A.-L., Goldstein, L.D., Lehrbach, N.J., Le Pen, J., et al. (2012). piRNAs Can Trigger a Multigenerational Epigenetic Memory in the Germline of *C. elegans*. *Cell* 150, 88–99.

Bartel, D.P. (2018). Metazoan MicroRNAs. *Cell* 173, 20–51.

Barucci, G., Cornes, E., Singh, M., Li, B., Ugolini, M., Samolygo, A., Didier, C., Dingli, F., Loew, D., Quarato, P., et al. (2020). Small-RNA-mediated transgenerational silencing of histone genes impairs fertility in piRNA mutants. *Nat. Cell Biol.* 22, 235–245.

Billi, A.C., Fischer, S.E.J., and Kim, J.K. (2014). Endogenous RNAi pathways in *C. elegans*. *WormBook* 1–49.

Bosher, J.M., Dufourcq, P., Sookhareea, S., and Labouesse, M. (1999). RNA interference can target pre-mRNA: Consequences for gene expression in a *Caenorhabditis elegans* operon. *Genetics* 153, 1245–1256.

Brown, K.C., and Montgomery, T.A. (2017). Transgenerational Inheritance: Perpetuating RNAi. *Curr. Biol.* 27, R383–R385.

Buckley, B.A., Burkhart, K.B., Gu, S.G., Spracklin, G., Kershner, A., Fritz, H., Kimble, J., Fire, A., and Kennedy, S. (2012). A nuclear Argonaute promotes multigenerational epigenetic inheritance and germline immortality. *Nature* 489, 447–451.

Burkhart, K.B., Guang, S., Buckley, B.A., Wong, L., Bochner, A.F., and Kennedy, S. (2011). A pre-mrna-associating factor links endogenous sirnas to chromatin regulation. *PLoS Genet.* 7, e1002249.

Burton, N.O., Burkhart, K.B., and Kennedy, S. (2011). Nuclear RNAi maintains heritable gene silencing in *Caenorhabditis elegans*. *Proc. Natl. Acad. Sci. U. S. A.* 108, 19683–19688.

Carthew, R.W., and Sontheimer, E.J. (2009). Origins and Mechanisms of miRNAs and siRNAs. *Cell* 136, 642–655.

Castel, S.E., and Martienssen, R.A. (2013). RNA interference in the nucleus: Roles for small RNAs in transcription, epigenetics and beyond. *Nat. Rev. Genet.* 14, 100–112.

Chi, W., and Reinke, V. (2006). Promotion of oogenesis and embryogenesis in the *C. elegans* gonad by EFL-1/DPL-1 (E2F) does not require LIN-35 (pRB). *Development* 133, 3147–3157.

Claycomb, J.M., Batista, P.J., Pang, K.M., Gu, W., Vasale, J.J., van Wolfswinkel, J.C., Chaves, D.A., Shirayama, M., Mitani, S., Ketting, R.F., et al. (2009). The Argonaute CSR-1 and Its 22G-RNA Cofactors Are Required for Holocentric Chromosome Segregation. *Cell* 139, 123–134.

Czech, B., and Hannon, G.J. (2016). One Loop to Rule Them All: The Ping-Pong Cycle and piRNA-Guided Silencing. *Trends Biochem. Sci.* 41, 324–337.

Dernburg, A.F., McDonald, K., Moulder, G., Barstead, R., Dresser, M., and Villeneuve, A.M. (1998). Meiotic recombination in *C. elegans* initiates by a conserved mechanism and is dispensable for homologous chromosome synapsis. *Cell* 94, 387–398.

Dodson, A.E., and Kennedy, S. (2019). Germ Granules Coordinate RNA-Based Epigenetic Inheritance Pathways. *Dev. Cell* 50, 704-715.e4.

Dodson, A.E., and Kennedy, S. (2020). Phase Separation in Germ Cells and Development. *Dev. Cell* 55, 4–17.

El-Brolosy, M.A., Kontarakis, Z., Rossi, A., Kuenne, C., Günther, S., Fukuda, N., Kikhi, K., Boezio, G.L.M., Takacs, C.M., Lai, S.L., et al. (2019). Genetic compensation triggered by mutant mRNA degradation. *Nature* 568, 193–197.

Fire, A., Xu, S., Montgomery, M.K., Kostas, S.A., Driver, S.E., and Mello, C.C. (1998). Potent and specific genetic interference by double-stranded RNA in *Caenorhabditis elegans*. *Nature* 391, 806–811.

Gao, M., and Arkov, A.L. (2013). Next generation organelles: Structure and role of germ granules in the germline. *Mol. Reprod. Dev.* 80, 610–623.

Grishok, A., Tabara, H., and Mello, C.C. (2000). Genetic Requirements for Inheritance of RNAi in *C. elegans*. *Science* (80-.). 287, 2494–2497.

Gu, S.G., Pak, J., Guang, S., Maniar, J.M., Kennedy, S., and Fire, A. (2012). Amplification of siRNA in *Caenorhabditis elegans* generates a transgenerational sequence-targeted histone H3 lysine 9 methylation footprint. *Nat. Genet.* 44, 157–164.

Guang, S., Bochner, A.F., Pavelec, D.M., Burkhart, K.B., Harding, S., Lachowiec, J., and Kennedy, S. (2008). An Argonaute Transports siRNAs from the Cytoplasm to the Nucleus. *Science* (80-). 321, 537–541.

Guang, S., Bochner, A.F., Burkhart, K.B., Burton, N., Pavelec, D.M., and Kennedy, S. (2010). Small regulatory RNAs inhibit RNA polymerase II during the elongation phase of transcription. *Nature* 465, 1097–1101.

Hoogstrate, S.W., Volkers, R.J., Sterken, M.G., Kammenga, J.E., and Snoek, L.B. (2014). Nematode endogenous small RNA pathways. *Worm* 3, e28234.

Ishidate, T., Ozturk, A.R., Durning, D.J., Sharma, R., Shen, E.-Z., Chen, H., Seth, M., Shirayama, M., and Mello, C.C. (2018). ZNFX-1 Functions within Perinuclear Nuage to Balance Epigenetic Signals. *Mol. Cell* 70, 639-649.e6.

Kalinava, N., Ni, J.Z., Peterman, K., Chen, E., and Gu, S.G. (2017). Decoupling the downstream effects of germline nuclear RNAi reveals that H3K9me3 is dispensable for heritable RNAi and the maintenance of endogenous siRNA-mediated transcriptional silencing in *Caenorhabditis elegans*. *Epigenetics Chromatin* 2017 10:10, 1–14.

Kim, J.K., Gabel, H.W., Kamath, R.S., Tewari, M., Pasquinelli, A., Rual, J.-F., Kennedy, S., Dybbs, M., Bertin, N., Kaplan, J.M., et al. (2005). Functional Genomic Analysis of RNA Interference in *C. elegans*. *Science* (80-). 308, 1164–1167.

Lev, I., Gingold, H., and Rechavi, O. (2019). H3K9me3 is required for inheritance of small RNAs that target a unique subset of newly evolved genes. *Elife* 8.

Liao, S., Chen, X., Xu, T., Jin, Q., Xu, Z., Xu, D., Zhou, X., Zhu, C., Guang, S., and Feng, X. (2020). Co-surveillance of ribosomal RNA by the exosome complex and nucleolar RNAi in *C. elegans*. *BioRxiv* 2020.11.23.395020.

Liu, J., Valencia-Sanchez, M.A., Hannon, G.J., and Parker, R. (2005). MicroRNA-dependent localization of targeted mRNAs to mammalian P-bodies. *Nat. Cell Biol.* 7, 719–723.

Lui, D.Y., and Colaiácovo, M.P. (2013). Meiotic development in *Caenorhabditis elegans*. *Adv. Exp. Med. Biol.* 757, 133–170.

Luo, Y., Na, Z., and Slavoff, S.A. (2018). P-Bodies: Composition, Properties, and Functions. *Biochemistry* 57, 2424–2431.

Macqueen, A.J., Nica, M., Colaiá Covo, P., Mcdonald, K., and Villeneuve, A.M. (2002). Synapsis-dependent and-independent mechanisms stabilize homolog pairing during meiotic prophase in *C. elegans*.

Manage, K.I., Rogers, A.K., Wallis, D.C., Uebel, C.J., Anderson, D.C., Nguyen, D.A.H., Arca, K., Brown, K.C., Rodrigues, R.J.C., de Albuquerque, B.F.M., et al. (2020). A tudor domain protein, SIMR-1, promotes sirna production at pirna-targeted mrnas in *C. Elegans*. *Elife* 9.

Mao, H., Zhu, C., Zong, D., Weng, C., Yang, X., Huang, H., Liu, D., Feng, X., and Guang, S. (2015). The Nrde Pathway Mediates Small-RNA-Directed Histone H3 Lysine 27 Trimethylation in *Caenorhabditis elegans*. *Curr. Biol.* 25, 2398–2403.

Marré, J., Traver, E.C., and Jose, A.M. (2016). Extracellular RNA is transported from one generation to the next in *Caenorhabditis elegans*. *Proc. Natl. Acad. Sci. U. S. A.* 113, 12496–12501.

Martienssen, R., and Moazed, D. (2015). RNAi and heterochromatin assembly. *Cold Spring Harb. Perspect. Biol.* 7.

Martínez, G., and Slotkin, R.K. (2012). Developmental relaxation of transposable element silencing in plants: Functional or byproduct? *Curr. Opin. Plant Biol.* 15, 496–502.

Motamedi, M.R., Verdel, A., Colmenares, S.U., Gerber, S.A., Gygi, S.P., and Moazed, D. (2004). Two RNAi complexes, RITS and RDRC, physically interact and localize to noncoding centromeric RNAs. *Cell* 119, 789–802.

Newman, M.A., Ji, F., Fischer, S.E.J., Anselmo, A., Sadreyev, R.I., and Ruvkun, G. (2018). The surveillance of pre-mRNA splicing is an early step in *C. Elegans* RNAi of endogenous genes. *Genes Dev.* 32, 670–681.

Ni, J.Z., Kalinava, N., Mendoza, S.G., and Gu, S.G. (2018). The spatial and temporal dynamics of nuclear RNAi-targeted retrotransposon transcripts in *Caenorhabditis elegans*. *Development* 145, dev167346.

Ouyang, J.P.T., Folkmann, A., Bernard, L., Lee, C.-Y., Seroussi, U., Charlesworth, A.G., Claycomb, J.M., and Seydoux, G. (2019). P Granules Protect RNA Interference Genes from Silencing by piRNAs. *Dev. Cell* 50, 716-728.e6.

Pak, J., and Fire, A. (2007). Distinct Populations of Primary and Secondary Effectors During RNAi in *C. elegans*. *Science* (80-.). 315, 241–244.

Pak, J., Maniar, J.M., Mello, C.C., and Fire, A. (2012). Protection from feed-forward amplification in an amplified RNAi mechanism. *Cell* 151, 885–899.

Phillips, C.M., Montgomery, T.A., Breen, P.C., and Ruvkun, G. (2012). MUT-16 promotes formation of perinuclear Mutator foci required for RNA silencing in the *C. elegans* germline. *Genes Dev.* 26, 1433–1444.

Rechavi, O., and Lev, I. (2017). Principles of Transgenerational Small RNA Inheritance in *Caenorhabditis elegans*. *Curr. Biol.* 27, R720–R730.

Rhind, N.R., Miller, L.M., Kopczynski, J.B., and Meyer, B.J. (1995). *xo1-1* acts as an early switch in the *C. elegans* male/hermaphrodite decision. *Cell* 80, 71–82.

Sapetschnig, A., Sarkies, P., Lehrbach, N.J., and Miska, E.A. (2015). Tertiary siRNAs Mediate Paramutation in *C. elegans*. *PLoS Genet.* 11, 1005078.

Schubert, C.M., Lin, R., de Vries, C.J., Plasterk, R.H., and Priess, J.R. (2000). MEX-5 and MEX-6 function to establish soma/germline asymmetry in early *C. elegans* embryos. *Mol. Cell* 5, 671–682.

Schwartz-Orbach, L., Zhang, C., Sidoli, S., Amin, R., Kaur, D., Zhebrun, A., Ni, J., and Gu, S.G. (2020). *Caenorhabditis elegans* nuclear RNAi factor set-32 deposits the transgenerational histone modification, h3k23me3. *Elife* 9, 1–21.

Seydoux, G. (2018). The P Granules of *C. elegans*: A Genetic Model for the Study of RNA–Protein Condensates. *J. Mol. Biol.* 430, 4702–4710.

Shen, E.-Z., Chen, H., Ozturk, A.R., Tu, S., Shirayama, M., Tang, W., Ding, Y.-H., Dai, S.-Y., Weng, Z., and Mello, C.C. (2018). Identification of piRNA Binding Sites Reveals the Argonaute Regulatory Landscape of the *C. elegans* Germline. *Cell* 172, 937–951.e18.

Shih, J.D., Waks, Z., Kedersha, N., and Silver, P.A. (2011). Visualization of single mRNAs reveals temporal association of proteins with microRNA-regulated mRNA. *Nucleic Acids Res.* 39, 7740.

Shirayama, M., Seth, M., Lee, H.-C., Gu, W., Ishidate, T., Conte, D., and Mello, C.C. (2012a). piRNAs initiate an epigenetic memory of nonself RNA in the *C. elegans* germline. *Cell* 150, 65–77.

Shirayama, M., Seth, M., Lee, H.C., Gu, W., Ishidate, T., Conte, D., and Mello, C.C. (2012b). PiRNAs initiate an epigenetic memory of nonself RNA in the *C. elegans* germline. *Cell* 150, 65–77.

Shukla, A., Yan, J., Pagano, D.J., Dodson, A.E., Fei, Y., Gorham, J., Seidman, J.G., Wickens, M., and Kennedy, S. (2020). poly(UG)-tailed RNAs in genome protection and epigenetic inheritance. *Nature* 582, 283–288.

Shukla, A., Perales, R., and Kennedy, S. (2021). piRNAs Coordinate poly(UG) Tailing to Prevent Aberrant and Permanent Gene Silencing. *BioRxiv* 2021.01.30.428010.

Sijen, T., Fleenor, J., Simmer, F., Thijssen, K.L., Parrish, S., Timmons, L., Plasterk, R.H.A., and Fire, A. (2001). On the role of RNA amplification in dsRNA-triggered gene silencing. *Cell* 107, 465–476.

Sijen, T., Steiner, F.A., Thijssen, K.L., and Plasterk, R.H.A. (2007). Secondary siRNAs Result from Unprimed RNA Synthesis and Form a Distinct Class. *Science* (80-.). 315, 244–247.

Strome, S., and Wood, W.B. (1982). Immunofluorescence visualization of germ-line-specific cytoplasmic granules in embryos, larvae, and adults of *Caenorhabditis elegans*. *Proc. Natl. Acad. Sci.* 79, 1558–1562.

Sundby, A.E., Molnar, R.I., and Claycomb, J.M. (2021). Connecting the Dots: Linking *Caenorhabditis elegans* Small RNA Pathways and Germ Granules. *Trends Cell Biol.* 31, 387–401.

Tabach, Y., Billi, A.C., Hayes, G.D., Newman, M.A., Zuk, O., Gabel, H., Kamath, R., Yacoby, K., Chapman, B., Garcia, S.M., et al. (2013). Identification of small RNA pathway genes using patterns of phylogenetic conservation and divergence. *Nature* 493, 694–698.

Tabara, H., Sarkissian, M., Kelly, W.G., Fleenor, J., Grishok, A., Timmons, L., Fire, A., and Mello, C.C. (1999). The *rde-1* Gene, RNA Interference, and Transposon Silencing in *C. elegans*. *Cell* 99, 123–132.

Tang, W., Seth, M., Tu, S., Shen, E.-Z., Li, Q., Shirayama, M., Weng, Z., and Mello, C.C. (2018). A Sex Chromosome piRNA Promotes Robust Dosage Compensation and Sex Determination in *C. elegans*. *Dev. Cell* 44, 762-770.e3.

Tsai, H.Y., Chen, C.C.G., Conte, D., Moresco, J.J., Chaves, D.A., Mitani, S., Yates, J.R., Tsai, M.D., and Mello, C.C. (2015). A ribonuclease coordinates siRNA amplification and mRNA Cleavage during NAI. *Cell* 160, 407–419.

Tyc, K.M., Nabih, A., Wu, M.Z., Wedeles, C.J., Sobotka, J.A., and Claycomb, J.M. (2017). The Conserved Intron Binding Protein EMB-4 Plays Differential Roles in Germline Small RNA Pathways of *C. elegans*. *Dev. Cell* 42, 256-270.e6.

Uebel, C.J., Anderson, D.C., Mandarino, L.M., Manage, K.I., Aynaszyan, S., and Phillips, C.M. (2018). Distinct regions of the intrinsically disordered protein MUT-16 mediate assembly of a small RNA amplification complex and promote phase separation of Mutator foci. *PLOS Genet.* 14, e1007542.

Updike, D., and Strome, S. (2010). P granule assembly and function in *Caenorhabditis elegans* germ cells. In *Journal of Andrology, (J Androl)*, pp. 53–60.

Vavassori, S., Chou, J., Faletti, L.E., Haunerding, V., Opitz, L., Joset, P., Fraser, C.J., Prader, S., Gao, X., Schuch, L.A., et al. (2021). Multisystem inflammation and susceptibility to viral infections in human ZNFX1 deficiency. *J. Allergy Clin. Immunol.*

Voronina, E., Seydoux, G., Sassone-Corsi, P., and Nagamori, I. (2011). RNA granules in germ cells. *Cold Spring Harb. Perspect. Biol.* 3.

Le Voyer, T., Neehus, A.L., Yang, R., Ogishi, M., Rosain, J., Alroqi, F., Alshalan, M., Blumental, S., Ali, F. Al, Khan, T., et al. (2021). Inherited deficiency of stress granule ZNFX1 in patients with monocytosis and mycobacterial disease. *Proc. Natl. Acad. Sci. U. S. A.* 118.

Wan, G., Fields, B.D., Spracklin, G., Shukla, A., Phillips, C.M., and Kennedy, S. (2018). Spatiotemporal regulation of liquid-like condensates in epigenetic inheritance. *Nature* 557, 679–683.

Wan, G., Yan, J., Fei, Y., Pagano, D.J., and Kennedy, S. (2020). A conserved NRDE-2/MTR-4 complex mediates nuclear RNAi in *Caenorhabditis elegans*. *Genetics* 216, 1071–1085.

Wang, E., and Hunter, C.P. (2017). SID-1 Functions in Multiple Roles To Support Parental RNAi in *Caenorhabditis elegans*. *Genetics* genetics.300067.2017.

Wang, Y., Yuan, S., Jia, X., Ge, Y., Ling, T., Nie, M., Lan, X., Chen, S., and Xu, A. (2019). Mitochondria-localised ZNFX1 functions as a dsRNA sensor to initiate antiviral responses through MAVS. *Nat. Cell Biol.* 21, 1346–1356.

Weiser, N.E., and Kim, J.K. (2019). Multigenerational Regulation of the *Caenorhabditis elegans* Chromatin Landscape by Germline Small RNAs. *Annu. Rev. Genet.* 53, 289–311.

Xu, F., Feng, X., Chen, X., Weng, C., Yan, Q., Xu, T., Hong, M., and Guang, S. (2018). A Cytoplasmic Argonaute Protein Promotes the Inheritance of RNAi. *Cell Rep.* 23, 2482–2494.

Yang, H., Zhang, Y., Vallandingham, J., Li, H., Florens, L., Mak, H.Y., and Mak, H.Y. (2012). The RDE-10/RDE-11 complex triggers RNAi-induced mRNA degradation by association with target mRNA in *C. elegans*. *Genes Dev.* 26, 846–856.

Yang, H., Vallandingham, J., Shiu, P., Li, H., Hunter, C.P., and Mak, H.Y. (2014). The DEAD box helicase RDE-12 promotes amplification of RNAi in cytoplasmic foci in *C. Elegans*. *Curr. Biol.* 24, 832–838.

Yigit, E., Batista, P.J., Bei, Y., Pang, K.M., Chen, C.-C.G., Tolia, N.H., Joshua-Tor, L., Mitani, S., Simard, M.J., and Mello, C.C. (2006). Analysis of the *C. elegans* Argonaute Family Reveals that Distinct Argonautes Act Sequentially during RNAi. *Cell* 127, 747–757.

Zalevsky, J., MacQueen, A.J., Duffy, J.B., Kempfues, K.J., and Villeneuve, A.M. (1999). Crossing over during *Caenorhabditis elegans* meiosis requires a conserved MutS-based pathway that is partially dispensable in budding yeast.

Zhang, C., Montgomery, T.A., Gabel, H.W., Fischer, S.E.J., Phillips, C.M., Fahlgren, N., Sullivan, C.M., Carrington, J.C., and Ruvkun, G. (2011). *mut-16* and other mutator class genes modulate 22G and 26G siRNA pathways in *Caenorhabditis elegans*. *Proc. Natl. Acad. Sci. U. S. A.* 108, 1201–1208.

Zhang, C., Montgomery, T.A., Fischer, S.E.J., Garcia, S.M.D.A., Riedel, C.G., Fahlgren, N., Sullivan, C.M., Carrington, J.C., and Ruvkun, G. (2012). The *Caenorhabditis elegans* RDE-10/RDE-11 Complex Regulates RNAi by Promoting Secondary siRNA Amplification. *Curr. Biol.* 22, 881–890.

Zhang, D., Tu, S., Stubna, M., Wu, W.-S., Huang, W.-C., Weng, Z., and Lee, H.-C. (2018). The piRNA targeting rules and the resistance to piRNA silencing in endogenous genes. *Science* (80-.). 359, 587–592.

Chapter 4: Conclusions and Final Remarks

Altogether, this body of work describes the complex relationship between germ granules and sRNA biology. We have described an instance where germ granules appear to protect transcripts against aberrant sRNA amplification induced by piRNAs (Chapter 2; Ouyang et al., 2019). Additionally, we have collected data that suggest that germ granules may be participating in maintaining a cycle of sRNA amplification that allows for the transgenerational perpetuation of RNAi (Chapter 3). How can these somewhat disparate findings be reconciled? One possible explanation to account for this is the difference in developmental stage during which we observe these phenomena. The proposed model of granule protection is based upon observations in the developing *C. elegans* embryo whereby loss of germ granules in the primordial germ cells results in cytoplasmic dispersion of transcripts and, in turn, increased sRNA amplification against these transcripts. The model of germ granules mediating sRNA amplification, however, is based upon observations in the adult *C. elegans* germline in which we find that cytoplasmically dispersed transcripts become enriched within germ granules upon RNAi and loss of this enrichment in the absence of ZNFX-1 weakens the silencing effect in the F1 generation. The difference in developmental context could certainly explain the discrepancy between our models, as the differences in germ granule composition at these respective stages has long been recognized (Sundby et al., 2021; Updike and Strome, 2010). For example, some granule components, such as MEG-3 and MEG-4, are known to be present only during the embryonic stages and are largely turned over by the first larval stage (Ouyang et al., 2019; Wang et al., 2014). Even the RNA composition of germ granules is also likely to be different at different stages, as *mex-6* and *puf-5* transcripts, which are strongly enriched within embryonic germ granules (Lee et al., 2020), are dispersed cytoplasmically in the adult germline (Chapter 3). Therefore, it is possible that the compositional differences that exist in germ granules between these two stages could account for possible differences in function.

This thesis puts forth exciting avenues of future exploration for both models of granule protection and granule sRNA amplification. Understanding why the *rde-11* and *sid-1* transcripts are so heavily targeted by piRNAs and why MEG-3 and MEG-4 function to protect them from

excessive silencing will be an interesting avenue for future research. It is possible that endogenous sRNA regulation of the *rde-11* and *sid-1* mRNAs functions to regulate sRNA related responses, such as exogenous RNAi. Perhaps external stimuli, such as the exposure of worms to dsRNA, could modulate the presence of these RNAs inside vs outside the granule, fine tuning the duration of the RNAi response by silencing this core RNAi machinery. With respect to the germ granule sRNA amplification model, the discovery of the ZNFX-1 dependent germ granule sRNA amplification cycle begs the question of how mechanistically this cycle is maintained. Because of ZNFX-1's interaction with both secondary Argonautes and RdRPs (Barucci et al., 2020; Ishidate et al., 2018b; Wan et al., 2018), we speculate that ZNFX-1 may be serving as a molecular bridge between Argonaute recognition, pUGylation, and RdRP-dependent sRNA amplification. Future experiments probing how ZNFX-1 coordinates continuous pUGylation will be of particular interest to the field.

Curriculum Vitae - John Paul T. Ouyang

2917 North Calvert Street, Apt 3FF, Baltimore, Maryland, 21218

(240)-383-6188

jpouyang314@gmail.com

EDUCATION

The Johns Hopkins University School of Medicine (JHU SOM) Fall 2016-Summer 2021
Thesis Advisor: Geraldine Seydoux, PhD
Biochemistry, Cellular, and Molecular Biology PhD Program

University of Maryland College Park Fall 2013- Spring 2016
Major: Cell Biology and Genetics
Honors College (Integrated Life Sciences)
GPA: 4.000

RESEARCH EXPERIENCE

PhD Candidate in the JHU SOM lab of Dr. Geraldine Seydoux May 2017-Present
-Utilizing transcriptomic and cell biological approaches to study the relationship between germ granules and RNA-mediated interference in *Caenorhabditis elegans*.

Undergraduate Honors Thesis Researcher in the UMD Cell Biology and Molecular Genetics Lab of Dr. Caren Chang May 2013-July 2016
-Conducted library screens to identify interactors with EIN2, a key regulator of the ethylene signaling pathway.
-Worked on testing the ethylene sensing capabilities of a novel prokaryotic protein containing an ethylene binding domain.

Summer Intern at the National Institutes of Health in the National Cancer Institute Lab of Dr. Michael Lichten 2014, 2015
-Worked on creating a system of DNA reporter cassettes to aid in the study of meiotic homologous recombination in budding yeast.

PUBLICATIONS

Lee, C. Y. S., Putnam, A., Lu, T., He, S., Ouyang, J. P. T., & Seydoux, G. (2020). Recruitment of mRNAs to P granules by condensation with intrinsically-disordered proteins. *ELife*, 9. <https://doi.org/10.7554/eLife.52896>

Pike, A. M., Strong, M. A., Ouyang, J. P. T., & Greider, C. W. (2019). TIN2 Functions with TPP1/POT1 To Stimulate Telomerase Processivity. *Molecular and Cellular Biology*, 39(21). <https://doi.org/10.1128/MCB.00593-18>

Ouyang, J. P. T., Folkmann, A., Bernard, L., Lee, C.-Y., Seroussi, U., Charlesworth, A. G., ... Seydoux, G. (2019). P Granules Protect RNA Interference Genes from Silencing by piRNAs. *Developmental Cell*, 50(6), 716-728.e6. <https://doi.org/10.1016/j.devcel.2019.07.026>

Krohn, D., Marino-Johnson, D., Ouyang, J. P. T. (2014). The KMO Method for Solving Non-Homogenous, m^{th} Order Differential Equations. *Rose-Hulman Undergraduate Mathematics Journal*. 15, 132-142.

HONORS/AWARDS

The DiMaio Graduate Student Award, MBG Department, JHU SOM	2021
Ruth L. Kirschstein Predoctoral Individual National Research Service Award, NICHD	2020
Journal Club Award, MBG Department, JHU SOM	2019
UMD Summa Cum Laude	2016
UMD Appleman-Norton Award in Plant Biology	2016
UMD Cell Biology and Molecular Genetics Thesis Honors	2016
HHMI Undergraduate Research Fellow	2015-2016
NIH Summer Internship	2014, 2015
UMD Integrated Life Sciences Honors Citation	2016
UMD's Dean's Scholarship	2013-2015
UMD's Dean's List	2013-2016

ORAL PRESENTATIONS

Genetics Society of America: International *C. elegans* Conference. Virtual Conference, June 2021: "Independent nuclear and cytoplasmic silencing mechanisms contribute to transgenerational RNAi." (selected oral presentation)

Cold Spring Harbor: Germ Cells. Virtual Conference, October 2020: "mRNAs targeted by silencing small RNAs accumulate in germ granules." (selected oral presentation)

Cold Spring Harbor: Regulatory & Non-Coding RNAs. Virtual Conference, May 2020: "mRNAs targeted by silencing small RNAs accumulate in germ granules." (selected oral presentation)

Genetics Society of America: The Allied Genetics Conference (TAGC). Virtual conference, April, 2020: "mRNAs targeted by silencing small RNAs accumulate in germ granules." (selected oral presentation)

Keystone Symposium on Molecular and Cellular Biology: Small Regulator RNAs. Daejeon, South Korea. April, 2019: "Loss of Germ Granule Integrity during the Oocyte-to-Embryo Transition Disrupts Small RNA Homeostasis in *Caenorhabditis elegans*." (selected oral presentation)

The Johns Hopkins University School of Medicine, Department of Molecular Biology and Genetics Colloquium. Baltimore, Maryland. November 2018: "A link between maternal inheritance of germ granules and small RNA homeostasis in *C. elegans*."

University of Maryland College Park's Cell Biology and Molecular Genetics Honors Program Thesis Defense. College Park, Maryland. April 2016: "Characterizing Phytohormone Response in Bacterial and Algal Hormone Receptor Homologs."

National Institutes of Health's Summer Student Seminar Series. Bethesda, Maryland. July 2014 and August 2015: "Constructing a DNA cassette for the Analysis of Meiotic Recombination in Budding Yeast."

POSTER PRESENTATIONS

HHMI Science Conference. Chevy Chase, Maryland. September, 2019: "Defining the role of biomolecular condensates in small RNA-mediated gene regulation"

EMBO | EMBL Symposium: The complex Life of RNA. Heidelberg, Germany. October, 2018: "A link between maternal inheritance of germ granules and small RNA homeostasis in *C. elegans*."

National Institutes of Health's Summer Poster Day. Bethesda Maryland. August 2014 and 2015: "Constructing a DNA cassette for the Analysis of Meiotic Recombination in Budding Yeast."

TEACHING EXPERIENCE

Undergraduate Research Mentor	2018-Present
-Mentored two undergraduate students through their research projects.	
Teaching Academy, Johns Hopkins University	2018-Present
-Undergoing pedagogical training to become a certified instructor.	
YO! Baltimore Tutoring Project	Fall 2020
-Tutored local Baltimore residents pursuing their GED.	
Thread Volunteer/Mentor	2016-2018
-Served as a weekly after-school math and science tutor at Dunbar High School, Baltimore, Maryland.	
Principles of Genetics Teaching Assistant	Fall 2018
-Designed problem sets and assisted the instructor in a flipped classroom setting.	
Tutor in UMD's Integrated Life Sciences AP Biology Tutoring Program	2013-2015
-Volunteered as an AP Biology tutor at Northwestern High School, Hyattsville, Maryland.	
-Served as the student coordinator of the program for the 2014-2015 academic year.	
Assistant Teacher at English as a Second Language (ELS) classes	2011-2013
-Volunteered for ESL classes at the Seven Locks Baptist Church, Potomac Maryland.	
High School Latin Tutor	2011-2013